

Fault Diagnosis of Gas Turbine Engines by Using Multiple Model Approach

Zahra Abbasfard

A Thesis in
The Department
of
Electrical and Computer Engineering

Presented in Partial Fulfillment of the Requirements
for the Degree of
Master of Applied Science (Electrical and Computer Engineering) at
Concordia University
Montreal, Quebec, Canada

April 2013

© Zahra Abbasfard, 2013

CONCORDIA UNIVERSITY
School of Graduate Studies

This is to certify that the thesis prepared

By: Zahra Abbasfard

Entitled: Fault Diagnosis of Gas Turbine Engines by Using Multiple Model Approach

and submitted in partial fulfillment of the requirements for the degree of
Master of science

complies with the regulations of the University and meets the accepted standards with respect to originality and quality.

Signed by the final examining committee:

___ Dr. R. Raut _____ Chair

___ Dr. S. Gleason _____ Examiner

___ Dr. Z. Tian _____ Examiner

___ Dr. K. Khorasani _____ Supervisor

Approved by _____

Chair of Department or Graduate Program Director

Dean of Faculty

Date _____

ABSTRACT

Fault Diagnosis of Gas Turbine Engines by Using Multiple Model Approach

Zahra Abbasfard

The field of fault detection and isolation (FDI) has attracted much attention in control theory during the last three decades which has resulted in development of sophisticated FDI algorithms. However, increasing the complexity of FDI algorithms is not necessarily feasible. Particularly for on-line FDI, the FDI unit must have the minimum possible computation cost to prevent any long delays in fault detection.

In this research, we try to address the FDI problem of a single spool jet engine by using a modified linear multiple model (MM). We first develop a novel symbolic computation-based method for linearization purposes such that the obtained linear models are subjected to the symbolic fault variables. By substituting certain values for these symbolic variables, one can obtain different linear models, which describe mathematically the healthy and faulty models. In order to select the operating point, we use this fact that for a given constant fuel flow (W_f), the system reaches a steady state, that is varying for different values of W_f . Therefore, the operating points for linearization can be determined by the level of the Power Level Angel (PLA) (different values of W_f). These operating points are selected such that an observer, which is designed as a candidate for the healthy mode, can accurately estimates the states of the system in healthy scenario and the number of false alarm then would be kept to minimum. If the

system works at different operating points one can then discretize the W_f into different intervals such that in each interval a linear model represents the behavior of the original system. By using the obtained models for different operating points, one designs the corresponding FDI units.

Second, we provide a modified multiple model (MM) approach to investigate the FDI problem of a single spool jet engine. The main advantage of this method lies in the fact that the proposed MM consists of a certain set of linear Kalman filter banks rather than using nonlinear Kalman filters such as the Extended Kalman Filter which requires more computational cost. Moreover, a hierarchical structural multiple model is used to detect and isolate multiple faults. The simulation results show the capability of the proposed method when it is applied to a single spool jet engine model.

To :

my husband and my little son

Alireza and Sourena

my brother and my sister

Mohammadreza and Shadi

ACKNOWLEDGMENTS

I would like to express deep gratitude to my dissertation advisor Prof. K. Khorasani for his consistent encouragement, motivation, guidance and support through-out my study at Concordia University. He has provided me with unquenchable enthusiasm, vision, and wisdom, which inspired me from the beginning to the end.

My special thanks are to my comities member, Dr. R. Raut , Dr. S. Gleason, Dr. Z. Tian for devoting their valuable time in guiding and evaluating my work.

My good friends, Najmeh Darougheh, Amir Baniamerian and Zahra Gallehdary with whom I spent a lot of time both at work and in spare time, deserve big thanks. Also I wish to thank my manager at AECOM CO. Plamen Kurktchiev for supporting me during my study.

Last, but by no means least, my special thanks go to my husband Alireza, for his love and support over the years. He has always been a pillar of strength, inspiration and support. I could never thank my brother and sister for their unconditional love and prayers, without which I would never have come so far.

TABLE OF CONTENTS

LIST OF FIGURES.....	X
LIST OF TABLES	XVII
NOMENCLATURE	XIX
CHAPTER 1 : INTRODUCTION	1
1.1. INTRODUCTION.....	1
1.2. MOTIVATION OF THE RESEARCH	3
1.3. LITERATURE REVIEW	5
1.3.1. FDI for Gas Turbine.....	6
1.3.2. Multiple-Model Based FDI.....	7
1.3.3. Artificial Intelligence Based FDI.....	8
CHAPTER 2 : BACKGROUND	12
2.1. AIRCRAFT JET ENGINE MATHEMATICAL MODEL.....	12
2.1.1. Components	15
2.1.2. Complete Healthy Model	20
2.1.3. Faulty Model	21
2.2. MULTIPLE MODEL APPROACH	24
2.2.1. Kalman Filter.....	24
2.2.2. Linear Multiple Model.....	28
2.3. CONCLUSION	30
CHAPTER 3 : SYMBOLIC LINEARIZATION	31

3.1. INTRODUCTION.....	31
3.2. A NOVEL SYMBOLIC LINEARIZATION METHOD	32
3.3. COMPLETE SYMBOLIC LINEAR MODEL	39
3.4. SIMULATION RESULTS.....	42
3.5. CONCLUSION	46
 CHAPTER 4 : FAULT DIAGNOSIS OF GAS TURBINE	 47
4.1. MODIFIED MULTIPLE MODEL	47
4.1.1. FDI Logic for Single Faults.....	48
4.1.2. Normalization	50
4.1.3. Determining the Operating Points.....	52
4.2. SINGLE FAULT SIMULATION RESULTS.....	53
4.2.1. Faults with Magnitude 2%	55
4.2.2. Faults with Magnitude 5%	63
4.2.3. Faults with Magnitude 8%	69
4.2.4. Faults with Magnitude 10%	75
4.2.5. Effectiveness Loss of Fuel Flow	81
4.2.6. Summary.....	85
4.3. NUMBER OF OBSERVERS	89
4.4. CONCLUSION	94
 CHAPTER 5 MODIFICATIONS TO THE FDI APPROACH.....	 95
5.1. FDI DIAGNOSIS OF MULTIPLE FAULTS	95
5.1.1. Simulation Results.....	98
5.2. OUTPUT SELECTION	103
5.2.1. Investigation of the Observability.....	104
5.2.2. Simulation Results.....	106

5.3. CONCLUSION	113
CHAPTER 6 CONCLUSIONS AND SUGGESTIONS	114
6.1. CONTRIBUTIONS OF THE THESIS.....	114
6.1.1. Develop a Novel Symbolic Linearization Method	114
6.1.2. Develop the Modified Multiple Model FDI.....	115
6.1.3. The FDI problem of the Single Spool Gas Turbine	115
6.2. SUGGESTIONS	116
6.2.1. Suggestions on the Theory	116
6.2.2. Suggestions on the Application.....	117
BIBLIOGRAPHY	118

LIST OF FIGURES

Figure 2.1: The Schematic of single spool jet engine [55].	13
Figure 2.2: Schematic of the gas turbine working cycle [16].	14
Figure 2.3: The single spool jet engine (basic model) [19].	15
Figure 3.1: The compressor decomposition block.	33
Figure 3.2: Turbine block decomposition.	35
Figure 3.3: The single spool gas turbine in which compressor and turbine decomposed in the sub-blocks (also see Figure 3.1 and Figure 3.2).	39
Figure 3.4: One profile of the fuel flow selected for the healthy scenario.	42
Figure 3.5: The output N of the linearized and the original system for the healthy scenario.	43
Figure 3.6: The output TC of the linearized and the original system for the healthy scenario.	43
Figure 3.7: The output TT of the linearized and the original system for the healthy scenario.	44
Figure 3.8: The output PC of the linearized and the original system for the healthy scenario.	44
Figure 3.9: The output PT of the linearized and the original system for the healthy scenario.	45
Figure 4.1: The probability of multiple model for the scenario in which a fault occurs in the compressor efficiency at $t=5sec$. It takes 1 sec for the probability of the corresponding model reaches to 0.91 ($P1$ denotes the healthy mode and $P2 - P6$ correspond to various faulty cases).	49
Figure 4.2: The simulation result for the fault which occurs at $t=5$ sec in compressor efficiency (noise free measurement).	50
Figure 4.3: The simulation result for the fault which occurs at $t=5$ sec in compressor efficiency (noisy measurement).	51

Figure 4.4: The simulation result for the fault which occurs at $t=5$ sec in compressor efficiency (modified and normalized output). 52

Figure 4.5: Simulation result for the healthy scenario by using the proposed method with $\mathbf{Wf} = \mathbf{0.85}$. p_1 denotes the probability of the healthy mode validity (for the mode labels refer to Table 4.2). 56

Figure 4.6: Simulation result for the healthy scenario by using the approach proposed in [2] with $\mathbf{Wf} = \mathbf{0.85}$. p_1 denotes the probability of the healthy model validity (for the mode labels refer to Table 4.2) 56

Figure 4.7: The simulation result for the scenario II by using the proposed method with $\mathbf{Wf} = \mathbf{0.85}$. A fault with magnitude 0.02 ($F_{et} = 0.98$) occurs in the turbine efficiency at $t = 5sec$ (for the mode labels refer to Table 4.2). 57

Figure 4.8: The simulation result for the scenario II by using the approach proposed in [2] with $\mathbf{Wf} = \mathbf{0.85}$. A fault with magnitude 0.02 ($F_{et} = 0.98$) occurs in the turbine efficiency at $t = 5sec$ (for the mode labels refer to Table 4.2). 58

Figure 4.9: The simulation result for the scenario III by using the proposed method with $\mathbf{Wf} = \mathbf{0.85}$. A fault with magnitude 0.02 ($F_{ec} = 0.98$) occurs in the compressor efficiency at $t = 5sec$ (for the mode labels refer to Table 4.2). 59

Figure 4.10: The simulation result for the scenario III by using the approach proposed in [2] with $\mathbf{Wf} = \mathbf{0.85}$. A fault with magnitude 0.02 ($F_{ec} = 0.98$) occurs in the compressor efficiency at $t = 5sec$ (for the mode labels refer to Table 4.2). 59

Figure 4.11: The simulation result for the scenario IV by using the proposed method with $\mathbf{Wf} = \mathbf{0.85}$. A fault with magnitude 0.02 ($F_{mt} = 0.98$) occurs in the turbine mass flow at $t = 5sec$ (for the mode labels refer to Table 4.2). 60

Figure 4.12: The simulation result for the scenario IV by using the approach proposed in [2] with $\mathbf{Wf} = \mathbf{0.85}$. A fault with magnitude 0.02 ($F_{mt} = 0.98$) occurs in the turbine mass flow at $t = 5sec$ (for the mode labels refer to Table 4.2). 61

Figure 4.13: The simulation result the for scenario V by using the proposed method with $\mathbf{Wf} = \mathbf{0.85}$. A fault with magnitude 0.02 ($F_{mc} = 0.98$) occurs in the compressor mass flow at $t = 5sec$ (for the mode labels refer to Table 4.2). 62

Figure 4.14: The simulation result for the scenario V by using the approach proposed in [2] with $\mathbf{Wf} = \mathbf{0.85}$. A fault with magnitude 0.02 ($F_{mc} = 0.98$) occurs in the compressor mass flow at $t = 5sec$ (for the mode labels refer to Table 4.2). 62

Figure 4.15: The simulation result for the scenario II by using the proposed method with $\mathbf{Wf} = \mathbf{0.85}$. A fault with magnitude 0.05 ($F_{et} = 0.95$) occurs in the turbine efficiency at $t = 5\text{sec}$ (for the mode labels refer to Table 4.3). 63

Figure 4.16: The simulation result for the scenario II by using the approach proposed in [2] with $\mathbf{Wf} = \mathbf{0.85}$. A fault with magnitude 0.052 ($F_{et} = 0.95$) occurs in the turbine efficiency at $t = 5\text{sec}$ (for the mode labels refer to Table 4.3). 64

Figure 4.17: The simulation result for the scenario III by using the proposed method with $\mathbf{Wf} = \mathbf{0.85}$. A fault with magnitude 0.05 ($F_{ec} = 0.95$) occurs in the compressor efficiency at $t = 5\text{sec}$ (for the mode labels refer to Table 4.3). 65

Figure 4.18: The simulation result for the scenario III by using the approach proposed in [2] with $\mathbf{Wf} = \mathbf{0.85}$. A fault with magnitude 0.05 ($F_{ec} = 0.95$) occurs in the compressor efficiency at $t = 5\text{sec}$ (for the mode labels refer to Table 4.3). 65

Figure 4.19: The simulation result for the scenario IV by using the proposed method with $\mathbf{Wf} = \mathbf{0.85}$. A fault with magnitude 0.05 ($F_{mt} = 0.95$) occurs in the turbine mass flow at $t = 5\text{sec}$ (for the mode labels refer to Table 4.3). 66

Figure 4.20: The simulation result for the scenario IV by using the approach proposed in [2] with $\mathbf{Wf} = \mathbf{0.85}$. A fault with magnitude 0.05 ($F_{mt} = 0.95$) occurs in the turbine mass flow at $t = 5\text{sec}$ (for the mode labels refer to Table 4.3). 67

Figure 4.21: The simulation result for the scenario V by using the proposed method with $\mathbf{Wf} = \mathbf{0.85}$. A fault with magnitude 0.05 ($F_{mc} = 0.95$) occurs in the compressor mass flow at $t = 5\text{sec}$ (for the mode labels refer to Table 4.3). 68

Figure 4.22: The simulation result for the scenario V by using the approach proposed in [2] with $\mathbf{Wf} = \mathbf{0.85}$. A fault with magnitude 0.05 ($F_{mc} = 0.95$) occurs in the compressor mass flow at $t = 5\text{sec}$ (for the mode labels refer to Table 4.3). 68

Figure 4.23: The simulation result for the scenario II by using the proposed method with $\mathbf{Wf} = \mathbf{0.85}$. A fault with magnitude 0.08 ($F_{et} = 0.92$) occurs in the turbine efficiency at $t = 5\text{sec}$ (for the mode labels refer to Table 4.4). 69

Figure 4.24: The simulation result for the scenario II by using the approach proposed in [2] with $\mathbf{Wf} = \mathbf{0.85}$. A fault with magnitude 0.08 ($F_{et} = 0.92$) occurs in the turbine efficiency at $t = 5\text{sec}$ (for the mode labels refer to Table 4.4). 70

Figure 4.25: The simulation result for the scenario III by using the proposed method with $\mathbf{Wf} = \mathbf{0.85}$. A fault with magnitude 0.08 ($F_{ec} = 0.92$) occurs in the compressor

efficiency at $t = 5\text{sec}$ (for the mode labels refer to Table 4.4).....	71
Figure 4.26: The simulation result for the scenario III by using the approach proposed in [2] with $Wf = 0.85$. A fault with magnitude 0.08 ($F_{ec} = 0.92$) occurs in the compressor efficiency at $t = 5\text{sec}$ (for the mode labels refer to Table 4.4).	71
Figure 4.27: The simulation result for the scenario IV by using the proposed method with $Wf = 0.85$. A fault with magnitude 0.08 ($F_{mt} = 0.92$) occurs in the turbine mass flow at $t = 5\text{sec}$ (for the mode labels refer to Table 4.4).	72
Figure 4.28: The simulation result for the scenario IV by using the approach proposed in [2] with $Wf = 0.85$. A fault with magnitude 0.08 ($F_{mt} = 0.92$) occurs in the turbine mass flow at $t = 5\text{sec}$ (for the mode labels refer to Table 4.4).	73
Figure 4.29: The simulation result for the scenario V by using the proposed method with $Wf = 0.85$. A fault with magnitude 0.08 ($F_{mc} = 0.92$) occurs in the compressor mass flow at $t = 5\text{sec}$ (for the mode labels refer to Table 4.4).	74
Figure 4.30: The simulation result for the scenario V by using the approach proposed in [2] with $Wf = 0.85$. A fault with magnitude 0.02 ($F_{mc} = 0.92$) occurs in the compressor mass flow at $t = 5\text{sec}$ (for the mode labels refer to Table 4.4).	74
Figure 4.31: The simulation result for the scenario II by using the proposed method with $Wf = 0.85$. A fault with magnitude 0.1 ($F_{et} = 0.9$) occurs in the turbine efficiency at $t = 5\text{sec}$ (for the mode labels refer to Table 4.5).	75
Figure 4.32: The simulation result for the scenario II by using the approach proposed in [2] with $Wf = 0.85$. A fault with magnitude 0.1 ($F_{et} = 0.9$) occurs in the turbine efficiency at $t = 5\text{sec}$ (for the mode labels refer to Table 4.5).	76
Figure 4.33: The simulation result for the scenario III by using the proposed method with $Wf = 0.85$. A fault with magnitude 0.1 ($F_{ec} = 0.9$) occurs in the compressor efficiency at $t = 5\text{sec}$ (for the mode labels refer to Table 4.5).	77
Figure 4.34: The simulation result for scenario III by using the approach proposed in [2] with $Wf = 0.85$. A fault with magnitude 0.1 ($F_{ec} = 0.9$) occurs in the compressor efficiency at $t = 5\text{sec}$ (for the mode labels refer to Table 4.5).	77
Figure 4.35: The simulation result for the scenario IV by using the proposed method with $Wf = 0.85$. A fault with magnitude 0.1 ($F_{mt} = 0.9$) occurs in the turbine mass flow at $t = 5\text{sec}$ (for the mode labels refer to Table 4.5).	78
Figure 4.36: The simulation result for the scenario IV by using the approach proposed in	

[2] with $\mathbf{Wf} = \mathbf{0.85}$. A fault with magnitude 0.1 ($F_{mt} = 0.9$) occurs in the turbine mass flow at $t = 5sec$ (for the mode labels refer to Table 4.5).....	79
Figure 4.37: The simulation result for the scenario V by using the proposed method with $\mathbf{Wf} = \mathbf{0.85}$. A fault with magnitude 0.1 ($F_{mc} = 0.9$) occurs in the compressor mass flow at $t = 5sec$ (for the mode labels refer to Table 4.5).....	80
Figure 4.38: The simulation result for the scenario V by using the approach proposed in [2] with $\mathbf{Wf} = \mathbf{0.85}$. A fault with magnitude 0.1 ($F_{mc} = 0.9$) occurs in the compressor mass flow at $t = 5sec$ (for the mode labels refer to Table 4.5).....	80
Figure 4.39: The simulation result for the scenario VI by using the proposed method with $\mathbf{Wf} = \mathbf{0.85}$. A fault with magnitude 0.05 ($F_{w_f} = 0.95$) occurs in effectiveness of fuel flow actuator at $t = 5sec$ (for the mode labels refer to Table 4.2).....	81
Figure 4.40: The simulation result for the scenario VI by using the approach proposed in [2] with $\mathbf{Wf} = \mathbf{0.85}$. A fault with magnitude 0.05 ($F_{w_f} = 0.95$) occurs in effectiveness of fuel flow actuator at $t = 5sec$ (for the mode labels refer to Table 4.2).	82
Figure 4.41: The simulation result for the scenario VI by using the proposed method with $\mathbf{Wf} = \mathbf{0.85}$. A fault with magnitude 0.08 ($F_{w_f} = 0.92$) occurs in effectiveness of fuel flow actuator at $t = 5sec$ (for the mode labels refer to Table 4.4).....	83
Figure 4.42: The simulation result for the scenario IV by using the approach proposed in [2] with $\mathbf{Wf} = \mathbf{0.85}$. A fault with magnitude 0.08 ($F_{w_f} = 0.92$) occurs in effectiveness of fuel flow actuator at $t = 5sec$ (for the mode labels refer to Table 4.4).	83
Figure 4.43: The simulation result for the scenario VI with $\mathbf{Wf} = \mathbf{0.85}$. A fault with magnitude 0.1 ($F_{w_f} = 0.9$) occurs in effectiveness of fuel flow actuator at $t = 5sec$ (for the mode labels refer to Table 4.5).....	84
Figure 4.44: The simulation result for the scenario IV by using the approach proposed in [2] with $\mathbf{Wf} = \mathbf{0.85}$. A fault with magnitude 0.1 ($F_{w_f} = 0.9$) occurs in effectiveness of fuel flow actuator at $t = 5sec$ (for the mode labels refer to Table 4.5).....	85
Figure 4.45: The simulation result for the scenario II by using our proposed method. A fault with magnitude 3% ($F_{et} = 0.97$) occurs in the compressor efficiency at $t = 5sec$ (in this simulation we run all filters in parallel).	91
Figure 4.46: The simulation result for the scenario II by using our proposed method. A	

fault with magnitude 6% ($F_{et} = 0.94$) occurs in the compressor efficiency at $t = 5sec$ (in this simulation we run all filters in parallel).	91
Figure 4.47: The simulation result for the scenario II by using our proposed method. A fault with magnitude 7% ($F_{et} = 0.93$) occurs in the compressor efficiency at $t = 5sec$ (in this simulation we run all filters in parallel).	92
Figure 4.48: The simulation result for the scenario II by using our proposed method. A fault with magnitude 9% ($F_{et} = 0.91$) occurs in the compressor efficiency at $t = 5sec$ (in this simulation we run all filters in parallel).	92
Figure 4.49: The simulation result for the scenario IV by using our proposed method. A fault with magnitude 9% ($F_{mt} = 0.91$) occurs in the compressor efficiency at $t = 5sec$ (in this simulation we run all filters in parallel).	93
Figure 5.1: The probability of the models for a multiple-fault scenario. The faults with magnitude 2% and 5% occur in the turbine efficiency and mass flow at $t=8sec$ and $t=20sec$, respectively. The proposed method in the previous chapter cannot isolate the second fault.	96
Figure 5.2: Simulation results of Scenario I, multiple faults in the turbine efficiency and compressor mass flow with a magnitude of 2% occurs at $t=8sec$ and $t=20sec$, respectively.	100
Figure 5.3: Simulation results of Scenario II, multiple faults in the turbine efficiency and mass flow with a magnitude of 2% occurs at $t=8sec$ and $t=20sec$, respectively. ...	100
Figure 5.4: Simulation results of Scenario III, multiple faults in the turbine efficiency and fuel flow with a magnitude of 2% and 5% occur at $t=8sec$ and $t=20sec$, respectively.	101
Figure 5.5: Simulation results of Scenario IV, multiple faults in the compressor mass flow and fuel flow with a magnitude 2% and 5% occur at $t=8sec$ and $t=20sec$, respectively.	102
Figure 5.6: Simulation results of Scenario V, multiple faults in the turbine mass flow and compressor efficiency with a magnitude 2% occur at $t=8sec$ and $t=20sec$, respectively.	103
Figure 5.7: The probability of the models for Scenario I with $y = [N, T_C, P_C, P_t]$. A fault with a magnitude of 2% occurs in the turbine efficiency at $t=5sec$	107
Figure 5.8: The probability of the models for Scenario II with $y = [N, T_C, P_C, P_t]$. A fault with a magnitude of 2% occurs in the compressor efficiency at $t=5sec$	108

Figure 5.9: The probability of the models for Scenario III with $y = [N, T_C, P_C, P_t]$. A fault with a magnitude of 2% occurs in the turbine mass flow at $t=5sec$ 108

Figure 5.10: The probability of the models for Scenario IV with $y = [N, T_C, P_C, P_t]$. A fault with a magnitude of 2% occurs in the compressor mass flow at $t=5sec$ 109

Figure 5.11: The probability of the models for Scenario V with $y = [N, T_C, P_C, P_t]$. A loss of effectiveness of fuel flow with a magnitude of 5% occurs at $t=5sec$ 109

Figure 5.12: The probability of the models for Scenario I with $y = [T_C, P_C, P_t]$. A fault with a magnitude of 2% occurs in the turbine efficiency at $t=5sec$ 110

Figure 5.13: The probability of the models for Scenario II with $y = [T_C, P_C, P_t]$. A fault with a magnitude of 2% occurs in the compressor efficiency at $t=5sec$ 110

Figure 5.14: The probability of the models for Scenario III with $y = [T_C, P_C, P_t]$. A fault with a magnitude of 2% occurs in the turbine mass flow at $t=5sec$ 111

Figure 5.15: The probability of the models for Scenario IV with $y = [T_C, P_C, P_t]$. A fault with a magnitude of 2% occurs in the compressor mass flow at $t=5sec$ 111

Figure 5.16: The probability of the models for Scenario V with $y = [T_C, P_C, P_t]$. A loss of effectiveness of fuel flow with a magnitude of 5% occurs at $t=5sec$ 112

LIST OF TABLES

Table 2.1: The time-update phase in the Kalman filter.	27
Table 2.2: The measurement-update phase in the Kalamn filter.	27
Table 3.1: The average output difference (equation (3.21)) between the nonlinear single spool and the linear model obtained by the proposed symbolic linearization method.	46
Table 4.1: The FDI results for different incremental changes of nominal \mathbf{Wf} and $\mathbf{Wf} = \mathbf{0.9}$ in which the bank of observer is constructed. The symbol \times denotes false alarm flag.	53
Table 4.2: The different models corresponding to the healthy and faulty modes that are used in the simulation for each operating point.	55
Table 4.3: The different models corresponding to the healthy and faulty modes (5% magnitude) that are used in the simulation for each operating point.	63
Table 4.4: The different models corresponding to the healthy and faulty modes (8% magnitude) that are used in the simulation for each operating point.	69
Table 4.5: The different models corresponding to the healthy and faulty modes (10% magnitude) that are used in the simulation for each operating point.	75
Table 4.6: The summary of simulation results for different values of \mathbf{wf} by using our proposed approach. t_D and t_I denote the detection and isolation times, respectively. The magnitude of the faults is equal to 2%.	85
Table 4.7: The summary of simulation results for different values of \mathbf{wf} by using the proposed approach in [2]. t_D and t_I denote the detection and isolation times, respectively. The magnitude of the faults is equal to 2%.	86
Table 4.8: The summary of simulation results for different values of \mathbf{wf} by using our proposed approach. t_D and t_I denote the detection and isolation times, respectively. The magnitude of the faults is equal to 5%.	86
Table 4.9: The summary of simulation results for different values of \mathbf{wf} by using the proposed approach in [2]. t_D and t_I denote the detection and isolation times, respectively. The magnitude of the faults is equal to 5%.	87
Table 4.10 The summary of simulation results for different values of \mathbf{wf} by using our	

proposed approach. t_D and t_I denote the detection and isolation times, respectively. The magnitude of the faults is equal to 8%.	87
Table 4.11: The summary of simulation results for different values of \mathbf{wf} by using the proposed approach in [2]. t_D and t_I denote the detection and isolation times, respectively. The magnitude of the faults is equal to 8%.	88
Table 4.12: The summary of simulation results for different values of \mathbf{wf} by using our proposed approach. t_D and t_I denote the detection and isolation times, respectively. The magnitude of the faults is equal to 10%.	88
Table 4.13: The summary of simulation results for different values of \mathbf{wf} by using the proposed approach in [2]. t_D and t_I denote the detection and isolation times, respectively. The magnitude of the faults is equal to 10%.	89
Table 4.14: The summary of simulation results for different severity of faults such that these magnitudes are not match with the filters.....	93
Table 5.1: The selected Level 2 bank after isolating the fault $F_{et} = 0.02$. Note that all models include this fault.....	97
Table 5.2: The Level 1 bank used for multiple fault diagnosis.	98
Table 5.3: The Level 2 banks that are used for multiple fault diagnosis.....	98
Table 5.4: The detection and isolation time of scenarios I-V. \mathbf{TD} and \mathbf{TI} denote the detection and isolation time, respectively. In all the scenarios, first fault occurs at $t=8\text{sec}$ and second one occurs at $t=20\text{sec}$	103
Table 5.5: The Observability test results by using different sets of outputs and different values of W_f . The symbols \surd and \times designate the observability and unobservability, respectively.....	105
Table 5.6The summary of simulation results for different set of measurements by using $\mathbf{Wf} = \mathbf{0.8}$. t_D and t_I denote the detection and isolation times, respectively.....	112

NOMENCLATURE

Subscripts

<i>amb</i>	Ambient
<i>C</i>	Compressor
<i>CC</i>	Combustion Chamber
<i>d</i>	Intake
<i>W_f</i>	Fuel flow
<i>M</i>	Mixer
<i>mech</i>	Mechanical
<i>n</i>	Nozzle
<i>T</i>	Turbine

Variables

β	Bypass ratio
\dot{m}	Mass flow rate $\frac{kg}{s}$
η	Efficiency
γ	Heat capacity ratio
π	Pressure ratio
J	Rotor moment of inertia, $kg \cdot m^2$
c_p	Specific heat and constant pressure, $\frac{J}{kgK}$
c_v	Specific heat at constant volume, $\frac{J}{kgK}$
N	Fan speed, <i>rpm</i>
P	Pressure, <i>kPa</i> (kilo Pascal)
P_0	Pressure at sea level at standard day
R	Gas constant, $\frac{J}{kgK}$
T	Temperature, <i>K</i>
T_0	Temperature at sea level at standard day
V	Volume, m^3
W_c	Power consumed by compressor, <i>W</i> (watt)
W_T	Power generated by turbine, <i>W</i>

Chapter 1: INTRODUCTION

1.1. INTRODUCTION

There is a steady demand for man-made systems to be more efficient and accurate which calls for more sophisticated control algorithms. On the other hand, safety is a prominent requirement for every dynamical system [1]. The early fault detection can enable the system to be more reliable. Moreover, Fault Detection and Isolation (FDI) can play a critical role in decreasing the maintenance cost [2, 3]. Therefore, the FDI methods are inevitable part of each control system [4].

In the literature, fault diagnosis is used interchangeably to refer to the fault detection isolation and also fault detection, isolation and *identification*. The field of fault diagnosis has attracted much attention in control theory in the past few decades [5, 6]. Based on the fact that continuously increasing the complexity of dynamical systems calls for more sophisticated control algorithms, the FDI methods also have to be modified to overcome the complications. However, increasing the complexity of an FDI algorithm is not feasible in most of the applications particularly for on-line FDI in which the FDI unit must have the minimum possible computation cost to prevent any large delays in fault detection [5]. For example, if the fault detection information is supplied with delay it can result in total failure of the system, which leads to more cost and safety critical situations (a total fault in a jet engine may cause airplane crash [7]).

Faults can occur at any part of the system such as the sensors, actuators or even in the components. Generally, Fault Detection (FD) can be defined as in detecting any malfunction that has a negative effect on the performance of the investigated system

based on sensor measurements, while Fault Isolation (FI) involves determining the location of the detected fault. In other words, the isolation of a fault (which is the next step after detection) provides the necessary information to locate the fault [5]. For example, after detecting a fault in the actuators of a dynamical system the FI unit enables us to determine the faulty actuator. This information is useful for the recovery and maintenance action [8].

Traditional approach for FDI is hardware redundancy by using multiple sensors, actuators or components. In this approach, the FDI is based on the voting techniques [9]. However, hardware redundancy suffers from the couple of drawbacks, namely cost, complexity and physical limitations, which cause this approach to be impractical in many applications [8, 10, 11, 12]. For example, in an aircraft engine the fault in the efficiency of compressor cannot be resolved by hardware redundancy (using an extra compressor is not possible in this application).

Another approach for fault diagnosis can be accomplished by performing certain techniques and algorithms that are known as analytical redundancy. Based on the available knowledge of the system, analytical redundancy can be categorized into three main approaches, namely model based, data-driven based and expert systems [10, 11, 12]. In the model based approach the complete prior knowledge of the system allows one to represent the system as a mathematical model [5, 8, 6], while in the other approaches this mathematical model is not available. In the model based method, by using the mathematical model of the system and measured data the FDI objective is accomplished. In the data-driven based method [13], one first tries to fit a universal mathematical model (such as a neural network) to the available data (by performing a learning process) and then implements to FDI algorithms for this framework [9]. However, the third approach (expert systems) considers the investigated system as a set

of rules (for example, a certain number of fuzzy rules) obtained from experts [14, 15]. In this thesis we focus on the model based approach.

Each model based FDI approach consists of two main units, namely as a residual generator unit and a decision-making unit [5, 10, 11, 12]. The residuals are generated by using a set of estimators, where the discrepancy of measured signal and estimated signal (that is provided by the estimator) is defined as the residual [5, 8]. Therefore, the residual for a fault free system is close to zero and when a fault occurs the residuals diverges from zero which indicates the fault occurrence [6]. The residual evaluation (decision making) unit is in charge of detecting and isolating the faults based on the residuals. Generally, the decision-making unit applies a decoding method to the residuals to detect and isolate the faults [10, 11, 12].

1.2. MOTIVATION OF THE RESEARCH

The FDI problem of nonlinear systems is an active research area in the control theory of dynamical systems. A highly complex FDI unit results in an increasing cost of computation and time. For example, the nonlinear approaches such as nonlinear Kalman filter demands a differentiation (for constructing the Jacobinan matrices) in each time step. The idea of using approaches with lower complexity such as linear Kalman filter (with certain modifications) can overcome this problem. In this thesis, the FDI problem of the nonlinear systems is investigated by using a modified linear multiple model approach. As a case study, we apply the proposed method to a type of gas turbine namely a single spool jet engine [16] . We focus on the aircraft jet engines in the cruise mode. Nevertheless, the proposed method can be applied to the industrial gas turbines, since the dynamics of this engine is similar to the aircraft engines in the cruise mode [9, 16].

During the last two decades, the fault detection and isolation problem of gas turbines has attracted an increasing interest [3, 16 (and reference therein)]. In addition to reliability (which is critical quite for jet engines), since the maintenance of engines is a highly cost and time consuming task, the early fault detection in these systems can decrease the cost significantly [17, 18].

On one hand, in the analytical redundancy-based approaches, complexity of the FDI unit is directly influenced by the complexity of the corresponding system. For example, the FDI unit for nonlinear systems is more sophisticated than the linear ones [8]. On the other hand, complicated FDI algorithms do not necessarily result in a better and more accurate diagnosis achievement [3, 6]. Roughly speaking, sophisticated FDI algorithms consume more time to perform the corresponding computations and therefore, the delay in fault analysis is inevitable. Also, complex algorithms need more hardware requirements. Hence, one needs to simplify the FDI algorithms as much as possible. These requirements can be critical where the compactness plays a crucial role in the system (for example, in aircraft and satellites) [6].

In this thesis, a novel FDI algorithm for a single spool jet engine is developed. As we shall see, this system is a nonlinear dynamical system. However, the proposed method is based on the linearized model of the original system. This approach allows us to apply the linear FDI algorithms (for example Kalman filters) on the nonlinear original system with certain modifications. This approach results in an FDI method with lower complexity (compared with nonlinear algorithms such as unscented Kalman filters [19]) which is easy to implement. Based on the fact that the linearized model is only valid in small vicinity of the operating point¹ which is used for linearization, we

¹ By valid in small vicinity we mean that the discrepancy of the linearized system and the original one is negligible only in a small neighborhood of the operating point.

utilize a certain set of linearized systems for different operating points to capture the dynamical behavior of the original nonlinear system.

The original system of the single spool engine is a highly nonlinear system. The main reason for this nonlinearity lies on the compressor and turbine maps [16]. The compressor map describes the behavior of the compressor under different operating points and is different from one engine to another one. Therefore, in order to linearize the system one needs to utilize a computer-algebra based program. However, usually, the compressor map cannot be represented by a closed form function and is provided by manufactures as a look-up table, where linearization algorithms in MATLAB software can be performed numerically [20]. In this thesis, a new symbolic computation approach is developed to perform the linearization. By using this approach, one can add the faults to output of the certain blocks and compute a linear, symbolic model that is used to obtain different faulty models of the system for developing the multiple model FDI algorithm. Also, one only needs to linearize the system once and by substituting the corresponding value of faults obtains the different faulty models.

Moreover, for the FDI purpose, we develop a multiple model approach to detect, isolate and identify a certain set of faults in the engine. Furthermore, a hierarchical structure is developed to handle the diagnosis of the multiple fault scenarios. The robustness of the proposed method in the sensor total fault is investigated and it is shown that the approach is applicable with smaller set of measurements.

1.3. LITERATURE REVIEW

As mentioned earlier, in the model based FDI approach the mathematical model of the investigated system is necessary to develop a residual generation unit that is based on the difference between the measured and estimated variables [21]. It should be

mentioned that this knowledge includes the differential equations (and more precisely state space equations) of the dynamical system.

1.3.1. FDI for Gas Turbine

The gas turbine model is represented by a nonlinear dynamical system [2, 22]. In literature different methods for the FDI problem of gas turbine engines are provided. The survey [21] focuses on the model based FDI that are applicable for aerospace systems, and represents the key points of fault detection methods that rely on analytical redundancy. In [19], by using an extended Kalman filter the nonlinear FDI problem of a single spool jet engine is investigated. Because of complexity of the gas turbine engine model, the statistical and empirical models have also been used for the FDI [21, 23]. Neural networks (such as dynamic and autoassociative) have been utilized for the single spool jet engine FDI problem in [9]. The author in [9] uses the autoassociative neural network for noise reduction purpose and dynamic neural network to accomplish the FDI mission. The random forest method is used in [24]. The random forest method is classified as a supervised learning method for the decision-making tree [24]. The FDI problem of an aircraft engine is investigated by using fusion models in [25]. In [2] the FDI problem of a dual spool jet engine is addressed. The authors in [2] propose a linear multiple model (while the original system is nonlinear). In this thesis, we provide a linear multiple model for fault diagnosis of the single spool jet engine. This work has two main differences as compared with the approach proposed in [2]. First, here we develop a novel linearization method based on the symbolic computation. Second, we introduce a linear-based FDI algorithm for the single spool jet engines. This issue is not completely investigated in [2].

1.3.2. Multiple-Model Based FDI

One of the popular approaches for FDI purpose is the multiple model [2, 7]. In this subsection, we review the literature utilizing this scheme as an FDI approach. In the multiple model method, by using a bank of Kalman filters (linear or nonlinear), the FDI method has been performed. Particularly, this approach uses a set of Kalman filters (that each of them is designed for detecting a specific fault) such that all the filters but one have large output estimation error. According to the filter with the minimum error, one can detect and isolate the corresponding fault. This approach is also applied for nonlinear systems [26]. The author in [5] presents a survey on different model based methods in fault detection and isolation (FDI) in dynamical systems. It studies the robustness of the estimation (parameter and state) based techniques and investigates these methods for different systems. Comparing experimental results in different systems, it is pointed that the capability of the model based methods depends on the model accuracy; hence while these methods are really reasonable in some mechanical system such as aircraft, they are not very reliable in some other systems such as chemical plants. One of important aspect of the model-based FDI algorithm is the residual generation. In [5], the robustness of this unit is investigated on the number of available measurements.

The authors in [27] explore the nonlinear behavior of aircraft during the fault scenarios and create multiple linear models of the system with MATLAB and Simulink. The controllability of the system at various points in the linear analysis can show that multi linear model is useful. Also it is shown how to recreate the nonlinear system from linear models [27]. In [28], the FDI problem of nonlinear systems is investigated where the Lyapunov-based technique is used to show the stability of the filters.

As mentioned earlier, in the multiple model approach one uses a set of observers. The Kalman filter is a suitable observer for state estimation; it has low computational cost and low memory requirements. Kalman filters are very popular because they are easy to use. In fact the Kalman filter is a well-known recursive state estimator for linear systems. In practice the algorithm is often used for nonlinear systems by linearizing the system's process and measurement functions. Different Kalman filter variants linearize the functions in different ways. The quality of the estimates from different Kalman filter variants strongly depends on how these filters linearize the process and measurement functions and how they take linearization errors into account.

The nonlinear Kalman filters are generally categorized into two subclasses, as Unscented (UKF) and Extended (EKF) Kalman filters. The UKF linearize process and measurement functions by a statistical linear regression of the functions through some "sampling points" in the "uncertainty region" around the state estimate. It defines the uncertainty due to the linearization errors as the covariance matrix of the deviations between the function values of the nonlinear and the linearized function in the sampling points. The EKF on the other hand only uses the function evaluation and its Jacobian in the state estimate. Also it needs trial and error for each particular example to obtain good values for the covariance matrix, which models the linearization errors [29].

1.3.3. Artificial Intelligence Based FDI

Like other areas in the control theory, the artificial intelligence (AI) including fuzzy systems, neural networks and genetic algorithms has attracted a significant interest in the FDI problem. The authors in [30] outline some recent approaches to the generation of residual signals using methods by integrating quantitative and qualitative system knowledge, based on AI techniques. Also it gives an outline of AI methods that

are considered a powerful extension to quantitative analytical approaches for the FDI of dynamical systems.

An overview of the artificial intelligence techniques to identify the faults in HVDC (High Voltage Direct Current) transmission system is provided in [31]. By using a neural network, fault diagnosis of permanent magnet synchronous motors under dynamic and mixed eccentricity fault diagnosis is investigated in [32] with artificial neural network. In [33] a frequency pattern and competent criterion is introduced for short-circuit-fault recognition in permanent magnet synchronous motors. In this approach SVM cluster is used for fault isolation purpose. Also, the demagnetization state of permanent magnets during fault conditions in a permanent magnet synchronous motor is addressed in [34].

In [35] by using a fuzzy neural network, the authors first address the uncertainty modeling and then the fuzzy rules are used for the fault diagnosis of the gas turbine engines. Also, the dynamic neural networks is used for fault diagnosis purposes in [36]. This network is belongs to a special class of neural networks as locally recurrent globally feed-forward. In [37], the FDI problem of the fuel-cell system is investigated, and also the fault tolerant control is addressed. In particular, they derive the fuzzy rule based on the measurements obtained from different cells, and then based on which unit is faulty the corresponding controller is updated. In [38] the FDI of an aircraft jet engine is accomplished by using dynamic neural networks. First, dynamic neural network is utilized to learn the dynamics of jet engine and then this model is used for FDI purposes. The authors in [39] propose an FDI algorithm for the turbine. This method is based on fuzzy and support vector machine (SVM). First the normalized faulty symptoms are used for training the SVM. Then by combining the advantages of fuzzy theory with SVM a highly reliable FDI unit is designed. Moreover, in [40] condition

monitoring of a steam turbine by using neural networks is investigated. This approach is validated with the experimental data to detect and isolate the turbine bearings faults.

By analyzing insulation oil systems in the transforms, an artificial intelligence (AI) like neural network based FDI unit is developed in [41]. The fault detection is accomplished by using the statistical approaches in [42]. More precisely, the kurtosis and entropy of the output measurements are used to detect the fault. Then by using these two statistics as the input to a neural network, the detected fault is isolated. In [43], an artificial intelligence based approach is used for the FDI problem of a navigation system gyroscope. This method is based on the Radial Basis Networks (RBF), where in order to train the network a fuzzy-genetic algorithm is used. The FDI problem in presence of uncertainty is addressed in [44]. The authors use two RBF networks. First, one RBF is trained to approximate the unknown nonlinear dynamics of the systems, and then the second network is utilized for the FDI purpose.

In [45] the FDI problem of the rotating machinery is investigated by using time series analysis combined with artificial intelligence. Particularly, an Autoregressive (AR) model is used to detect the faults. Also, a neural network (with coefficients of the AR model as inputs and fault types as output) is applied to isolate the detected fault. In [46] by combining the discrete wavelet transform and auto-associative neural network an FDI algorithm is provided. The methodology for training neural networks in this paper is Levenberg–Marquardt (LM) algorithm. In [47] a new fault diagnosis technique is presented in which Extended State Observer (ESO) and soft computing are combined to overcome the lack of modeling knowledge.

Fault diagnosis in the computer networks has also made a great progress. In [48, 49] this problem is addressed by using three different artificial intelligent approaches.

These approaches are expert systems, Bayesian networks and neural networks. The authors in [50] develop an approach for the FDI problem of analog circuits. The hybrid system that uses artificial neural networks and fuzzy systems is designed for this purpose. In [51] a method of fault diagnosis of satellite attitude control system based on data-driven combined with artificial intelligence is proposed in order to improve the reliability of the navigation satellite during its mission.

Chapter 2: BACKGROUND

In this chapter, we will provide a review on the background required to realize the proposed approach in this thesis. First, the single spool jet engine model is described. Then it is followed by a brief introduction to the fault diagnosis methods based on the multiple model approach.

2.1. AIRCRAFT JET ENGINE MATHEMATICAL MODEL

A gas turbine engine is a complex system including upstream rotating compressor joined to a downstream turbine, and a combustion chamber between these two parts. Gas turbine is most commonly used for mobile propulsion in vehicles and portable machinery. The applications include jet aircraft, helicopters, large ships and electric generators [18]. In this section, the mathematical model of a single spool jet engine is reviewed. There are several representations of gas turbine mathematical model in the literature [16, 52, 22, 53]. By using thermodynamic and aerodynamic theories and basic laws in mechanics, one can develop a single model which includes all major components in the engine [19, 53, 52] such that the resulting nonlinear model can capture the functional relations between the engine variables, namely as pressures, temperatures and gas flow rates [53]. Particularly, rotor and volume dynamics are considered in order to obtain a nonlinear dynamics for the system [9]. In this thesis the modeling of the aircraft single spool jet engine which is available in [19] is used. The dynamics of this nonlinear model is represented in the MATLAB Simulink.

The model of the engine components such as compressor and turbine are obtained by the corresponding performance maps, which are following from Gas turbine

Simulation Program (GSP) software [54]. The complete explanation of the components and related equations corresponding to the engine dynamics are presented as follows.

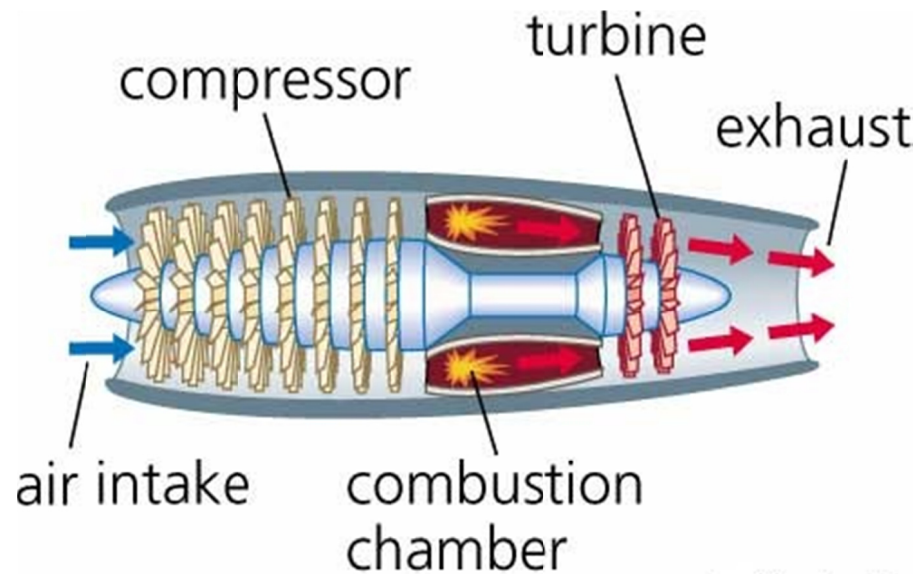


Figure 2.1: The Schematic of single spool jet engine [55].

Generally, each gas turbine has three main components namely compressor, combustion chamber and turbine (Figure 2.1). Compressor is used to increase the pressure of the inlet air. This component is followed by combustion chamber where the temperature of the fluid (high pressure air and fuel mixture) is increased by heating. It follows that combustion chamber is in charge of increasing the energy of the gas stream. The product of the combustion chamber is forced into the turbine section. Therefore, a large volume of the high velocity gas flow (that is output of the combustion chamber) is directed through a nozzle over the turbine blades. The energy is released to the turbine comes from the reduction in the temperature and pressure of the exhaust gas. A small part of this energy, which spins the turbine, powers the compressor to compress the inlet air. The rest of the energy is released as the thrust to generate the power. The schematic of this closed cycle is shown in Figure 2.2.

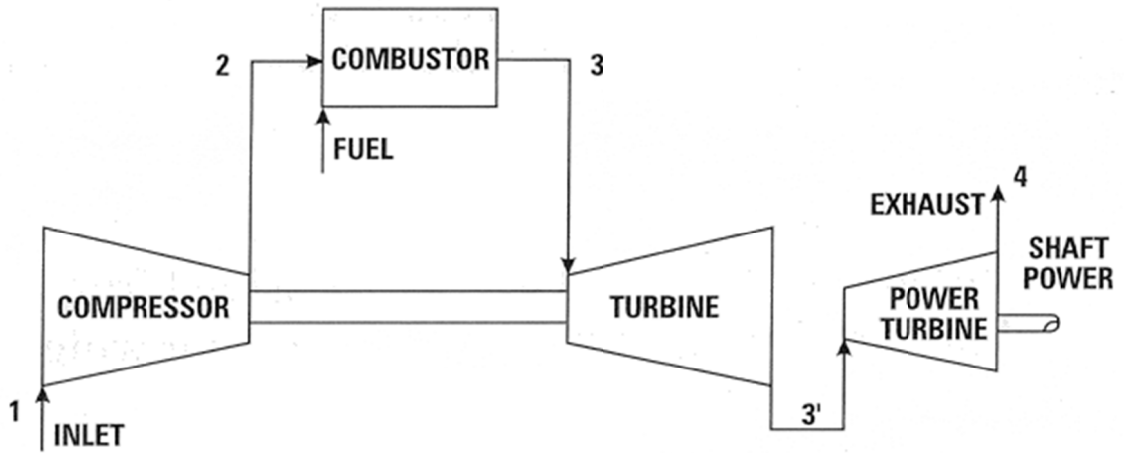


Figure 2.2: Schematic of the gas turbine working cycle [16].

Two basic equations that are inevitable to derive the mathematical model of the engine components are provided as follows:

Rotor Dynamics:

Energy balance equation between the shaft and the compressor is given by [19]

$$\frac{dE}{dt} = \eta_{\text{mech}} W_T - W_C$$

where J and N are the shaft moment of inertia and speed, respectively. In this work, we call N as the fan speed.

Volume Dynamic:

Generally, from an input-output point of view every component can be represented by the following equation

$$\dot{P} = \frac{RT}{V} (\sum \dot{m}_{in} - \sum \dot{m}_{out}) \quad (2.1)$$

where P, R, T, V and \dot{m} are pressure, gas constant, temperature, volume and mass flow rate respectively. This equation enables us to derive the compressor and turbine models. In the following we review the gas turbine components in more detail.

2.1.1. Components

As mentioned earlier, each gas turbine engine has three main components namely compressor, combustion and turbine. Nevertheless, in order to derive a comprehensive model we need to consider two additional components as intake duct and nozzle. Intake duct is used to improve the efficiency of the compressor by increasing the temperature and pressure of the inlet air. Nozzle actually produces the outlet thrust. Figure 2.3 shows the components of a single spool jet engine.

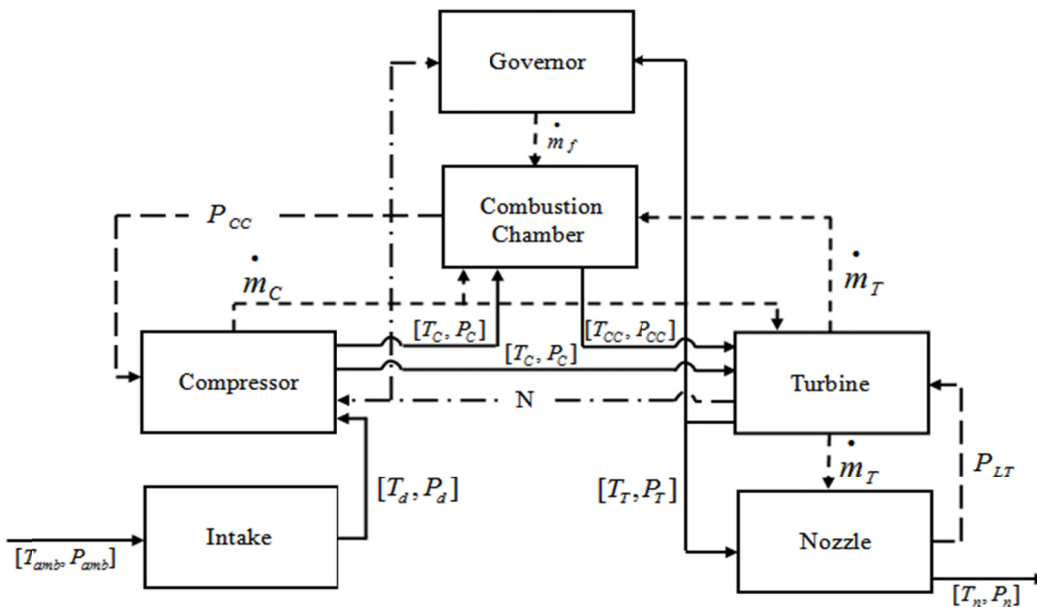


Figure 2.3: The single spool jet engine (basic model) [19].

2.1.1.1. Intake Duct

The intake duct is located before the compressor in order to recover as much of the total pressure of the free air stream as possible and to deliver this pressure to the front of the engine compressor. As a result, after intake duct, the temperature and the pressure of the inlet air are increased simultaneously [19, 53]. The input-output relation of the pressure in the intake duct is given by [19]

$$\frac{P_d}{P_{amb}} = \left[1 + \eta_d \frac{\gamma}{\gamma - 1} M^2 \right]^{\frac{\gamma}{\gamma - 1}} \quad (2.2)$$

where P_d , P_{amb} , η_d , γ and M are inlet pressure, ambient pressure, inlet efficiency, heat capacity ratio and Mach number, respectively. The inlet temperature ratio can be expressed in terms of M (M is the Mach number in the air temperature and pressure) as

$$\frac{T_d}{T_{amb}} = 1 + \frac{\gamma - 1}{2} M^2 \quad (2.3)$$

2.1.1.2. Compressor

The combustion of fuel and air at normal atmospheric pressure will not produce sufficient energy to produce useful work. The energy released by combustion is proportional to the mass of input stream and its pressure. Hence, the higher pressure input gas results in a more efficient combustion cycle. The compressor in a gas turbine engine is in charge of providing high-pressure air to the combustion chamber. The compressor model is obtained by the related performance maps, which are following from the GSP software [19, 54]. The compressor consists of three main parts [53]:

- Impeller
- Diffuser

- Manifold

Air leaves the Impeller at high speed, and flows through the diffuser, which converts high velocity, low-pressure fluid to the low-velocity, high-pressure stream. The diffuser also serves to lead airflow to the compressor manifold to increase the velocity and pressure that is satisfactory for high efficiency combustion cycle.

For a given pressure ratio (π_c) and the rotational speed ($\frac{N}{\sqrt{\theta}}$), the mass flow rate is obtained as $\dot{m}_c \frac{\sqrt{\theta}}{\delta}$ where $\theta = \frac{T_i}{T_o}$ and $\delta = \frac{P_i}{P_o}$. Also, the efficiency (η_c) is computed from the performance map by using an appropriate interpolation technique [21]. According to these parameters, one can formulate the compressor temperature and the mechanical power as:

$$T_c = T_d \left[1 + \frac{1}{\eta_c} (\pi_c^\gamma - 1) \right] \quad (2.4)$$

$$W_c = \dot{m}_c C_p (T_c - T_d) \quad (2.5)$$

where T_c and T_d are the input and output gas temperature of the compressor and W_c is the power consumed by compressor, and J and N are the shaft moment of inertia and speed, respectively. Note that T_d is the diffuser output, and the ambient conditions are set to standard condition and the Mach number is 0.7 as a typical Mach number in cruise mode [9, 56]. Standard temperature and pressure (informally abbreviated as STP) are temperature of 273.15 K (0°C, 32°F) and absolute pressure of 100 kPa (14.504 psi, 0.986 atm, 1 bar).

2.1.1.3. Combustion Chamber

In the combustion chamber, a large amount of fuel that are supplied through fuel spray nozzles, is burned with extensive volumes of air that are provided by the compressor. The releasing heat is performed such that the mixture gas is expanded and accelerated to provide a smooth and uniform stream of heated flow. This task must be accomplished with the minimum loss in pressure and with the maximum heat release within the limited space available. In other words, the combustion chamber represents both the energy accumulation and the volume dynamics between the pressure compressor and the pressure turbine at the same time [19, 22]. The following equations express the dynamics of the combustion chamber:

$$\dot{P}_{cc} = \frac{P_{cc}}{T_{cc}} \dot{T}_{cc} + \frac{\gamma R T_{cc}}{V_{cc}} (\dot{m}_c + \dot{m}_f - \dot{m}_T) \quad (2.6)$$

$$\dot{T}_{cc} = \frac{1}{C_v m_{cc}} \left[(C_p T_c \dot{m}_c + \eta_{CC} H_u \dot{m}_f - C_p T_{CC} \dot{m}_T) - C_v T_{CC} (\dot{m}_c + \dot{m}_f - \dot{m}_T) \right] \quad (2.7)$$

where T_{cc} and P_{cc} are the gas temperature and pressure in the combustion chamber respectively.

2.1.1.4. Turbine

The product of the combustion chamber is forced into the turbine section, where the high velocity and volume of the gas flow is directed through a nozzle over the turbine blades. This flow spins the turbine which provides the necessary power for the compressor. As compressor section, the behavior of the turbine is represented by performance maps which vary from one engine to another. Again, for a given pressure

ratio (π_T) and a specific fan speed ($\frac{N}{\sqrt{\theta}}$), the mass flow rate is obtained by ($\dot{m}_T \frac{\sqrt{\theta}}{\delta}$).

where $\theta = \frac{T_i}{T_o}$ and $\delta = \frac{P_i}{P_o}$.

Also, the turbine efficiency (η_T) is computed from the performance map. In this thesis we use the performance maps provided by the GSP software. According to these parameters one can obtain the turbine temperature drop T_T and the mechanical power W_T as:

$$T_T = T_{CC} \left[1 - \eta_T \left(1 - \pi_T^{\frac{\gamma-1}{\gamma}} \right) \right] \quad (2.8)$$

$$W_T = \dot{m}_T C_p (T_{CC} - T_T) \quad (2.9)$$

2.1.1.5. Nozzle

The nozzle is the exhaust duct of the jet engine. This is the final component of a jet engine which actually produces the thrust [22, 19]. The energy depleted airflow that passed the turbine, in addition to the colder air that bypassed the engine core, produces a force when exiting the nozzle that acts to propel the engine, and therefore the airplane, forward (or for the electrical generator this power is used to spin the shaft of the generator). The combination of the hot air and cold air are expelled to produce an exhaust, which causes a forward thrust. The relation between the input and output temperature of the nozzle T_{n_i} and T_{n_o} , respectively, is represented by the following equation:

$$T_{n_i} - T_{n_o} = \eta_n - T_{n_o} \left[1 - \left(\frac{P_{amb}}{P_{n_i}} \right)^{\frac{\gamma-1}{\delta}} \right] \quad (2.10)$$

In the next subsection, we summarize the equations and provide the mathematical model for the gas turbine engine system.

2.1.2. Complete Healthy Model

As in [3, 9], we assume that $P_{n_i} = P_T$ and $T_{n_i} = T_t$. Also, we assume that $T_{C_i} = T_d$ and $T_{T_i} = T_{CC}$ where T_{C_i} and T_{T_i} are the temperature of input flows to the compressor and turbine, respectively. Therefore, based on the preceding subsections and the fact that fan speeds of turbine section and compressor are identical, one can write

$$\begin{aligned} \dot{T}_{cc} &= \frac{1}{C_v m_{cc}} \left[(C_p T_C \dot{m}_c + \eta_{CC} H_u \dot{m}_f - C_p T_{CC} \dot{m}_t) - C_v T_{CC} (\dot{m}_c + \dot{m}_f - \dot{m}_t) \right] \\ \dot{N} &= \frac{\eta_{mach} \dot{m}_t C_p (T_{cc} - T_t) - \dot{m}_c C_p (T_c - T_d)}{JN \left(\frac{\pi}{30} \right)^2} \end{aligned} \quad (2.11)$$

$$\begin{aligned} \dot{P}_t &= \frac{RT_M}{V_M} \left(\dot{m}_t + \frac{\beta}{1+\beta} \dot{m}_c - \dot{m}_n \right) \\ \dot{P}_{cc} &= \frac{P_{cc}}{T_{cc}} \dot{T}_{cc} + \frac{\gamma RT_{cc}}{V_{cc}} (\dot{m}_c + \dot{m}_f - \dot{m}_t) \end{aligned}$$

where $T_M = \frac{\dot{m}_t T_t + \beta \dot{m}_c T_C}{\dot{m}_t + \beta \dot{m}_c}$ and T_C and T_t are given by

$$\begin{aligned} T_C &= T_d \left[1 + \frac{1}{\eta_C} (\pi_C^{\frac{\gamma-1}{\gamma}} - 1) \right] \\ T_t &= T_{CC} \left[1 - \eta_T (1 - \pi_T^{\frac{\gamma-1}{\gamma}}) \right] \end{aligned} \quad (2.12)$$

Note that we assume $P_t = P_{noz}$. It follows that the equation (2.11) is the state equation of the system. The output equation is given by [19]

$$y = [N, T_C, T_t, P_C, P_t]^T \quad (2.13)$$

In Section 5.1.1, we investigate the effects of different sets of outputs on the FDI performance.

2.1.3. Faulty Model

In this section, we provide the faulty model of a single spool gas turbine engine. First, let us to introduce the potential sources of faults in the investigated nonlinear system.

2.1.3.1. Potential Faults

In this section, we define the faults that are considered in this work. As mentioned in the previous chapter, fault is summarized as a malfunctioning in one of the system components. As in other dynamical systems, all parts of a gas turbine engine are subject to faults. Generally, there are three types of faults, namely component fault, actuator fault and sensor fault. Investigation and finding the solution of component and actuator faults are more critical than sensor faults in the gas turbine because for preventing a sensor fault one can also use hardware redundancy but for the component and the actuator faults this method is not practical and monitoring the model plays an important role.

Also, the rotating parts of a gas turbine have high potential to be subjected to the faults than other parts. For example, a very small crack in the turbine or compressor blades is propagated easily because of the rotor speed [16]. Therefore, in this thesis, we

consider five different types of faults, namely:

Decrease in the compressor flow capacity: F_{mc}

Decrease in the compressor efficiency: F_{ec}

Decrease in the turbine flow capacity: F_{mt}

Decrease in the turbine efficiency: F_{et}

Decrease in the effectiveness of the fuel actuator: F_{wf}

where corresponding to the fault free (or healthy) system, one can write $F_{mc} = F_{ec} = F_{mt} = F_{et} = F_{wf} = 1$. For the faulty system we set $0 < F_{mc} \leq 1$, $0 < F_{ec} \leq 1$, $0 < F_{mt} \leq 1$, $0 < F_{et} \leq 1$ and $0 < F_{wf} \leq 1$. For example, $F_{ec} < 1$ indicates that we have a fault in the compressor that results in decrease in the compressor efficiency. Note that the sever faults are represented by smaller values of $F_{mc}, F_{ec}, F_{mt}, F_{et}, F_{wf}$. For instance, the $F_{ec} = 0.2$ denotes a fault in the compressor efficiency with a magnitude of 80%, where as $F_{ec} = 0.8$ denotes the fault with a magnitude of 20%.

2.1.3.2. State Space Equations

From equations (2.11) and (2.12), it follows that the state space equation of a single spool jet engine subjected to faults (as introduced above) is given by

$$\begin{aligned}\dot{T}_{cc} &= \frac{1}{C_v m_{cc}} [(C_p T_C F_{mc} \dot{m}_c + \eta_{CC} H_u F_{wf} \dot{m}_f - C_p T_{CC} F_{mt} \dot{m}_t) \\ &\quad - C_v T_{CC} (F_{mc} \dot{m}_c + F_{wf} \dot{m}_f - F_{mt} \dot{m}_t)] \\ \dot{N} &= \frac{\eta_{mach} F_{mt} \dot{m}_t C_p (T_{cc} - T_t) - F_{mc} \dot{m}_c C_p (T_c - T_d)}{JN \left(\frac{\pi}{30} \right)^2}\end{aligned}\tag{2.14}$$

$$\begin{aligned}\dot{P}_t &= \frac{RT_M}{V_M} \left(F_{mt} \dot{m}_t + \frac{\beta}{1+\beta} F_{mc} \dot{m}_c - \dot{m}_n \right) \\ \dot{P}_{cc} &= \frac{P_{cc}}{T_{cc}} \dot{T}_{cc} + \frac{\gamma R T_{cc}}{V_{cc}} (F_{mc} \dot{m}_c + F_{wf} \dot{m}_f - F_{mt} \dot{m}_t)\end{aligned}$$

Note that $T_M = \frac{\dot{m}_t T_t + \beta \dot{m}_c T_c}{\dot{m}_t + \beta \dot{m}_c}$ and T_C and T_t are given by

$$T_C = T_d \left[1 + \frac{1}{F_{ec} \eta_C} (\pi_C^{\frac{\gamma-1}{\gamma}} - 1) \right]\tag{2.15}$$

$$T_t = T_{CC} \left[1 - F_{et} \eta_T (1 - \pi_T^{\frac{\gamma-1}{\gamma}}) \right]$$

and the output equation is given by (2.13).

Remark: Although the outputs T_C and T_t are subject to faults in the compressor and turbine efficiencies, respectively, these two faults are considered as sensor faults. The reason lies on the fact that in the sensor faults the measurements and actual outputs of the system have a discrepancy while here we assume that the measurement of all the outputs are accurate. Moreover, the sensor fault does not have any effect on the dynamics of the investigate system. However, by referring to equations (2.14) and (2.15), it follows that the faults in the compressor and turbine efficiencies affect the dynamics of the engine directly.

2.2. MULTIPLE MODEL APPROACH

The goal of a fault detection and isolation system is to improve the reliability, availability and safety of a system. As mentioned earlier the traditional method for FDI is to use the hardware redundancy, and therefore fault diagnosis is achieved by using extra instruments. By using this approach the number of sensors, components and actuators increase and it causes an increase in the cost, weight, and complexity [5]. Another approach is to use the relations among the measured variables of different system parts. This concept is known as analytical redundancy and applies the redundant analytical relations among the different measured variables. The analytical redundancy instead of using extra sensors or another equipment uses the mathematical model of the system [57].

Multiple model (MM) based approach is one of the analytical FDI approaches that has been proposed and applied to a large class of dynamical systems, such as jet engines [8, 58, 7, 59, 60, 28]. The goal of the MM approach is to provide a structure including a bank of filters for isolation and identification of faults. Typically, the filter used in the MM method is the Kalman filter. Therefore, we first review the Kalman filter briefly in the following.

2.2.1. Kalman Filter

The Kalman filter is a set of mathematical equations to produce a statistically optimal estimation of the underlying system state, recursively [58, 6] . The optimality is accomplished by minimizing the mean of the squared error [61]. The inputs of this algorithm are inputs and noisy measured outputs of the investigated linear dynamical system [61]. The filter is very powerful from several points of view: it supports estimations of past and present state. Also, practically it has been shown that the

estimation accuracy is still acceptable even when the precise nature of the modeled system is unknown and there is uncertainty in the modeling process [61]. Furthermore, because of the algorithm's recursive nature, it can run in real time using only the present measurements and the previous estimation information. In other words, no additional past information is required [62, 1, 63, 64]. Based on these benefits as well as simplicity of the implementation, this filter has been extensively applied to a wide range of dynamical systems from chemical processes to flight control problems [61, 65, 66].

The Kalman filter has been extended to nonlinear systems through different schemes namely the Extended Kalman filter and Unscented Kalman filter [67]. However, in this thesis we focus on the linear Kalman filter. In the following subsection, the linear Kalman filter is reviewed in more detail.

The Kalman filter tries to estimate the state $x \in R^n$ of a discretized controlled system with input signal $u \in R^l$ that is expressed by the following linear stochastic difference equation

$$x_k = Ax_{k-1} + Bu_{k-1} + w_k \tag{2.16}$$

where A and B are the dynamic (state) and input matrices, respectively. The measurement of the system $z \in R^m$ is given by

$$z_k = Hx_k + v_k \tag{2.17}$$

The random variables w_k and v_k denote the process and measurement noise, respectively. These random variables are assumed to be independent with the Gaussian probability distributions as

$$\begin{aligned} p(w) &\sim N(0, Q) \\ p(v) &\sim N(0, R) \end{aligned} \tag{2.18}$$

In practice, the process noise covariance Q and the measurement noise covariance R matrices might change with each time step or measurement, however here we assume that they are constant.

The Kalman filter can be written as a single equation, however it is most often conceptualized as two distinct phases, namely as "Predict (Time update)" and "Update (Measurement Update)" [61]. The predict phase uses the estimate state from the previous time step to produce a primary estimation at the current time step. This estimation is also known as the priori prediction (it does not include observation information from the current time step). In the update phase, the priori prediction is combined with current observation information to refine the final state estimation for the current time step. This improved estimate is termed as the posterior estimation [61].

Typically, the two phases alternate, with the prediction advancing the state until the next scheduled observation, and the update incorporating the observation. Also, if an observation is unavailable for some reason, the update may be skipped and multiple prediction steps performed. Likewise, if multiple independent observations are available at the same time, multiple update steps may be performed (typically with different observation matrices H_k) [61]. These features optimize the computation time, which is crucial for the online estimation purposes. In the next subsection, the equations of a typical Kalman filter are provided.

2.2.1.1. Kalman Filter Equations

In this subsection, the equations of the Kalman filter are provided. As mentioned

earlier, the filter has two set of operations namely predict and update [61]. These two steps are summarized in Table 2.1 and Table 2.2 where $\hat{x}_{k|k}$ is the estimation of x_k .

Table 2.1: The time-update phase in the Kalman filter.

Predicted (<i>a priori</i>) state estimate	$\hat{x}_{k k-1} = F_k \hat{x}_{k-1 k-1} + B_k U_k$
Predicted (<i>a priori</i>) estimate covariance	$P_{k k-1} = F_k P_{k-1 k-1} F_k^T + Q_k$

Table 2.2: The measurement-update phase in the Kalamn filter.

Innovation or measurement residual	$\tilde{y}_k = z_k - H_k \hat{x}_{k k-1}$
Innovation (or residual) covariance	$S_k = H_k P_{k k-1} H_k^T + R_k$
Optimal Kalman gain	$K_k = P_{k k-1} H_k^T + R_k$
Updated (<i>a posteriori</i>) state estimate	$\hat{x}_{k k} = \hat{x}_{k k-1} + K_k \tilde{y}_k$
Updated estimate covariance	$P_{k k} = (I - K_k H_k) P_{k k-1}$

If the investigated model is accurate (there is no error in the modeling process) and the values for $\hat{x}_{0|0}$ and $P_{0|0}$ accurately reflect the distribution of the initial state values which are unknown, then the following invariants are preserv (all estimates have a mean error of zero):

$$\begin{aligned}
 E[x_k - \hat{x}_{k|k}] &= E[x_k - \hat{x}_{k|k-1}] = 0 \\
 E[\tilde{y}_k] &= 0
 \end{aligned}
 \tag{2.19}$$

where $E[\cdot]$ denotes the expected value operator.

The covariance matrices accurately reflect the covariance of estimates as follows:

$$\begin{aligned}
 P_{k|k} &= \text{cov}(x_k - \hat{x}_{k|k}) \\
 P_{k|k-1} &= \text{cov}(x_k - \hat{x}_{k|k-1}) \\
 S_k &= \text{cov}(\tilde{y}_k)
 \end{aligned} \tag{2.20}$$

2.2.2. Linear Multiple Model

The primary feature of MM approach is a bank of K Kalman filters operating in parallel. These filters are dynamical systems with a vector of measurements z_k and a vector of actuator control commands u_k as inputs and estimated output as the outputs. At every sample period, each of these K filters produces an estimate of state \hat{x}^j , and a vector of residuals r^j , for $j = 1, 2, \dots, K$. The idea is that the filter which produces the most well-behaved residuals, represent to the model that best matches the true failure status of the system [61, 59]. For more clarification, consider following linear system:

$$\begin{aligned}
 x(k+1) &= A_k x(k) + B_k u(k) + w(k) \\
 y(k) &= C x(k) + v(k)
 \end{aligned} \tag{2.21}$$

where w and v are the input and output noise with known variances Q and R , respectively. If a fault (for example a component fault) occurs at the time instant k_f then $A_{k_f} = A_f, A_{k_f-1} = A_h$. In other words, at time k_f the matrix A is changed. Therefore, the dynamics of the system is changed from healthy to a faulty one. In the MM model, a bank of observers is run in parallel such that each observer simulates a mode of the system, for example healthy or faulty system. Based on the output error of the observers (residuals), one can realize the valid observer. In another explanation, if the valid observer (the observer with the minimum output error) is the healthy one, no fault is detected in the system, otherwise based on which observer is selected then the fault is

detected, isolated and identified (the observers are constructed for different values of the fault magnitude). For more clarification assume that we have only two models, healthy and faulty, respectively as

$$\begin{cases} x_h(k+1) = A_h x_h(k) + B_h u(k) + v_k \\ y_h(k) = C x_h(k) + w_k \end{cases} \quad (2.22)$$

$$\begin{cases} x_f(k+1) = A_f x_f(k) + B_f u(k) + v_k \\ y_f(k) = C x_f(k) + w_k \end{cases}$$

where v_k and w_k are the system and output noise respectively. In the MM approach, an observer is designed for each model. Therefore, for the above equation, the observers are given by

$$\begin{cases} \hat{x}_h(k+1) = A_h \hat{x}_h(k) + B_h u(k) + L_1 y(k) \\ \hat{y}_h(k) = C \hat{x}_h(k) \end{cases} \quad (2.23)$$

$$\begin{cases} \hat{x}_f(k+1) = A_f \hat{x}_f(k) + B_f u(k) + L_2 y(k) \\ \hat{y}_f(k) = C \hat{x}_f(k) \end{cases}$$

where L_1 and L_2 are the gain of the observers. Then based on the output error of the observers the fault can be detected.

The selection of the valid observer is based on the hypothesis conditional probability that can be formulated as [3]

$$p_i(k) = \frac{f_z(y(k) | i, y(k-1)) p_i(k-1)}{\sum_{j=1}^2 f_z(y(k) | j, y(k-1)) p_j(k-1)} \quad (2.24)$$

where $f_z(y(k) | i, y(k-1))$ is the conditional probability density for current measurement for the i th observer [2].

Based on the value of p_i 's, one can obtain the valid model. For example, assume that at the time step k , the value of p_1 is close to one and consequently the value of other p_i 's are close to zero. In other words, the probability of model 1 is higher than the other models. This information shows that the model 1 is the valid model at the time step k . This approach is used in the FDI approach so that based on the highest probability one can determine the valid model. If the valid model is the faulty model the corresponding fault is detected and isolated.

2.3. CONCLUSION

In the model based FDI approaches, one needs the mathematical model of the investigated system. In this chapter, the mathematical model of a single spool jet engine has been reviewed. Generally, this model is a nonlinear dynamical system with four states, namely the combustion pressure and temperature, fan speed and turbine pressure. Also, five types of potential faults (that are loss of the turbine and compressor mass flows and efficiencies and fuel flow) are formulated and the faulty nonlinear model has been derived. Moreover, the multiple model approach which has a crucial role in the proposed FDI approach has been briefly reviewed. In particular, we reviewed Kalman filter that is followed by formulation for the probability of each model in the multiple model approach.

Chapter 3: SYMBOLIC LINEARIZATION

3.1. INTRODUCTION

In the engineering area computation usually refers to numerical manipulation which deals with floating point numbers. However, during the last two decades another area in mathematics and computer science has increasingly attracted the attention which is called computer algebra or symbolic computation [20]. In this thesis this is known as Symbolic Computation (SC). While the numerical manipulation is performed (possibly with approximation) by the set of arithmetic operations on floating point numbers, the SC method emphasizes the computations (necessarily exact) on the mathematical expression containing variables and floating point numbers [20]. Based on the strong condition of the exact computation, the SC methods cannot be developed for systems with high complexity. Another limitation of the SC methods is presence of uncertainty in the investigated system [20]. For example, in the MATLAB software the equation including approximator unit such as neural networks or lookup tables cannot be solved by using the SC toolbox [20]. As mentioned earlier in Section 2.1, the Simulink model that is used in this work includes two lookup tables. Therefore, and based on the above explanation the linearization on the system (nonlinear single spool jet engine) cannot be accomplished by using the SC toolbox. However, to obtain the linear faulty models one needs first to linearize the system symbolically where the faults are expressed as variables. In this section we propose a novel method to overcome this problem.

3.2. A NOVEL SYMBOLIC LINEARIZATION METHOD

In this thesis an approach to utilize the symbolic computation is proposed which is a cornerstone of the following FDI method explained in next chapters. Generally, the proposed method is based on this idea that if the faults can be presented by multiplication of fault variables and output of certain components of the system, then each component is linearized numerically and the fault symbolic variables are multiplied in the corresponding outputs. Before going into more details, it must be mentioned that in order to numerically linearize a Simulink model, one can use the linearize function that is embedded in MATLAB. The output of this function is four matrices (i.e. A , B , C and D) which determine the state space equation of the linearized system [20]. It is worth noting that this function also can be used for the algebraic model (that is $y = h(u)$). In this case the output of the function would be $y = Du = \frac{\partial h}{\partial u}$, and the matrices A , B and C are not defined.

In this section, we first explain the symbolic-based approach for the compressor and turbine in details. Then the results for the single spool jet engine are provided. Let us consider the compressor model that is presented in Figure 3.1.

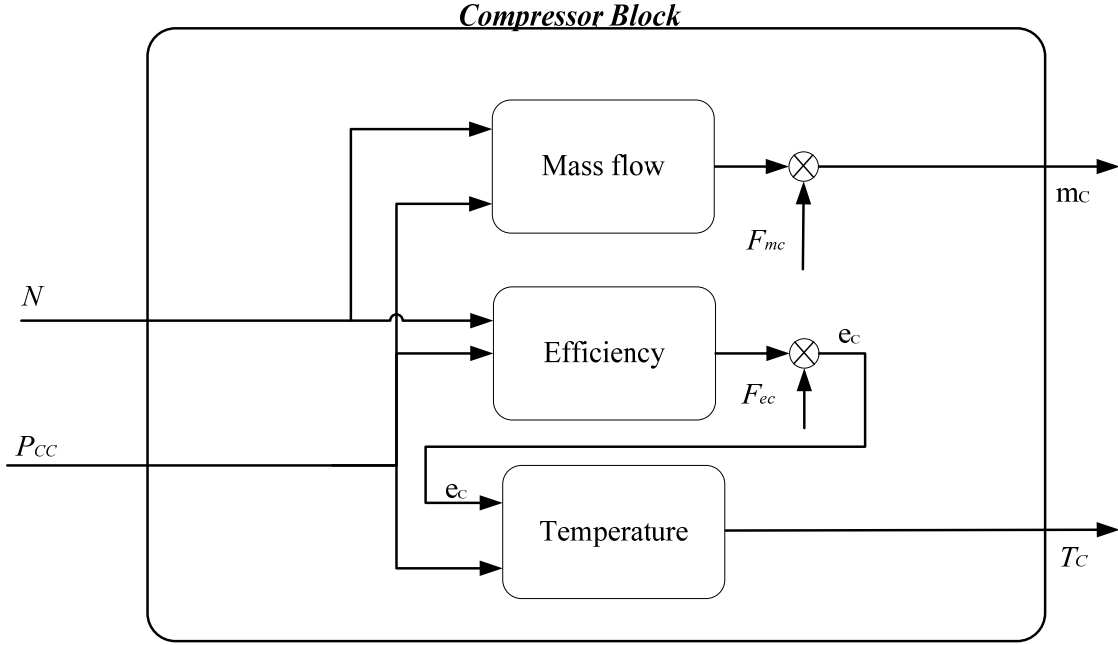


Figure 3.1: The compressor decomposition block.

The model of each sub-block in Figure 3.1 is presented by

$$\begin{aligned}
 m_C &= g_m(N, P_{CC}) \\
 e_C &= g_e(N, P_{CC}) \\
 T_C &= g_T(e_C, P_{CC})
 \end{aligned} \tag{3.1}$$

where m_C , e_C and T_C are the compressor mass flow, efficiency and temperature, respectively. Also, N and P_{CC} denote fan speed and combustion chamber pressure. Note that the sub-block models are algebraic (there is no dynamics in the compressor block).

Therefore, one can represent the compressor subsystem as

$$y_{cmp} = \begin{bmatrix} m_C \\ T_C \end{bmatrix} = g_{cmp}(u_{cmp}) \tag{3.2}$$

where $u_{cmp} = \begin{bmatrix} N \\ P_{CC} \end{bmatrix}$. Note that each sub-block is an algebraic system. For example, in the mass flow block u_{cmp} is the input and m_C is the output. The input for the temperature

sub-block is $u_{Tc} = \begin{bmatrix} e_c \\ P_{CC} \end{bmatrix}$. As mentioned above, one can linearize each block numerically and our proposed method relates to how one combines these linear systems to obtain the complete symbolic linearized model. Therefore, let us assume that the linearized models of the sub-blocks shown in Figure 3.1 are available. It follows that the linear model of the sub-blocks are given by

$$\begin{aligned} m_C &= D_{mc} u_{cmp} \\ e_C &= D_{ec} u_{cmp} \\ T_C &= D_{Tc} u_{Tc} \end{aligned} \tag{3.3}$$

where

$$\begin{aligned} D_{mc} &= [F_{mc} D_{mc}^1, F_{mc} D_{mc}^2] \\ D_{ec} &= [F_{ec} D_{ec}^1, F_{ec} D_{ec}^2] \\ D_{Tc} &= [D_{Tc}^1, D_{Tc}^2] \end{aligned} \tag{3.4}$$

Note that all sub-blocks in the compressor are algebraic and as mentioned earlier the linearized system does not have the matrices A , B and C . Therefore, the linear model of the compressor is given by

$$\begin{aligned} y_{cmp} &= D_{cmp} u_{cmp} \\ D_{cmp} &= \begin{bmatrix} 0 & 0 \\ D_{Tc}^2 & 0 \end{bmatrix} + \begin{bmatrix} 0 & 0 \\ F_{ec} D_{Tc}^1 D_{ec}^1 & F_{ec} D_{Tc}^1 D_{ec}^2 \end{bmatrix} + \begin{bmatrix} F_{mc} D_{mc}^1 & F_{mc} D_{mc}^2 \\ 0 & 0 \end{bmatrix} \\ &= \begin{bmatrix} F_{mc} D_{mc}^1 & F_{mc} D_{mc}^2 \\ D_{Tc}^2 + F_{ec} D_{Tc}^1 D_{ec}^1 & F_{ec} D_{Tc}^1 D_{ec}^2 \end{bmatrix} \end{aligned} \tag{3.5}$$

It should be mentioned that one can compute the matrices D_{mc} , D_{ec} and D_{Tc} numerically and multiply the fault symbolic variables with the corresponding block output. Hence, one can compute the symbolic linear model of the compressor by using the numerically linearized model of the sub-blocks that are shown in Figure 3.1.

Remark: In order to utilize the linearized function in the way explained above, one should decompose the compressor in sub-blocks such that the fault variables are multiplied with the output of certain sub-blocks. Also, these sub-blocks are not real components in the engine. For example, the compressor component may not be physically decomposed into them. However, we know that combination of these sub-blocks express the compressor model and capture the nonlinear behaviour of this component.

We can use the same approach to symbolically linearize the turbine component. Consider the turbine block of the engine as provided in Figure 3.2. As shown in Figure 3.2, the turbine component can be presented as four interconnected sub-blocks such that the corresponding faults are multiplied with certain outputs.

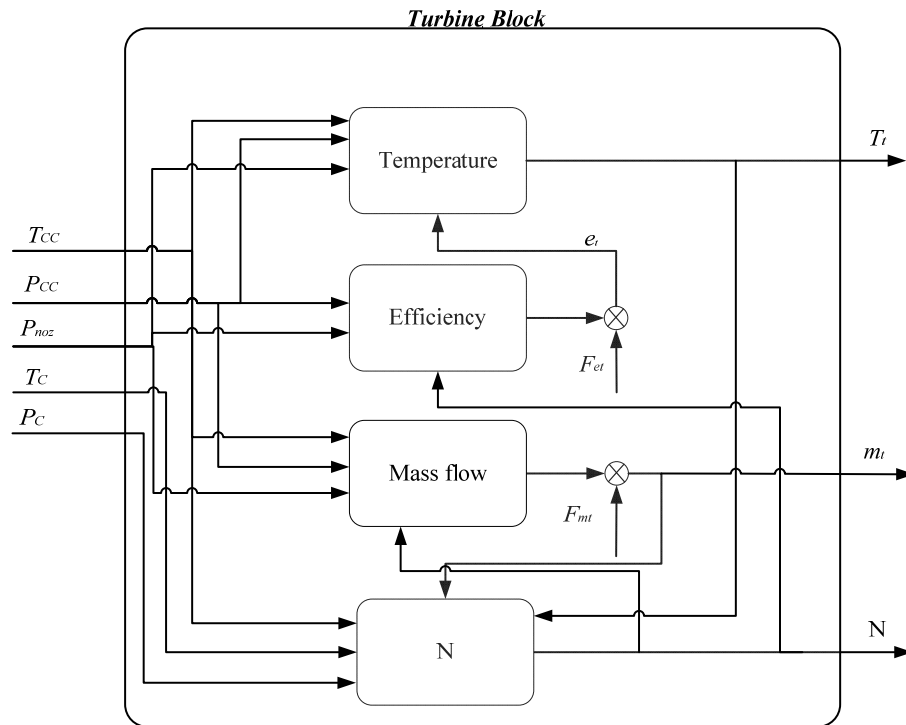


Figure 3.2: Turbine block decomposition.

Note that the sub-block N is the only one which is a dynamical system. In other words, for the turbine block N is the state, and although T_{CC} , P_{CC} and P_{noz} are the states for the single spool gas turbine, they are considered as input to the turbine block. Also, as can be observed from Figure 3.2 by decomposing the turbine component one can present the faults as the multiplication variable in certain point (efficiency and mass flow sub-blocks). Note that the symbolic variables denoting the faults (refer to Section 2.1.3.1) are added to the output of the corresponding sub-blocks. We merge these four sub-blocks by using the method explained earlier to obtain a single state space model for the turbine. Therefore, the turbine subsystem has the fault variable in the matrices A , B , C , D (the state space model for the turbine). The nonlinear model of the turbine is given by

$$\begin{aligned} \dot{N} &= g_{tr}(N, u_{tr}) \\ y_{tr} &= \begin{bmatrix} T_t \\ m_t \\ N \end{bmatrix} = h(N, u_{tr}) \end{aligned} \quad (3.6)$$

where $u_{tr} = \begin{bmatrix} T_{CC} \\ P_{CC} \\ P_{noz} \\ T_C \\ P_C \end{bmatrix}$ and N is the fan speed.

Recall that T_{CC} and P_{CC} are combustion chamber temperature and pressure, respectively. Also, P_{noz} , T_C and P_C are the nozzle pressure and compressor temperature and pressure, respectively. The nonlinear model of the sub-blocks shown in Figure 3.2 is given by

$$\begin{aligned} \dot{N} &= g_N(N, u_N) \\ y_N &= N \end{aligned} \quad (3.7)$$

$$\begin{aligned}
T_t &= g_{T_t}(u_{T_t}) \\
m_t &= g_{m_t}(u_{m_t}) \\
e_t &= g_{e_t}(u_{e_t})
\end{aligned} \tag{3.8}$$

where T_t , m_t and e_t are the turbine temperature, mass flow and efficiency, respectively.

Also,

$$u_N = \begin{bmatrix} T_{CC} \\ T_C \\ P_C \\ m_t \\ T_t \end{bmatrix}, u_{T_t} = \begin{bmatrix} T_{CC} \\ P_{CC} \\ P_{noz} \\ e_t \end{bmatrix}, u_{m_t} = \begin{bmatrix} T_{CC} \\ P_{CC} \\ P_{noz} \\ N \end{bmatrix}, u_{e_t} = \begin{bmatrix} P_{CC} \\ P_{noz} \\ N \end{bmatrix} \tag{3.9}$$

The linear model of these blocks are given by

$$\begin{aligned}
\dot{N} &= A_N N + B_N u_N \\
y_N &= N
\end{aligned} \tag{3.10}$$

$$\begin{aligned}
T_t &= D_{T_t} u_{T_t} \\
m_t &= D_{m_t} u_{m_t} \\
e_t &= D_{e_t} u_{e_t}
\end{aligned} \tag{3.11}$$

Integration of the above sub-blocks result in the following faulty linear model for the turbine that is given by

$$\begin{aligned}
\dot{N} &= A_{tr} N + B_{tr} u_{tr} \\
y_{tr} &= C_{tr} N + D_{tr} u_{tr}
\end{aligned}$$

where

$$\begin{aligned}
A_{tr} &= A_N + B_N^4 D_{mt}^4 F_{mt} + B_N^5 D_{Tt}^4 D_{et}^1 F_{et} \\
B_{tr} &= [B_N^1, 0, 0, B_N^2, B_N^3] + B_N^5 [D_{Tt}^1, D_{Tt}^2, D_{Tt}^3, 0, 0] \\
&\quad + [0, F_{et} B_N^5 D_{Tt}^5 D_{et}^1, F_{et} B_N^5 D_{Tt}^5 D_{et}^2, 0, 0] + [F_{mt} B_N^4 D_{mt}^1, F_{mt} B_N^4 D_{mt}^2, F_{mt} B_N^4 D_{mt}^3, 0, 0]
\end{aligned} \tag{3.12}$$

and

$$\begin{aligned}
C_{tr} &= \begin{bmatrix} 0 \\ 1 \\ 0 \end{bmatrix} + \begin{bmatrix} D_{Tt}^5 D_{et}^3 F_{et} \\ 0 \\ 0 \end{bmatrix} + \begin{bmatrix} 0 \\ 0 \\ D_{mt}^4 F_{mt} \end{bmatrix} \\
D_{tr} &= \begin{bmatrix} (D_{Tt}^1, D_{Tt}^2, D_{Tt}^3, 0, 0) \\ 0_{1 \times 5} \\ 0_{1 \times 5} \end{bmatrix} + \begin{bmatrix} (0, F_{et} D_{Tt}^5 D_{et}^1, F_{et} D_{Tt}^5 D_{et}^2, 0, 0) \\ 0_{1 \times 5} \\ 0_{1 \times 5} \end{bmatrix} + \begin{bmatrix} 0_{1 \times 5} \\ 0_{1 \times 5} \\ (F_{mt} D_{mt}^1, F_{mt} D_{mt}^2, F_{mt} D_{mt}^3, 0, 0) \end{bmatrix}
\end{aligned} \tag{3.13}$$

where the superscripts denote the elements of the corresponding vector (or row-vector). For example, D_{et}^1 denotes the first element of D_{et} or B_N^4 denotes the fourth element of B_N .

Based on the assumption that there is no fault in the nozzle and combustion chamber block, one can linear these blocks numerically. The linear model of the nozzle is given by

$$\begin{aligned}
\dot{P}_{noz} &= A_{noz} P_{noz} + B_{noz} u_{noz} \\
y_{noz} &= P_{noz}
\end{aligned} \tag{3.14}$$

where P_{noz} is the nozzle pressure and $u_{noz} = \begin{bmatrix} T_t \\ m_t \end{bmatrix}$. Note that A_{noz} and B_{noz} are 1×1 and 1×2 matrices, respectively. The linear model of the combustion chamber is also given by

$$\begin{bmatrix} \dot{T}_{CC} \\ \dot{P}_{CC} \end{bmatrix} = A_{CC} \begin{bmatrix} T_{CC} \\ P_{CC} \end{bmatrix} + B_{CC} \begin{bmatrix} W_f \\ P_c \\ T_c \\ m_t \end{bmatrix} \quad (3.15)$$

$$y_{CC} = \begin{bmatrix} T_{CC} \\ P_{CC} \end{bmatrix}$$

where A_{CC} and B_{CC} are 2×2 and 2×4 matrices, respectively.

In the next section, we provide the linear model of the single spool gas turbine by using the linear models of the compressor, turbine, nozzle and combustion chamber.

3.3. COMPLETE SYMBOLIC LINEAR MODEL

In this section, we summarize the symbolic linearize model of the single spool gas turbine. As mentioned earlier, we need to decompose the component such that the fault variables are multiplied to the corresponding outputs. Figure 3.3 shows the decomposition of the single spool gas turbine.

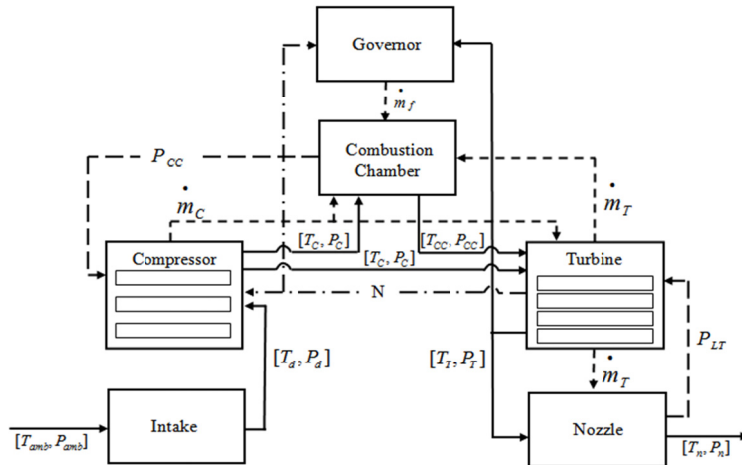


Figure 3.3: The single spool gas turbine in which compressor and turbine decomposed in the sub-blocks (also see Figure 3.1 and Figure 3.2).

Based on the symbolic model of each component (compressor and turbine), one can find the symbolic linear model of the single spool gas turbine as follows. The linear model of the system is given by

$$\begin{aligned} \dot{x} &= Ax + Bu \\ y &= Cx \end{aligned} \quad (3.16)$$

where $x = \begin{bmatrix} T_{CC} \\ P_{CC} \\ N \\ P_{noz} \end{bmatrix}$ and $u = wf$ and y is defined in equation (2.13).

The matrix A is given by

$$\begin{aligned} A_1 &= [A_{CC}, 0_{2 \times 2}] + \begin{bmatrix} B_{CC}^{1,2} & B_{CC}^{1,3} \\ B_{CC}^{2,2} & B_{CC}^{2,3} \end{bmatrix} \begin{bmatrix} 0 & D_C^{1,1} & D_C^{1,2} & 0 \\ 0 & D_C^{2,1} & D_C^{2,2} & 0 \end{bmatrix} + \begin{bmatrix} B_{CC}^{1,4} \\ B_{CC}^{2,4} \end{bmatrix} [C_{tr_n}^{3,1}, C_{tr_n}^{3,2}, C_{tr_n}^{3,3}, C_{tr_n}^{3,4}] \\ A_2 &= [B_{tr}^{1,1}, B_{tr}^{1,2}, A_{tr}, B_{tr}^{1,3}] + [B_{tr}^{1,4}, B_{tr}^{1,5}] \begin{bmatrix} 0 & 0 \\ 0 & D_{cmp}, 0 \end{bmatrix} \\ A_3 &= [0_{1 \times 3}, A_{noz}] + B_{noz} \begin{bmatrix} C_{tr_n}^{2,1} & C_{tr_n}^{2,2} & C_{tr_n}^{2,3} & C_{tr_n}^{2,4} \\ C_{tr_n}^{1,1} & C_{tr_n}^{1,2} & C_{tr_n}^{1,3} & C_{tr_n}^{1,4} \end{bmatrix} \\ A &= \begin{bmatrix} A_1 \\ A_2 \\ A_3 \end{bmatrix} \end{aligned} \quad (3.17)$$

where

$$C_{tr_n} = \begin{bmatrix} D_{tr}^{1,1} & D_{tr}^{1,2} & D_{tr}^{1,3} \\ D_{tr}^{2,1} & D_{tr}^{2,2} & D_{tr}^{2,3} \\ D_{tr}^{3,1} & D_{tr}^{3,2} & D_{tr}^{3,3} \end{bmatrix}, C_{tr} = \begin{bmatrix} D_{tr}^{1,2} & D_{tr}^{1,3} \\ D_{tr}^{2,2} & D_{tr}^{2,3} \\ D_{tr}^{3,2} & D_{tr}^{3,3} \end{bmatrix} \begin{bmatrix} 0 & 0 \\ 0 & D_{cmp}, 0 \end{bmatrix}$$

The input matrix is given by

$$B = \begin{bmatrix} F_{wf} B_{CC}^{1,1} \\ F_{wf} B_{CC}^{2,1} \\ 0 \\ 0 \end{bmatrix} \quad (3.18)$$

and finally the output matrix is provided by

$$C = \begin{bmatrix} C_1 \\ C_2 \\ C_3 \\ C_4 \\ C_5 \end{bmatrix} \quad (3.19)$$

where

$$\begin{aligned} C_1 &= [D_{tr}^{1,1}, D_{tr}^{1,2}, C_{tr}^{1,1}, D_{tr}^{1,3}] + [D_{tr}^{1,4}, D_{tr}^{1,5}] \begin{bmatrix} 0 & D_{cmp} & 0 \\ 0 & D_{cmp} & 0 \end{bmatrix} \\ C_2 &= [0, D_{cmp}^{2,1}, D_{cmp}^{2,2}, 0] \\ C_3 &= [D_{tr}^{3,1}, D_{tr}^{3,2}, C_{tr}^{3,1}, D_{tr}^{3,3}] + [D_{tr}^{3,4}, D_{tr}^{3,5}] \begin{bmatrix} 0 & D_{cmp} & 0 \\ 0 & D_{cmp} & 0 \end{bmatrix} \\ C_4 &= [C_{CC}, 0_{2 \times 2}] \\ C_5 &= [0_{1 \times 3}, 1] \end{aligned} \quad (3.20)$$

Note that each element of the linear system matrices is a symbolic polynomial of the faults values. Also, based on the fact that a single spool engine is a strictly proper system [54, 16], the matrix D is always equal to the zero matrix. In order to obtain a faulty system with certain fault magnitude, one can substitute the corresponding value of the fault parameters ($F_{mc}, F_{ec}, F_{mt}, F_{et}, F_{wf}$) in the symbolic state space model represented by equations (3.17) to (3.20).

3.4. SIMULATION RESULTS

In this section, we simulate the linearized system that is obtained in the previous section for the fault free case. Moreover, we compare the linear and nonlinear systems to show that the linear system can capture the dynamics of the original nonlinear system. It must be mentioned that the linear system, in fact, includes a set of linear systems for different operating points. As we explain in the next chapter the different operating point of the single spool jet engine can be determined by different values of fuel flow (W_f). We use the operating point with $W_f \in \{0.3, 0.5, 0.7, 0.9\}$ (the reason for this selection is explained in the next chapter) to obtain the linearized systems. The profile of W_f for the simulations below is shown in Figure 3.4.

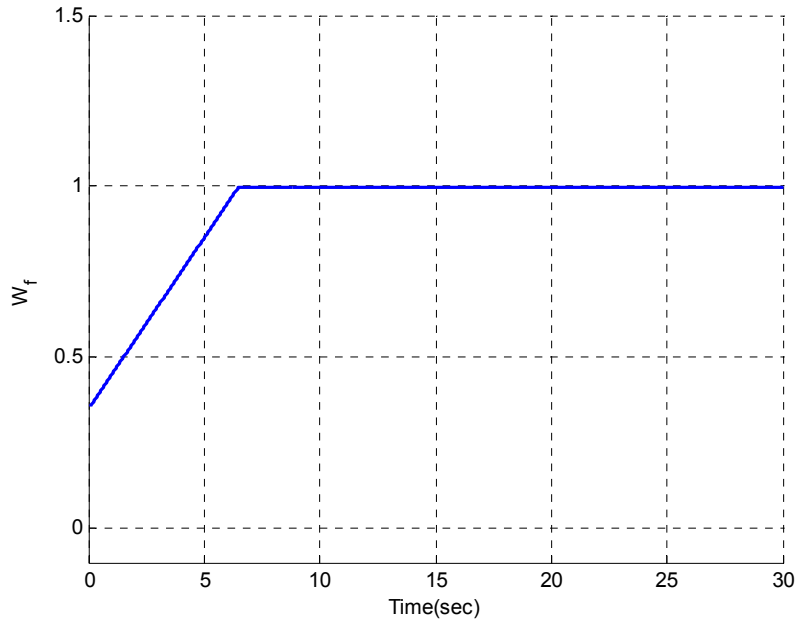


Figure 3.4: One profile of the fuel flow selected for the healthy scenario.

The outputs of the linear and nonlinear systems are summarized in Figure 3.5 to Figure 3.9.

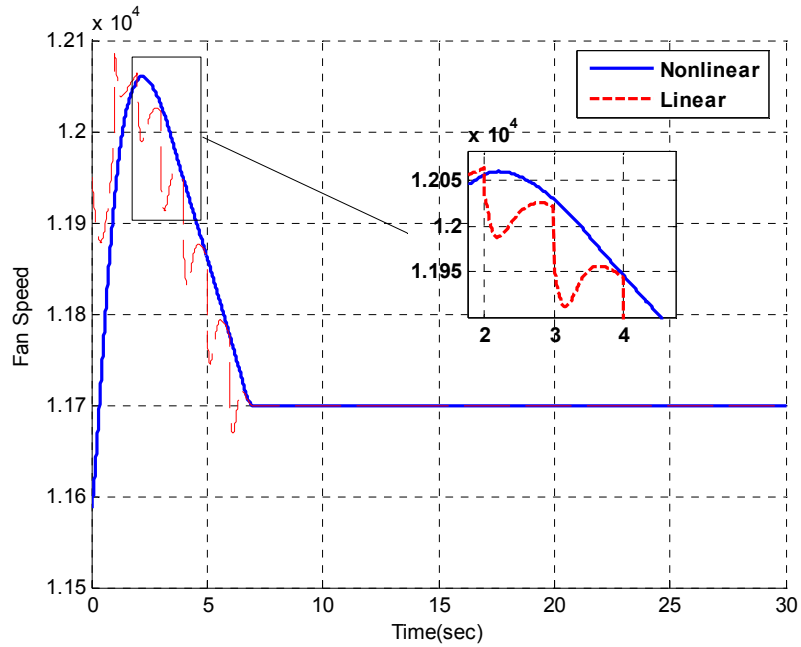


Figure 3.5: The output N of the linearized and the original system for the healthy scenario.

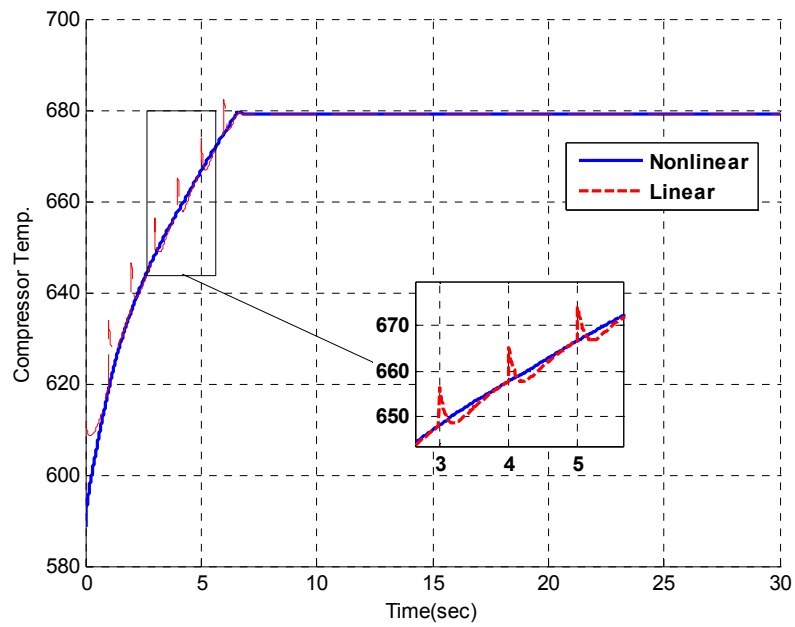


Figure 3.6: The output T_C of the linearized and the original system for the healthy scenario.

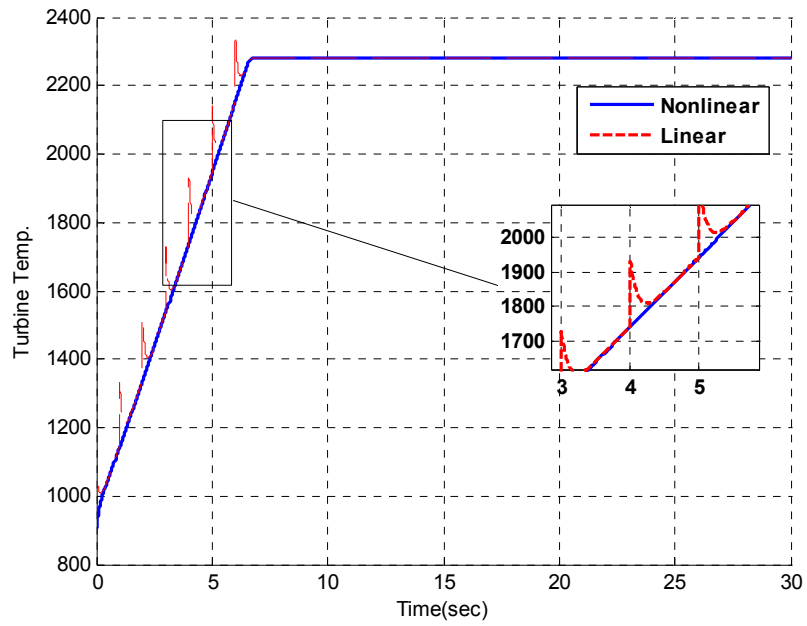


Figure 3.7: The output T_T of the linearized and the original system for the healthy scenario.

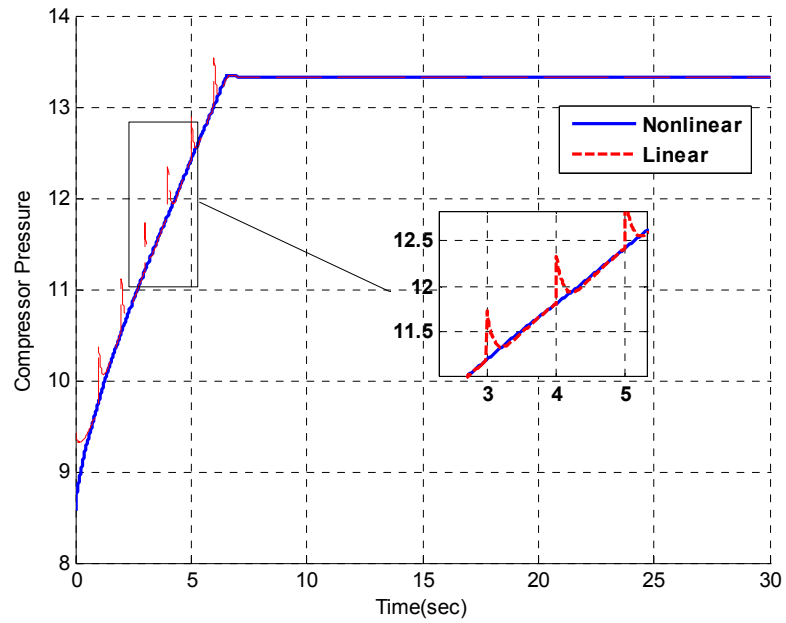


Figure 3.8: The output P_C of the linearized and the original system for the healthy scenario.

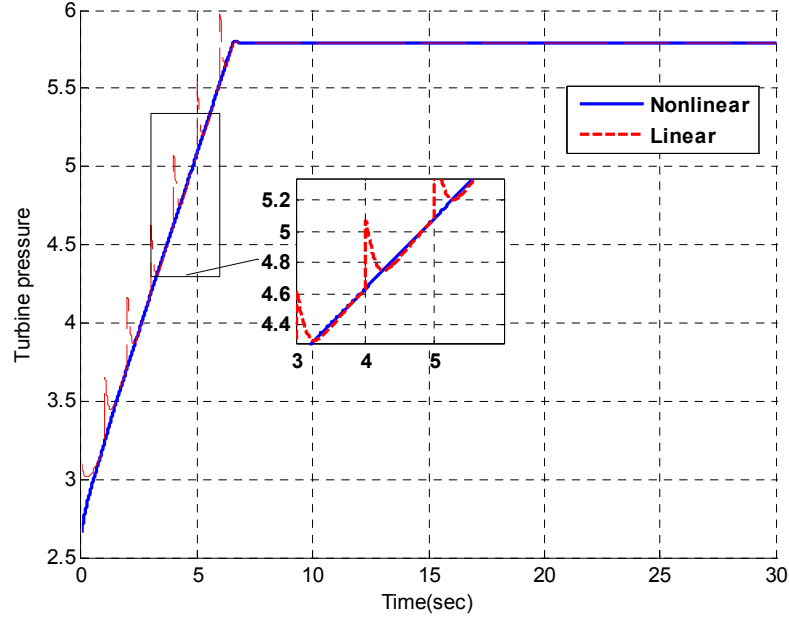


Figure 3.9: The output P_T of the linearized and the original system for the healthy scenario.

It should be mentioned that the initial conditions for the simulations are the steady state values of T_{CC} , P_{CC} , N and P_T when $W_f = 0.3$. In other words, by setting $W_f = 0.3$, we run the Simulink model and the steady state values have been selected as the initial conditions for the simulations. As follows we show the results for different sets of initial conditions. In order to quantify the ability of the linearized model to capture the nonlinear model, we define the metric as the mean value of the difference between the linear and nonlinear models, namely

$$E_m = \frac{1}{N_d} \sum_{i=1}^{N_d} |out_L^i - out_N^i| \quad (3.21)$$

in which N_d is number of all the available simulation data. Also, out_L^i and out_N^i are the i^{th} data for the investigated output of the linear and nonlinear models, respectively.

The simulation results for different values of the initial conditions are shown in Table 3.1 where the initial conditions are determined by different values of W_f . Also, for

each output we use equation (3.21) to compute the average error.

Table 3.1: The average output difference (equation (3.21)) between the nonlinear single spool and the linear model obtained by the proposed symbolic linearization method.

Initial condition (W_f)	0.1	0.2	0.3	0.4	0.5	0.6	0.7	0.8	0.9	1
Outputs										
N	33.79	23.29	14.41	8	8.8	8.11	9.67	11.69	13.49	15.05
T_C	1.43	0.84	0.5	0.25	0.32	0.33	0.37	0.43	0.48	0.53
T_T	6.67	5.83	5.32	4.7	5.45	6.21	7	7.78	8.61	9.5
P_C	0.05	0.03	0.02	0.01	0.01	0.02	0.02	0.03	0.03	0.03
P_T	0.03	0.02	0.02	0.01	0.01	0.01	0.02	0.02	0.02	0.02

By considering Figure 3.5 to Figure 3.9 and Table 3.1, it follows that the linearized model can capture the behaviour of the nonlinear system quite closely. As we shall see in the next chapter this linearized model can be utilized for the FDI purpose.

3.5. CONCLUSION

In this chapter a novel symbolic linearization method is developed for systems that cannot be linearized symbolically by using the existing symbolic computation toolboxes. By using this method, one can obtain the linearized model of a nonlinear system such that the fault variables are represented as a set of symbolic variables. This symbolic model enables us to track the effects of each fault in the linear system. Also, the different faulty models corresponding to different values of the fault can be easily obtained by substituting the value of the fault in the symbolic model. This method has been applied to the nonlinear single spool jet engine to obtain the symbolic linearized system for different operating points. The simulation results have also been provided to show the capability of the linearized model. These results have been performed for different set of initial conditions to show the accuracy of the obtained linear models.

Chapter 4: FAULT DIAGNOSIS OF GAS TURBINE

In this chapter, we provide the FDI logics that is used in this thesis for single fault scenarios. In the next chapter, we provide a hierarchical structure for multiple fault scenarios. The main difference between this approach and the approach proposed in [2] can be viewed in the decision making unit. Here, we introduce a methodology to measure the detection and isolation time. For this purpose, one needs to define a threshold. This threshold is defined on the probability values rather than on the observer errors. This threshold is obtained by Monte Carlo simulations.

4.1. MODIFIED MULTIPLE MODEL

As well-known, at a sufficiently small vicinity of each operating point, the dynamics of a nonlinear system can be captured by a linear model [2], and hence in this region the healthy and faulty models (that are used in multiple model approach) can be expressed by the corresponding linear models. Therefore, one can accomplish the FDI objective by using the linear multiple model provided that the original system operates in this vicinity.

The operating points of the jet engine can be determined by the value of the fuel flow (i.e. W_f) [2]. If the system works at different operating point one can discretize the W_f into different intervals such that in each interval a linear model captures the behavior of the original system. Then using the obtained models for different operating points one performs the FDI objective. In this approach, we modify the multiple model (MM) approach that is proposed in [3], which is a standard MM, equipped by a tool to

select the correct linear bank of observers that are based on the value of W_f for distinguishing the fault detection and isolation. This enables us to quantify the multiple model approaches which is useful for comparison purposes. In the proposed approach, the current bank of observers in the MM method is selected based on the value of W_f . Then the current operating mode of the engine (healthy or faulty) is determined based on the maximum probability of the current operating point that is selected based on the value of W_f . Finally, by defining a threshold on the model probabilities one can detect and isolate the faults.

Furthermore, we show that with a smaller set of operating points as compared to [3], the FDI objective can be accomplished. Moreover, it should be noted that in the proposed method one needs to linearize the nonlinear model once, while in the approach proposed in [2], for each fault, the nonlinear model must be linearized separately. Therefore, our proposed method has lower computational cost, although as we shall see in Section 4.2.6, the FDI approach is accomplished with the same accuracy as that obtained in [2]. Below, we define a methodology for the FDI logic.

4.1.1. FDI Logic for Single Faults

As mentioned in Chapter 1, in the multiple model approach the probability of different model enables us to determine the valid model. If the valid model is the healthy one, then no fault is detected otherwise based on which model is valid the corresponding fault is detected and isolated. However, when a fault occurs in the system, it generally takes some time so that the probability of a corresponding model reaches an acceptable level. For further clarification, consider the following Figure 4.1.

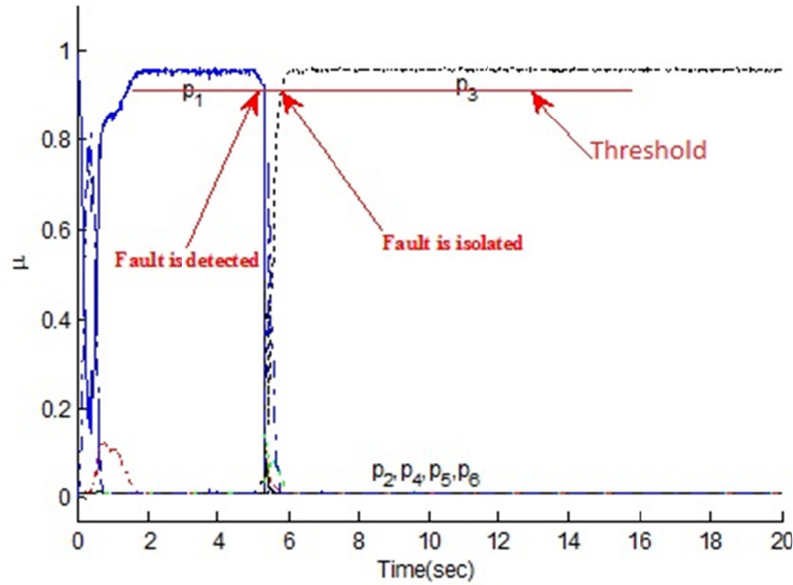


Figure 4.1: The probability of multiple model for the scenario in which a fault occurs in the compressor efficiency at $t=5\text{sec}$. It takes 1 sec for the probability of the corresponding model reaches to 0.91 (P_1 denotes the healthy mode and $P_2 - P_6$ correspond to various faulty cases).

As can be observed from Figure 4.1, the probability of the healthy mode before the fault occurrence is not exactly equal to one, and also there are some small fluctuation in the probabilities which may result in false alarm flags. To overcome this problem, we define a threshold such that the valid model is the model with a probability larger than this threshold. In other words, if any probability is lower than this threshold the corresponding model is not valid (refer to Figure 4.1). In this thesis, we assume the threshold $Thr = 0.91$. We obtain this threshold after fifty (50) runs by using flag generated Monte Carlo simulations randomly generated scenarios corresponding to different operating conditions for the healthy case such that there are no false alarms.

Moreover, it follows from Figure 4.1 that the probability of the healthy model decreases before the corresponding fault model probability reaches the threshold. Hence, by defining the threshold one can obtain the detection time (the time instant that probability of the healthy model exceeds the threshold and decreases) and the isolation

time (the time when the corresponding faulty model passes the threshold and remains above it). The isolation and detection times are shown in Figure 4.1. In the reminder of this chapter the detection and isolation times are determined by using the method that is explained above.

4.1.2. Normalization

In this section, we provide a method to decrease the false alarm flags that are caused by noisy measurements. For the noise free case, the FDI method can detect and isolate the faults. However, in the presence of noise the number of false alarms increases significantly. For example assume a fault scenario in which a fault in the compressor efficiency occurs at $t = 5$ sec with a magnitude of 0.02 ($f_{ec} = 0.98$). The simulation result for the bank obtained (by using the proposed method in Section 4.1) is shown in Figure 4.2. On the other hand, the result for noisy measurement is provided in Figure 4.3.

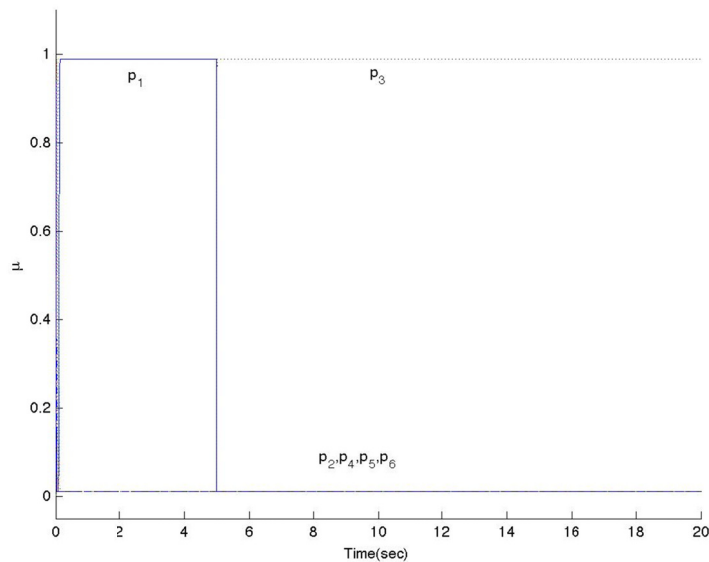


Figure 4.2: The simulation result for the fault which occurs at $t=5$ sec in compressor efficiency (noise free measurement).

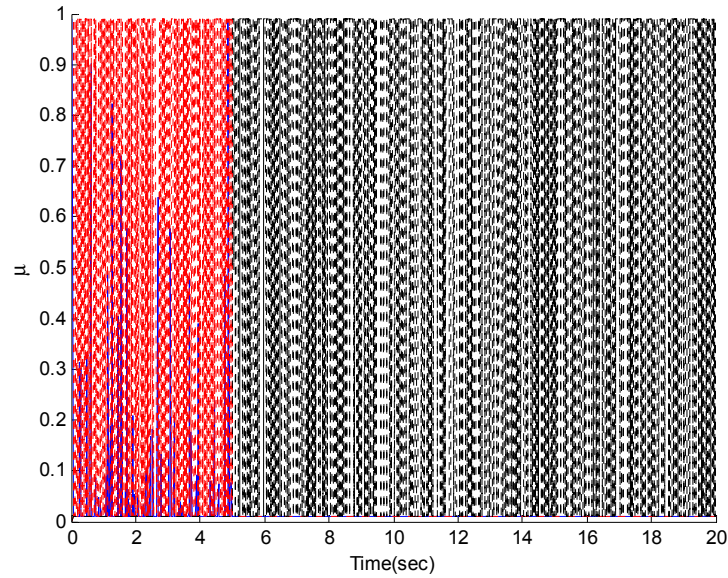


Figure 4.3: The simulation result for the fault which occurs at $t=5$ sec in compressor efficiency (noisy measurement).

In order to address this problem we normalize the output of the models by using a set of multiplicative factors. These scaling numbers are also used for the actual corresponding measurements. Towards this end the following vector is used for this purpose

$$[12000, 590, 900, 8, 3]$$

where 12000, 590, 900, 8 and 3 represent the nominal values of the outputs y_1 to y_5 , respectively in equation (2.13). The simulation results for the same scenario shown in Figure 4.3 is now provided in Figure 4.4. However, as can be seen the detection and isolation times are increased in this case (as compared to Figure 4.2).

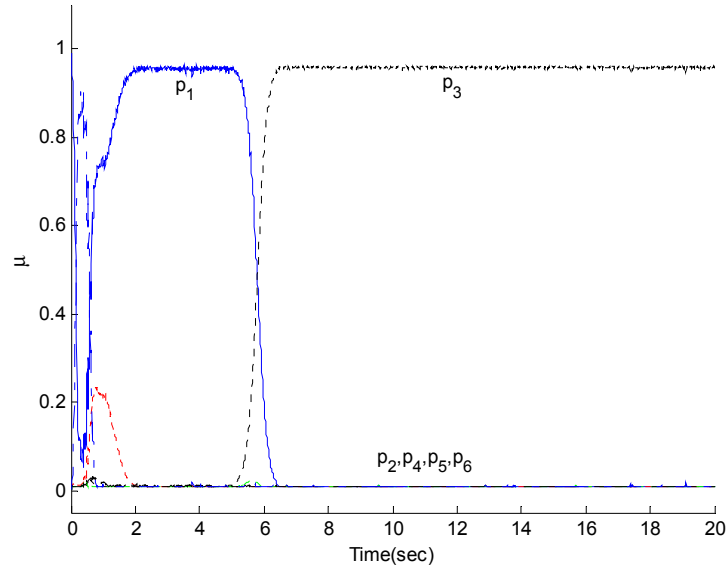


Figure 4.4: The simulation result for the fault which occurs at $t=5$ sec in compressor efficiency (modified and normalized output).

4.1.3. Determining the Operating Points

As mentioned earlier, in this thesis we use a set of bank of filters where each filter is valid for a vicinity of an operating point. With higher number of filters the results are more accurate however the computational cost will be higher too. Therefore, there is a trade-off between the number of operating points and computational cost. In this subsection, we obtain the minimum number of operating points such that all the considered faults are detectable.

To obtain the minimum interval between the operating points, we use a bank that is obtained for $W_f = 0.9$ (the typical value of the fuel flow for the cruise mode changes from 0.85 to 0.95 [2]). The proposed FDI approach is then performed for single fault scenarios for different values of W_f . Table 4.1 shows the results of the FDI for all faults where \times and \checkmark denote the false alarm flag and correct detection and isolation flag, respectively. Note that the FDI logic that was explained in the preceding subsection was

used to obtain the resolution Table 4.1.

Table 4.1: The FDI results for different incremental changes of nominal W_f and $W_f = 0.9$ in which the bank of observer is constructed. The symbol \times denotes false alarm flag.

Incremental Change from Nominal W_f	0.05	0.1	0.2	0.25	0.3
Faults					
f_{et}	√	√	√	×	×
f_{ec}	√	√	√	√	×
f_{mt}	√	√	√	×	×
f_{mc}	√	√	√	×	×
f_{wf}	√	√	√	√	×

It follows from Table 4.1 that the incremental changes of 0.05, 0.1 and 0.2 yield acceptable FDI results. According to the fact that with an interval of 0.2 we need less bank of observers we select the interval as 0.2. Therefore, we construct the banks for $W_f = \{0.3, 0.5, 0.7, 0.9\}$. Note that although the typical value of the W_f is between 0.85 and 0.95, however the banks of observers for $W_f = \{0.3, 0.5, 0.7, 0.9\}$ are used. In this way, one can tackle the FDI problem for the other values of W_f which can occur (not common) in the cruise mode.

4.2. SINGLE FAULT SIMULATION RESULTS

In this section, the simulation results for different scenarios are provided. The results are categorized into several subsections corresponding to various scenarios. In the single fault scenarios, a comprehensive set of results for different magnitudes of faults are provided. Furthermore, the simulation results by using the approach that is proposed in [2] are also reported in this section for comparative study. Finally,

summarizing tables are provided in the summary subsection of this section.

The simulations are performed on the cruise condition with four different values of $W_f = \{0.4, 0.55, 0.7, 0.85\}$. The ambient conditions are set to standard condition; that is the Mach number is 0.7 as a typical number in the cruise mode [56]. Standard temperature and pressure (informally abbreviated as STP) are temperature of 273.15 K (0°C, 32°F) and absolute pressure of 100 kPa (14.504 psi, 0.986 atm, 1 bar).

By using several linearized models, which are obtained corresponding to several operating points, we construct the bank of observers (Kalman filters). These operating points are obtained based on different values of W_f . For the simulations we choose as the nominal W_f given by $W_f = \{0.3, 0.5, 0.7, 0.9\}$, as explained in Section 4.1.3. The scenarios in this section are as follows:

Scenario I (healthy scenario): In this scenario, no fault occurs in the system.

Scenario II (single fault in the turbine efficiency): In this scenario we assume that a fault (decrease in the turbine efficiency) occurs at the time instant $t = 5$ sec.

Scenario III (single fault in the compressor efficiency): In this scenario a fault (decrease in the compressor efficiency) occurs at the time instant $t = 5$ sec.

Scenario IV (single fault in the mass flow of turbine): This scenario simulates a fault (decrease in the turbine mass flow) which occurs at the time instant $t = 5$ sec.

Scenario V (single fault in the mass flow of compressor): This scenario simulates a fault (decrease in the compressor mass flow) which occurs at the time instant $t = 5$ sec.

Scenario VI (single fault in the effectiveness of fuel flow): In this scenario a loss

of fuel flow effectiveness occurs at the time instant $t = 5$ sec.

Note that the above scenarios with certain magnitudes are provided in the following subsections. Each subsection is devoted to a specific magnitude. Also, we show the results for $W_f = 0.85$ and the results for the other values of W_f are only summarized in Section 4.2.6.

4.2.1. Faults with Magnitude 2%

In this subsection, the simulation results for the scenarios I-V are provided. The magnitude of all the faults is 2%. The faulty models that are used for this subsection are summarized in Table 4.2.

Table 4.2: The different models corresponding to the healthy and faulty modes that are used in the simulation for each operating point.

Model Mode	#1	#2	#3	#4	#5	#6
	Healthy	2% fault in F_{et}	2% fault in F_{ec}	2% fault in F_{mt}	2% fault in F_{mc}	5% fault in W_f

It is worth noting that the minimum detectable magnitude of the fault in the fuel flow effectiveness (W_f) is 5%. For this reason we only consider this level of fault severity in W_f .

4.2.1.1. Scenario I

The simulation results for the healthy scenario are shown in Figure 4.5. The probability of each model is shown by p_i where i denotes the model mode as provided in Table 4.2. Also, μ denotes the value of the probabilities which is between zero and one.

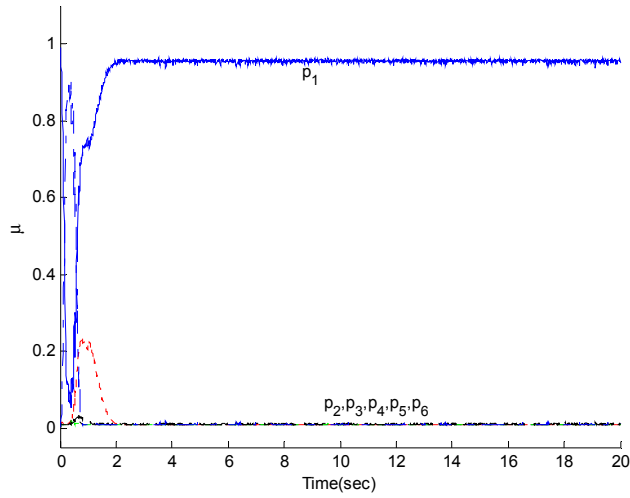


Figure 4.5: Simulation result for the healthy scenario by using the proposed method with $W_f = 0.85$. p_1 denotes the probability of the healthy mode validity (for the mode labels refer to Table 4.2).

The simulation result by using the approach proposed in [2] is provided in Figure 4.6.

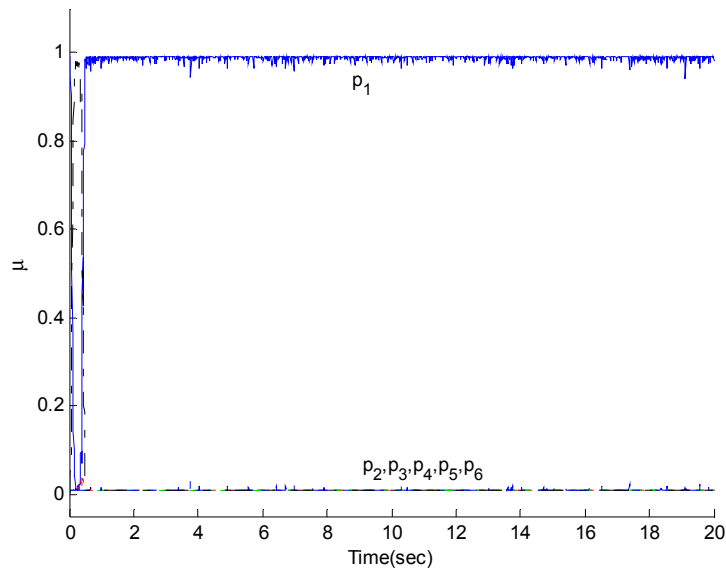


Figure 4.6: Simulation result for the healthy scenario by using the approach proposed in [2] with $W_f = 0.85$. p_1 denotes the probability of the healthy model validity (for the mode labels refer to Table 4.2) .

4.2.1.2. Scenario II

In this scenario, one fault occurs in the turbine efficiency at the time instant $t = 5$ sec. The magnitude of the fault is 0.02 ($F_{et} = 0.98$). Figure 4.7 shows the results for this scenario. Figure 4.8 shows the results that are obtained by using the approach that is proposed in [2] for comparison.

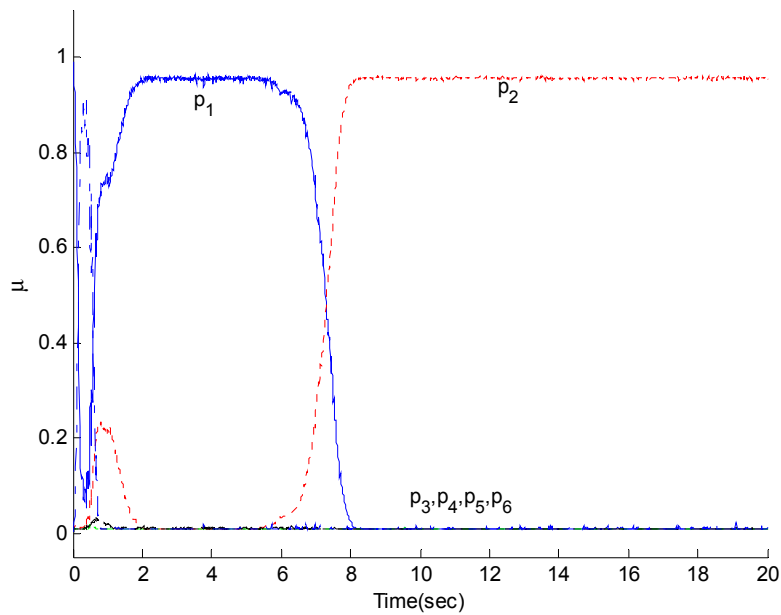


Figure 4.7: The simulation result for the scenario II by using the proposed method with $W_f = 0.85$. A fault with magnitude 0.02 ($F_{et} = 0.98$) occurs in the turbine efficiency at $t = 5$ sec (for the mode labels refer to Table 4.2).

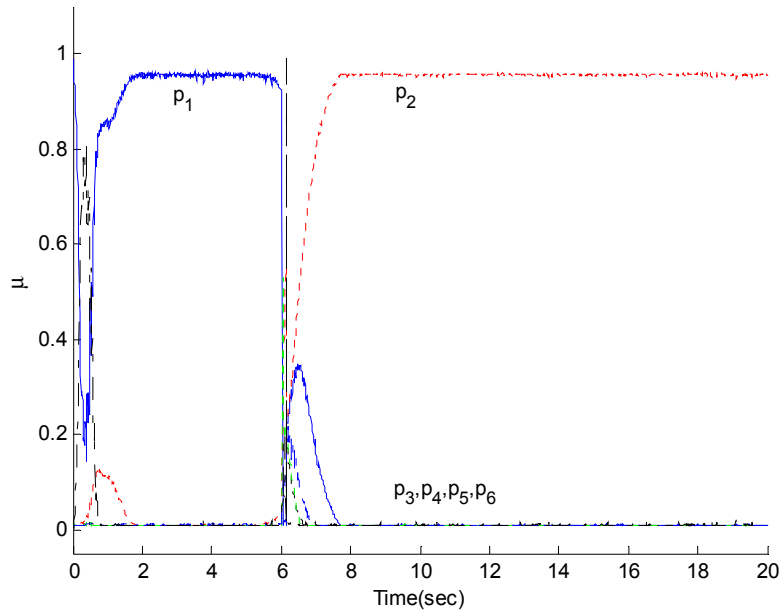


Figure 4.8: The simulation result for the scenario II by using the approach proposed in [2] with $W_f = 0.85$. A fault with magnitude 0.02 ($F_{et} = 0.98$) occurs in the turbine efficiency at $t = 5$ sec (for the mode labels refer to Table 4.2).

4.2.1.3. Scenario III

In this scenario, one fault occurs in the compressor efficiency at time instant $t = 5$ sec. The magnitude of the fault is 0.02 ($F_{ec} = 0.98$). Figure 4.9 shows the result for this scenario. Figure 4.10 shows the results that are obtained by using the approach that is proposed in [2] for comparison.

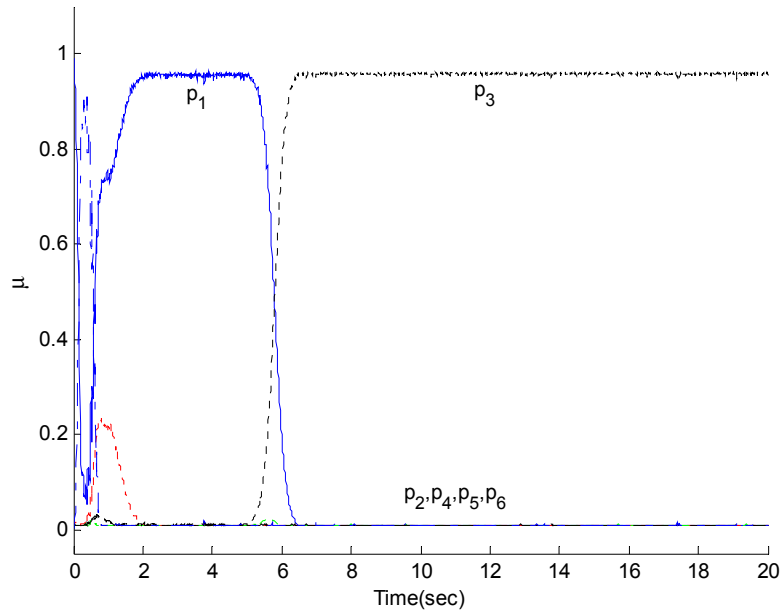


Figure 4.9: The simulation result for the scenario III by using the proposed method with $W_f = 0.85$. A fault with magnitude 0.02 ($F_{ec} = 0.98$) occurs in the compressor efficiency at $t = 5\text{sec}$ (for the mode labels refer to Table 4.2).

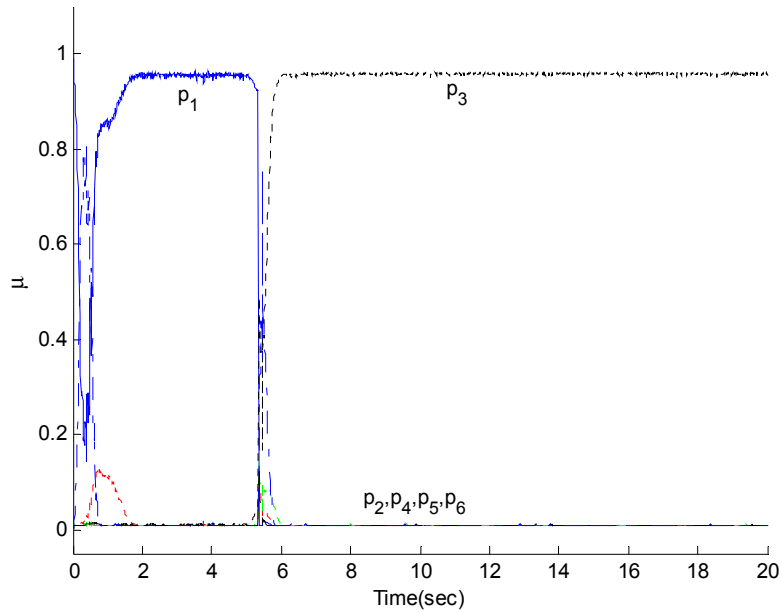


Figure 4.10: The simulation result for the scenario III by using the approach proposed in [2] with $W_f = 0.85$. A fault with magnitude 0.02 ($F_{ec} = 0.98$) occurs in the compressor efficiency at $t = 5\text{sec}$ (for the mode labels refer to Table 4.2).

4.2.1.4. Scenario IV

In this scenario, we assume that the system is subjected to a fault in the turbine mass flow at time instant $t = 5 \text{ sec}$. The magnitude of the fault is 0.02 ($F_{mt} = 0.98$). Figure 4.12 shows the results that are obtained by using the approach that is proposed in [2] for comparison.

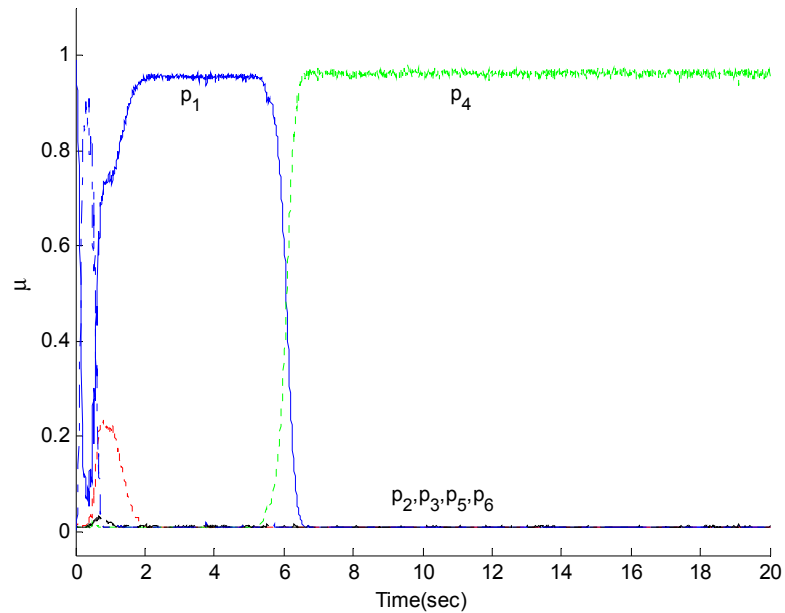


Figure 4.11: The simulation result for the scenario IV by using the proposed method with $W_f = 0.85$. A fault with magnitude 0.02 ($F_{mt} = 0.98$) occurs in the turbine mass flow at $t = 5 \text{ sec}$ (for the mode labels refer to Table 4.2).

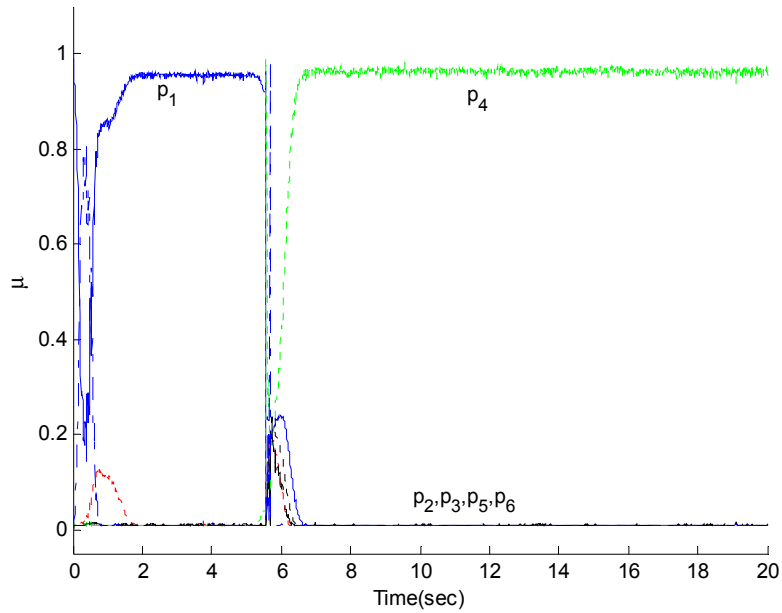


Figure 4.12: The simulation result for the scenario IV by using the approach proposed in [2] with $W_f = 0.85$. A fault with magnitude 0.02 ($F_{mt} = 0.98$) occurs in the turbine mass flow at $t = 5\text{sec}$ (for the mode labels refer to Table 4.2).

4.2.1.5. Scenario V

In this scenario a fault occurs in the compressor mass flow at $t = 5\text{sec}$. the magnitude of the fault is 0.02 ($F_{mc} = 0.98$). Figure 4.14 shows the results that are obtained by using the approach that is proposed in [2] for comparison.

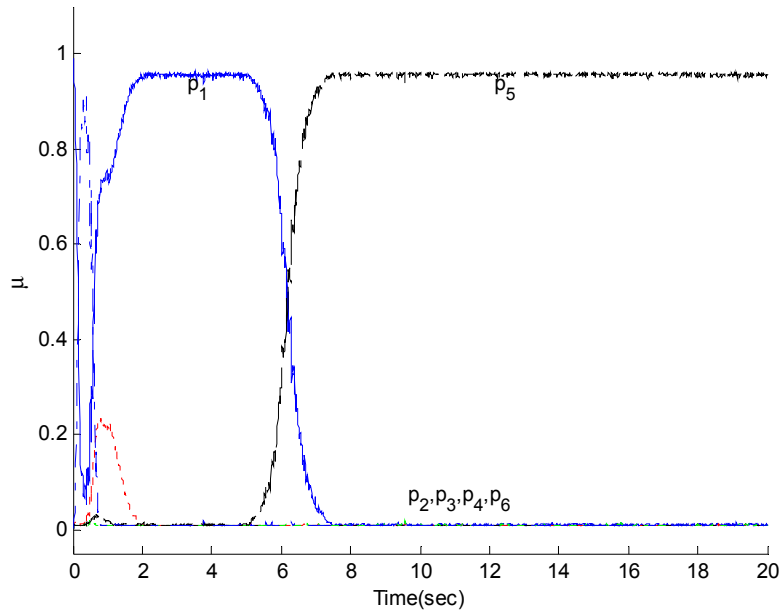


Figure 4.13: The simulation result the for scenario V by using the proposed method with $W_f = 0.85$. A fault with magnitude 0.02 ($F_{mc} = 0.98$) occurs in the compressor mass flow at $t = 5sec$ (for the mode labels refer to Table 4.2).

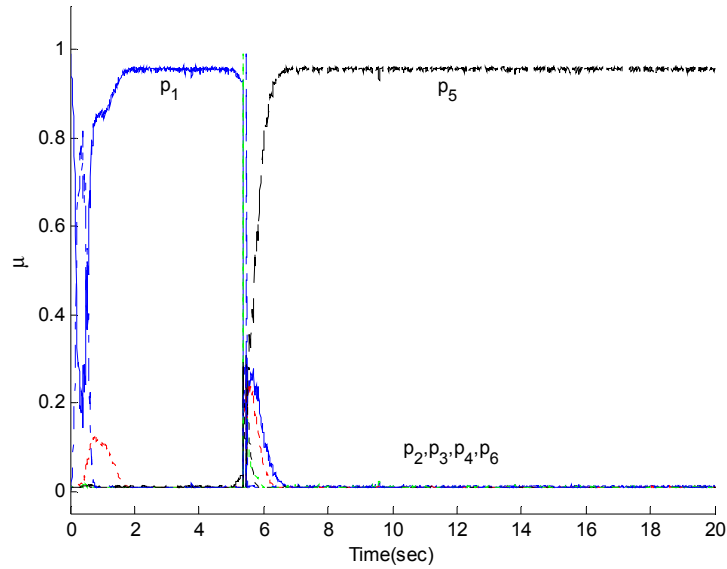


Figure 4.14: The simulation result for the scenario V by using the approach proposed in [2] with $W_f = 0.85$. A fault with magnitude 0.02 ($F_{mc} = 0.98$) occurs in the compressor mass flow at $t = 5sec$ (for the mode labels refer to Table 4.2)

4.2.2. Faults with Magnitude 5%

In this subsection, the simulation results for the scenarios I-V are presented. The magnitude of all the faults is 5%. The faulty models that are used for this subsection are summarized in Table 4.3.

Table 4.3: The different models corresponding to the healthy and faulty modes (5% magnitude) that are used in the simulation for each operating point.

Model Mode	#1	#2	#3	#4	#5	#6
	Healthy	5% fault in F_{et}	5% fault in F_{ec}	5% fault in F_{mt}	5% fault in F_{mc}	5% fault in W_f

4.2.2.1. Scenario II

In this scenario, one fault occurs in the turbine efficiency at time instant $t = 5 \text{ sec}$. The magnitude of the fault is 0.05 ($F_{et} = 0.95$). Figure 4.15 shows the result for this scenario. Figure 4.16 shows the results that are obtained by using the approach that is proposed in [2] for comparison.

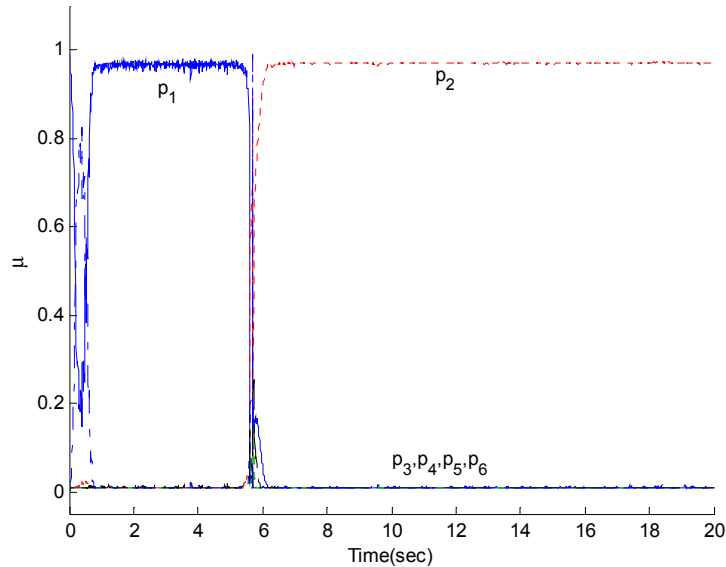


Figure 4.15: The simulation result for the scenario II by using the proposed method with $W_f = 0.85$. A fault with magnitude 0.05 ($F_{et} = 0.95$) occurs in the turbine efficiency at $t = 5 \text{ sec}$ (for the mode labels refer to Table 4.3).

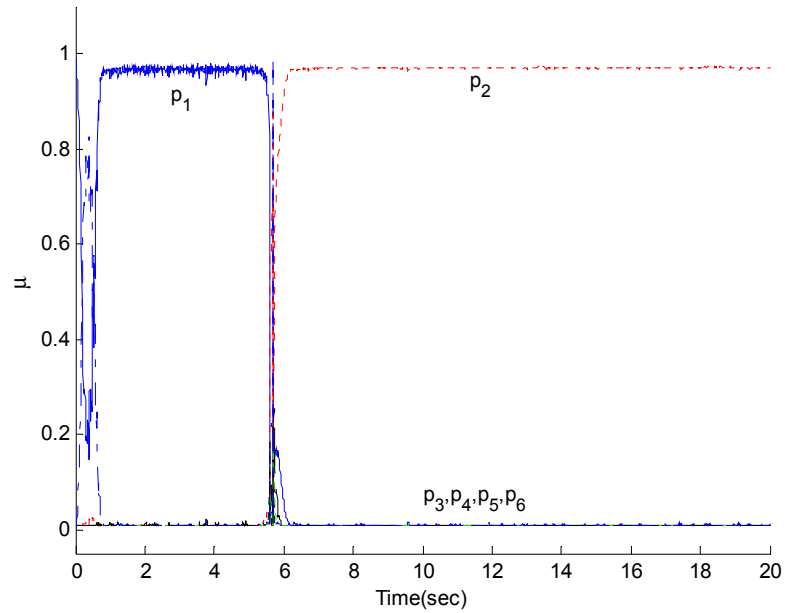


Figure 4.16: The simulation result for the scenario II by using the approach proposed in [2] with $W_f = 0.85$. A fault with magnitude 0.052 ($F_{et} = 0.95$) occurs in the turbine efficiency at $t = 5$ sec (for the mode labels refer to Table 4.3).

4.2.2.2. Scenario III

In this scenario, one fault occurs in the compressor efficiency at time instant $t = 5$ sec. The magnitude of the fault is 0.05 ($F_{ec} = 0.95$). Figure 4.17 shows the result for this scenario. Figure 4.18 shows the results that are obtained by using the approach that is proposed in [2] for comparison.

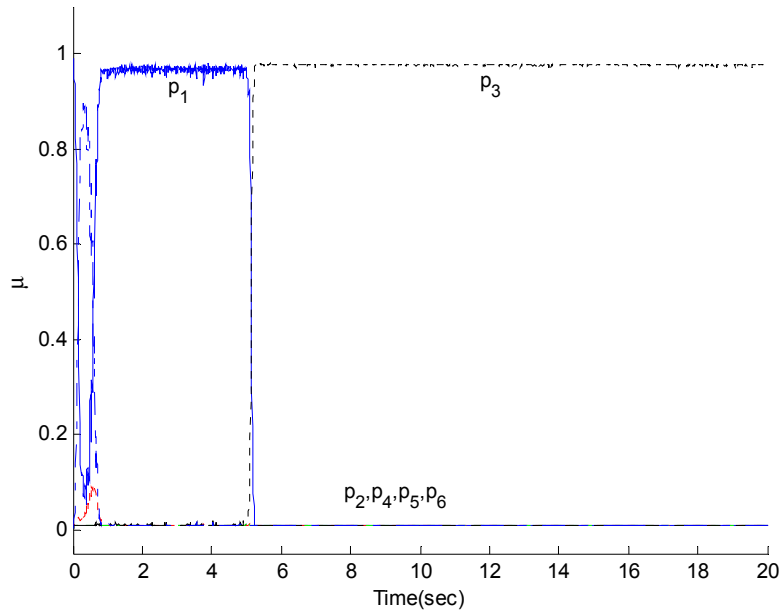


Figure 4.17: The simulation result for the scenario III by using the proposed method with $W_f = 0.85$. A fault with magnitude 0.05 ($F_{ec} = 0.95$) occurs in the compressor efficiency at $t = 5\text{sec}$ (for the mode labels refer to Table 4.3).

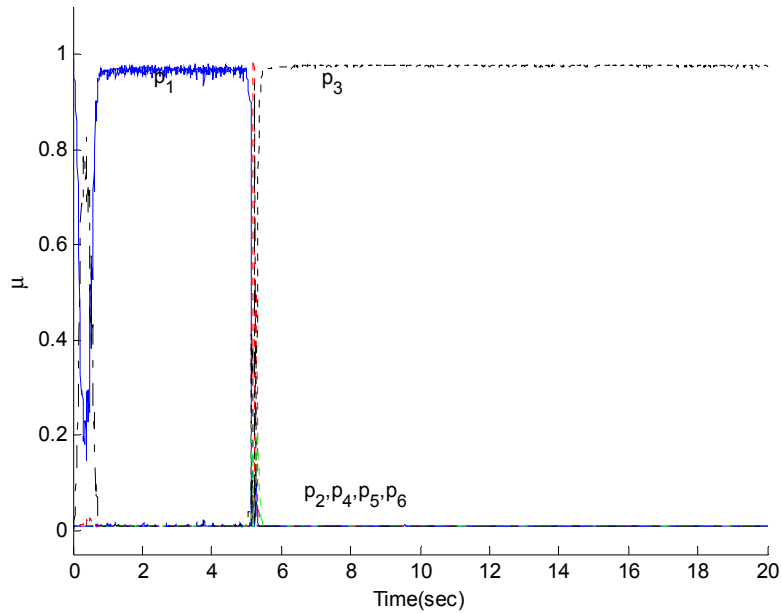


Figure 4.18: The simulation result for the scenario III by using the approach proposed in [2] with $W_f = 0.85$. A fault with magnitude 0.05 ($F_{ec} = 0.95$) occurs in the compressor efficiency at $t = 5\text{sec}$ (for the mode labels refer to Table 4.3).

4.2.2.3. Scenario IV

In this scenario, we assume that the system is subjected to a fault in the turbine mass flow at time instant $t = 5 \text{ sec}$. The magnitude of the fault is 0.05 ($F_{mt} = 0.95$). Figure 4.20 shows the results that are obtained by using the approach that is proposed in [2] for comparison.

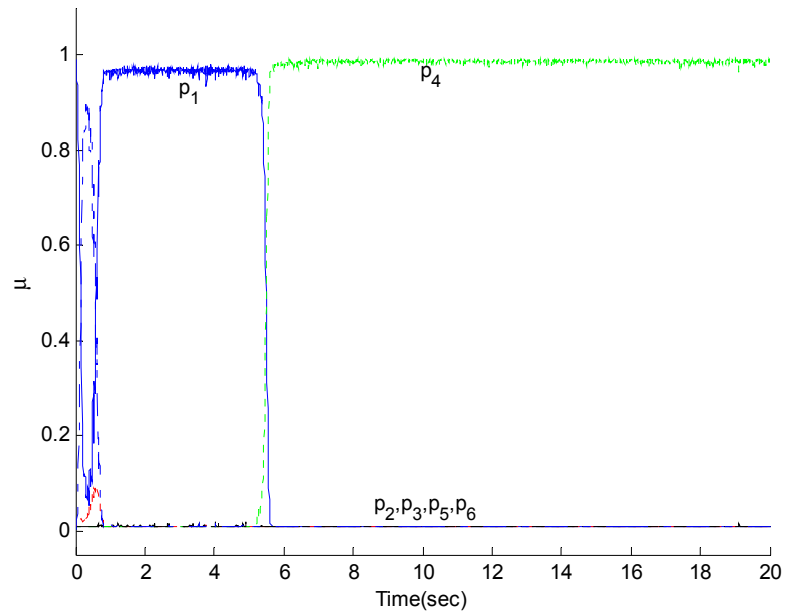


Figure 4.19: The simulation result for the scenario IV by using the proposed method with $W_f = 0.85$. A fault with magnitude 0.05 ($F_{mt} = 0.95$) occurs in the turbine mass flow at $t = 5 \text{ sec}$ (for the mode labels refer to Table 4.3).

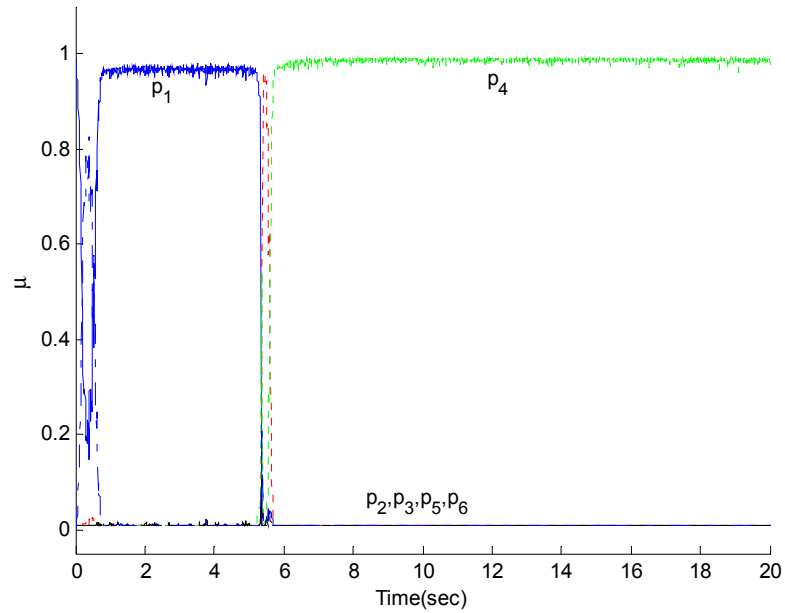


Figure 4.20: The simulation result for the scenario IV by using the approach proposed in [2] with $W_f = 0.85$. A fault with magnitude 0.05 ($F_{mt} = 0.95$) occurs in the turbine mass flow at $t = 5\text{sec}$ (for the mode labels refer to Table 4.3).

4.2.2.4. Scenario V

In this scenario a fault occurs in the compressor mass flow at $t = 5\text{sec}$. the magnitude of the fault is 0.05 ($F_{mc} = 0.95$). Figure 4.22 shows the results that are obtained by using the approach that is proposed in [2] for comparison.

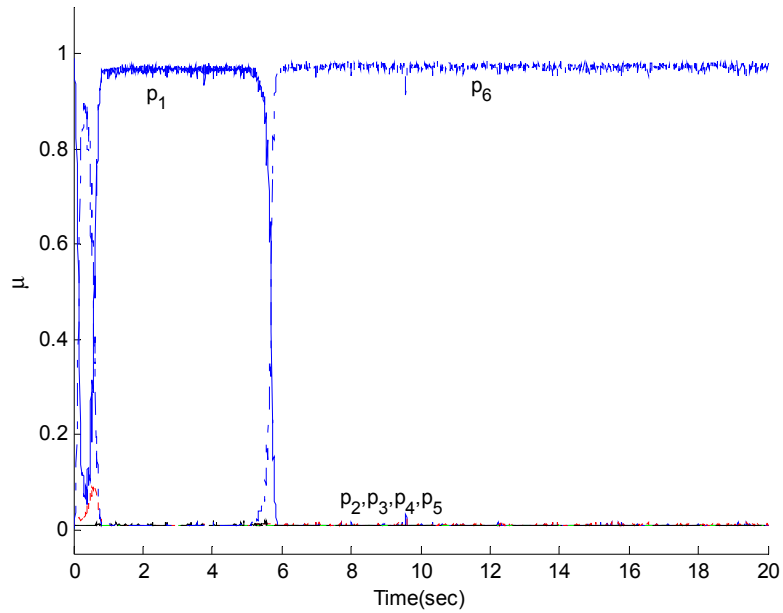


Figure 4.21: The simulation result for the scenario V by using the proposed method with $W_f = 0.85$. A fault with magnitude 0.05 ($F_{mc} = 0.95$) occurs in the compressor mass flow at $t = 5\text{sec}$ (for the mode labels refer to Table 4.3).

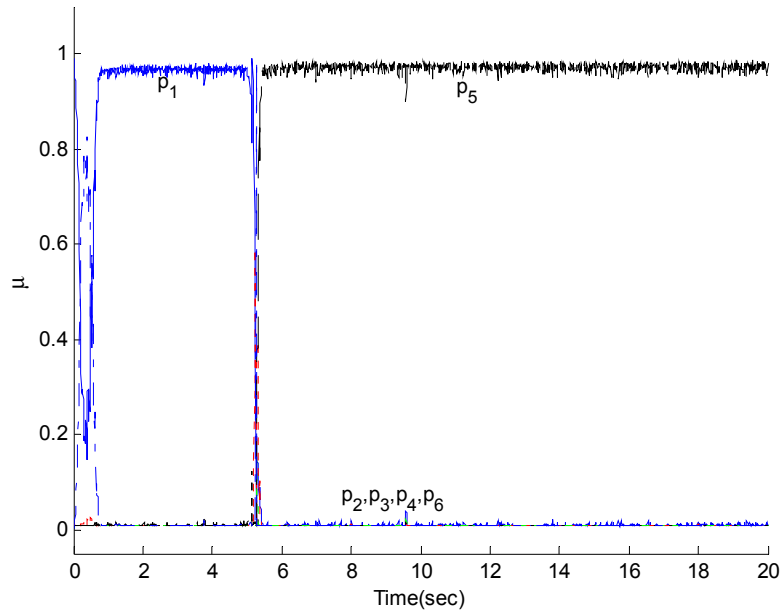


Figure 4.22: The simulation result for the scenario V by using the approach proposed in [2] with $W_f = 0.85$. A fault with magnitude 0.05 ($F_{mc} = 0.95$) occurs in the compressor mass flow at $t = 5\text{sec}$ (for the mode labels refer to Table 4.3).

4.2.3. Faults with Magnitude 8%

In this subsection, the simulation results for the scenarios I-V are presented. The magnitude of all the faults is 8%. The faulty models that are used for this subsection are summarized in Table 4.4.

Table 4.4: The different models corresponding to the healthy and faulty modes (8% magnitude) that are used in the simulation for each operating point.

Model Mode	#1	#2	#3	#4	#5	#6
	Healthy	8% fault in F_{et}	8% fault in F_{ec}	8% fault in F_{mt}	8% fault in F_{mc}	8% fault in W_f

4.2.3.1. Scenario II

In this scenario, one fault occurs in the turbine efficiency at time instant $t = 5$ sec. The magnitude of the fault is 0.08 ($F_{et} = 0.92$). Figure 4.23 shows the result for this scenario. Figure 4.24 shows the results that are obtained by using the approach that is proposed in [2] for comparison.

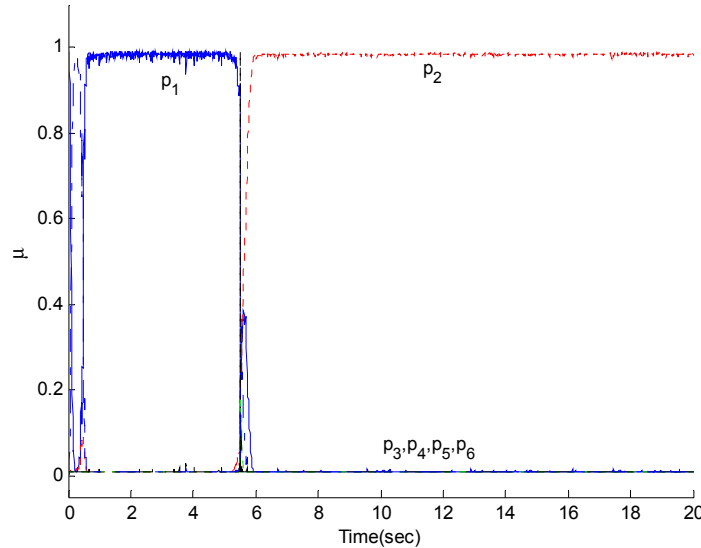


Figure 4.23: The simulation result for the scenario II by using the proposed method with $W_f = 0.85$. A fault with magnitude 0.08 ($F_{et} = 0.92$) occurs in the turbine efficiency at $t = 5$ sec (for the mode labels refer to Table 4.4).

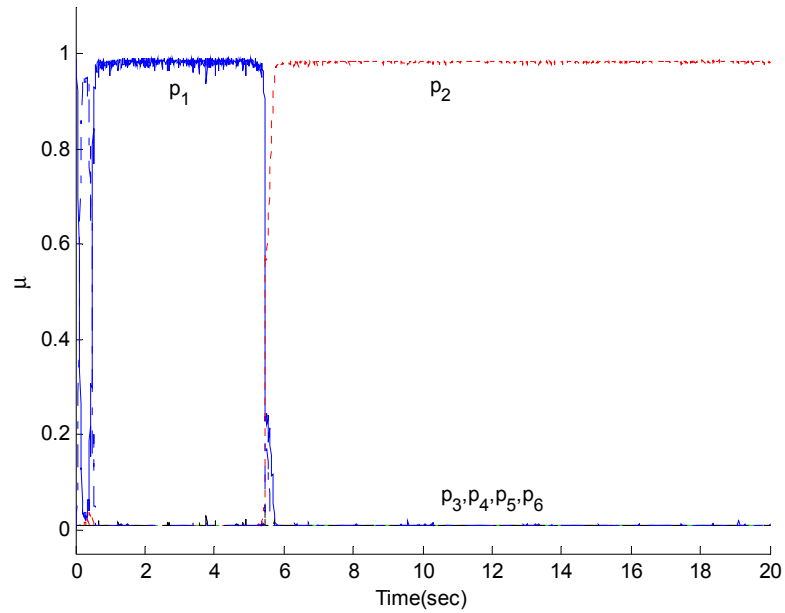


Figure 4.24: The simulation result for the scenario II by using the approach proposed in [2] with $W_f = 0.85$. A fault with magnitude 0.08 ($F_{et} = 0.92$) occurs in the turbine efficiency at $t = 5$ sec (for the mode labels refer to Table 4.4).

4.2.3.2. Scenario III

In this scenario, one fault occurs in the compressor efficiency at time instant $t = 5$ sec. The magnitude of the fault is 0.08 ($F_{ec} = 0.92$). Figure 4.25 shows the result for this scenario. Figure 4.26 shows the results that are obtained by using the approach that is proposed in [2] for comparison.

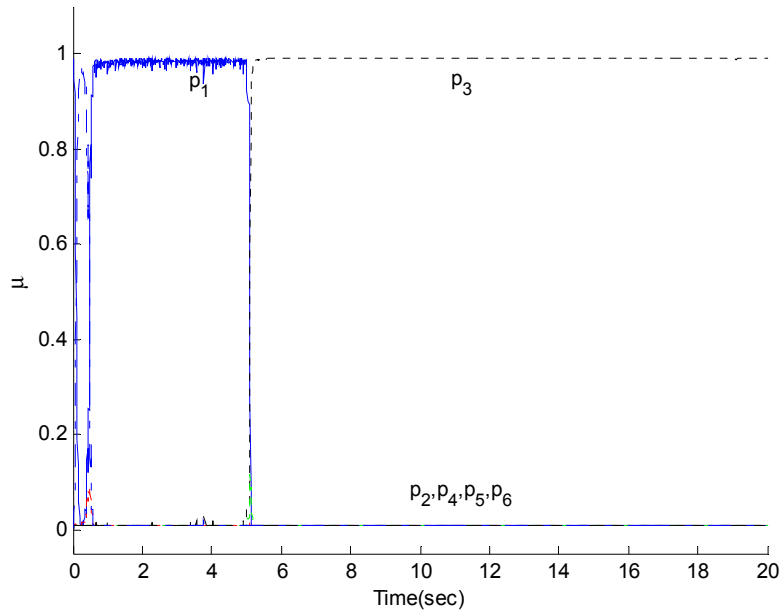


Figure 4.25: The simulation result for the scenario III by using the proposed method with $W_f = 0.85$. A fault with magnitude 0.08 ($F_{ec} = 0.92$) occurs in the compressor efficiency at $t = 5\text{sec}$ (for the mode labels refer to Table 4.4).

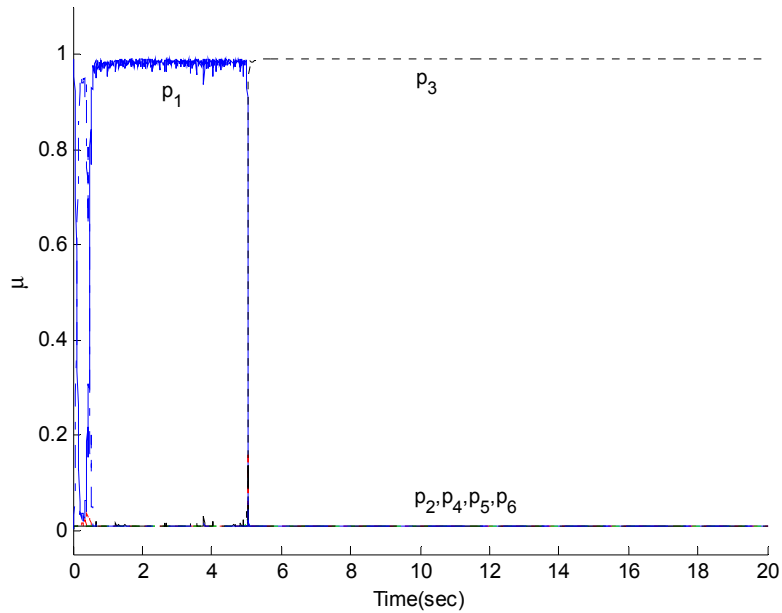


Figure 4.26: The simulation result for the scenario III by using the approach proposed in [2] with $W_f = 0.85$. A fault with magnitude 0.08 ($F_{ec} = 0.92$) occurs in the compressor efficiency at $t = 5\text{sec}$ (for the mode labels refer to Table 4.4).

4.2.3.3. Scenario IV

In this scenario, we assume that the system is subjected to a fault in the turbine mass flow at time instant $t = 5 \text{ sec}$. The magnitude of the fault is 0.08 ($F_{mt} = 0.92$). Figure 4.28 shows the results that are obtained by using the approach that is proposed in [2] for comparison.

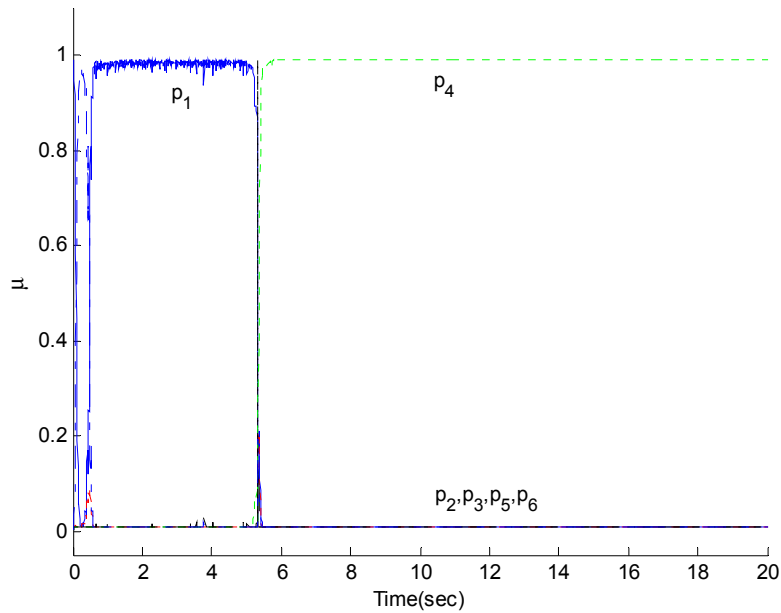


Figure 4.27: The simulation result for the scenario IV by using the proposed method with $W_f = 0.85$. A fault with magnitude 0.08 ($F_{mt} = 0.92$) occurs in the turbine mass flow at $t = 5 \text{ sec}$ (for the mode labels refer to Table 4.4).

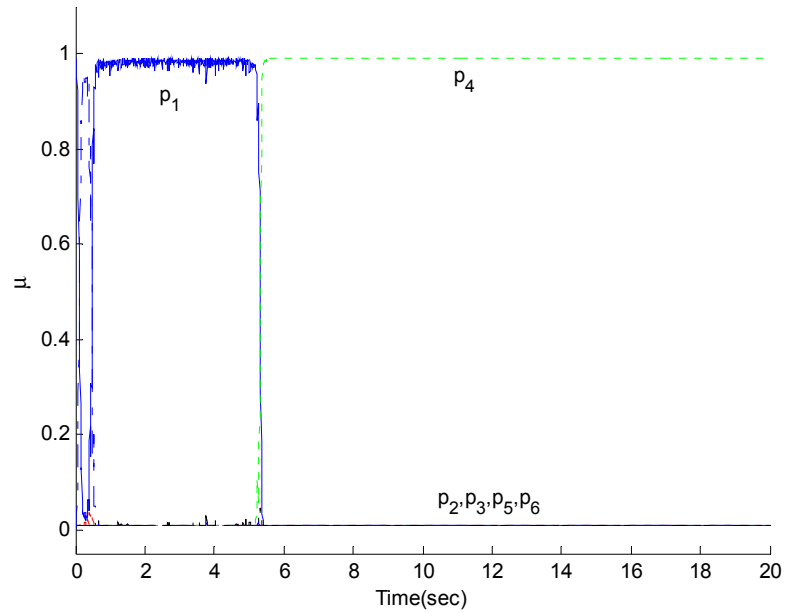


Figure 4.28: The simulation result for the scenario IV by using the approach proposed in [2] with $W_f = 0.85$. A fault with magnitude 0.08 ($F_{mt} = 0.92$) occurs in the turbine mass flow at $t = 5\text{sec}$ (for the mode labels refer to Table 4.4).

4.2.3.4. Scenario V

In this scenario a fault occurs in the compressor mass flow at $t = 5\text{sec}$. the magnitude of the fault is 0.08 ($F_{mc} = 0.92$). Figure 4.30 shows the results that are obtained by using the approach that is proposed in [2] for comparison.

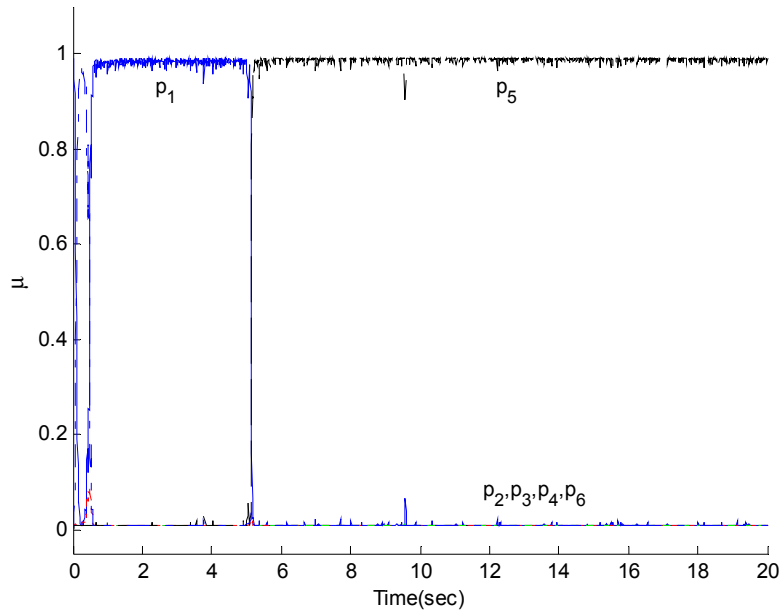


Figure 4.29: The simulation result for the scenario V by using the proposed method with $W_f = 0.85$. A fault with magnitude 0.08 ($F_{mc} = 0.92$) occurs in the compressor mass flow at $t = 5\text{sec}$ (for the mode labels refer to Table 4.4).

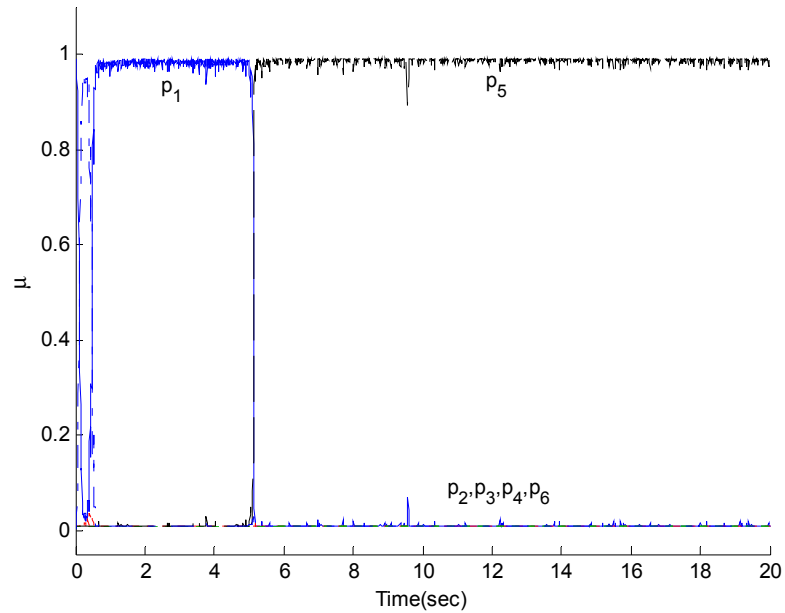


Figure 4.30: The simulation result for the scenario V by using the approach proposed in [2] with $W_f = 0.85$. A fault with magnitude 0.02 ($F_{mc} = 0.92$) occurs in the compressor mass flow at $t = 5\text{sec}$ (for the mode labels refer to Table 4.4).

4.2.4. Faults with Magnitude 10%

In this subsection, the simulation results for the scenarios I-V are presented. The magnitude of all the faults is 10%. The faulty models that are used for this subsection are summarized in Table 4.5.

Table 4.5: The different models corresponding to the healthy and faulty modes (10% magnitude) that are used in the simulation for each operating point.

Model Mode	#1	#2	#3	#4	#5	#6
	Healthy	10% fault in F_{et}	10% fault in F_{ec}	10% fault in F_{mt}	10% fault in F_{mc}	10% fault in W_f

4.2.4.1. Scenario II

In this scenario, one fault occurs in the turbine efficiency at time instant $t = 5 \text{ sec}$. The magnitude of the fault is 0.1 ($F_{et} = 0.9$). Figure 4.31 shows the result for this scenario. Figure 4.32 shows the results that are obtained by using the approach that is proposed in [2] for comparison.

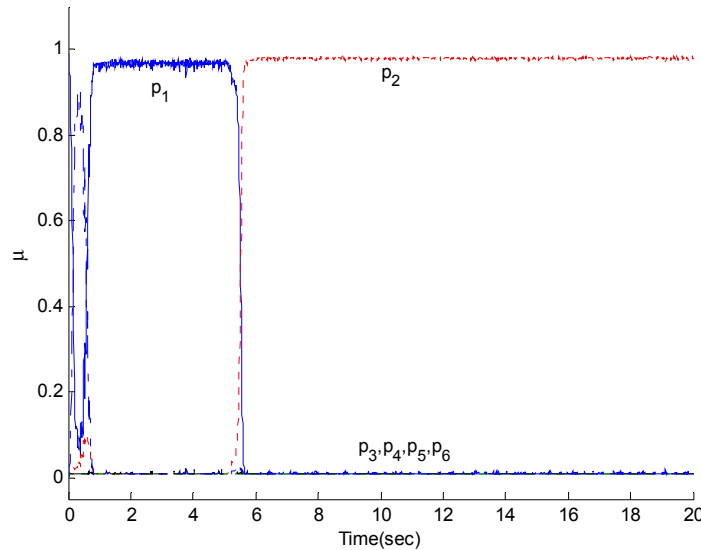


Figure 4.31: The simulation result for the scenario II by using the proposed method with $W_f = 0.85$. A fault with magnitude 0.1 ($F_{et} = 0.9$) occurs in the turbine efficiency at $t = 5 \text{ sec}$ (for the mode labels refer to Table 4.5).

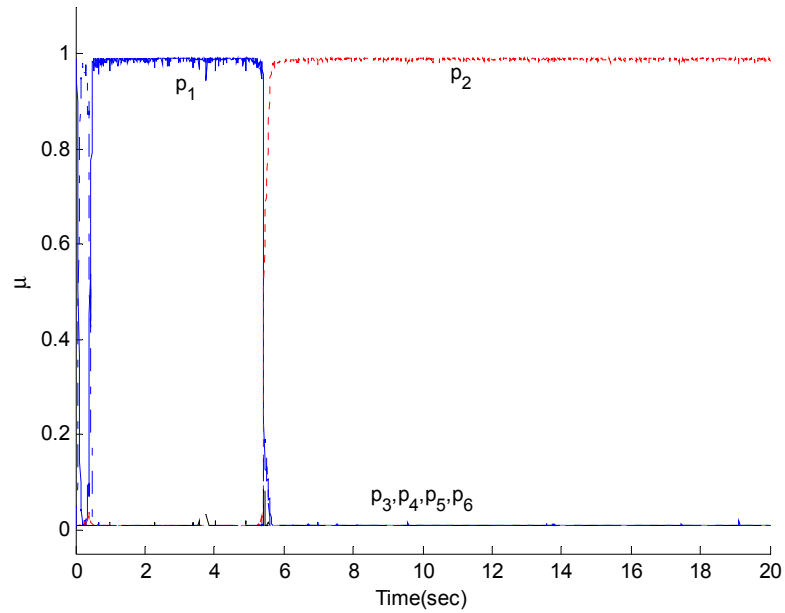


Figure 4.32: The simulation result for the scenario II by using the approach proposed in [2] with $W_f = 0.85$. A fault with magnitude 0.1 ($F_{et} = 0.9$) occurs in the turbine efficiency at $t = 5\text{sec}$ (for the mode labels refer to Table 4.5).

4.2.4.2. Scenario III

In this scenario, one fault occurs in the compressor efficiency at time instant $t = 5$ sec. The magnitude of the fault is 0.1 ($F_{ec} = 0.9$). Figure 4.33 shows the result for this scenario. Figure 4.34 shows the results that are obtained by using the approach that is proposed in [2] for comparison.

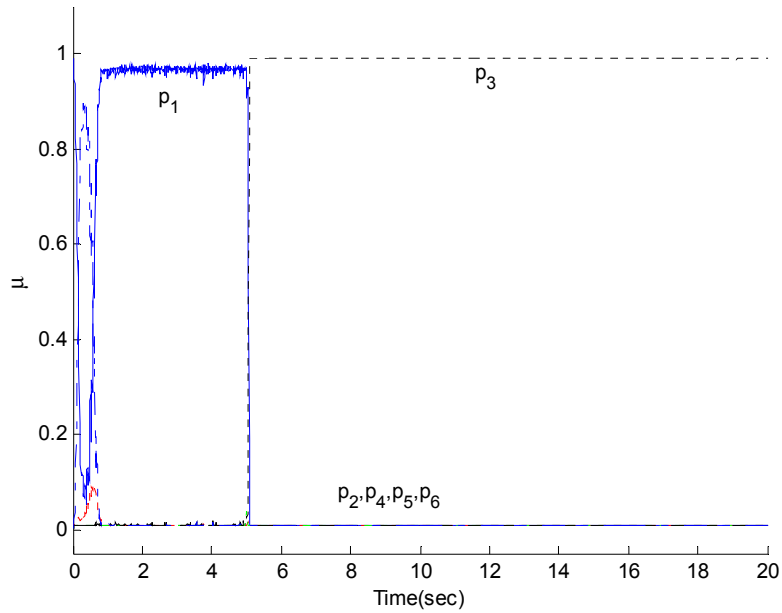


Figure 4.33: The simulation result for the scenario III by using the proposed method with $W_f = 0.85$. A fault with magnitude 0.1 ($F_{ec} = 0.9$) occurs in the compressor efficiency at $t = 5sec$ (for the mode labels refer to Table 4.5).

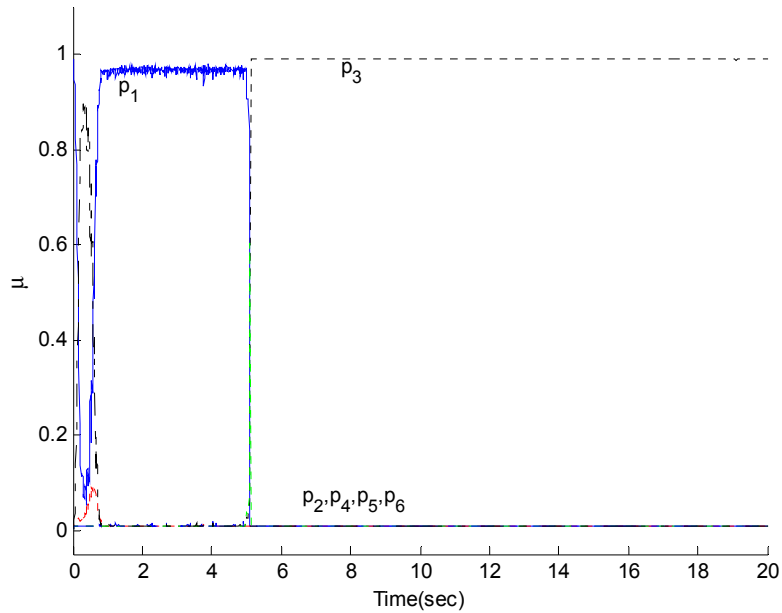


Figure 4.34: The simulation result for scenario III by using the approach proposed in [2] with $W_f = 0.85$. A fault with magnitude 0.1 ($F_{ec} = 0.9$) occurs in the compressor efficiency at $t = 5sec$ (for the mode labels refer to Table 4.5).

4.2.4.3. Scenario IV

In this scenario, we assume that the system is subjected to a fault in the turbine mass flow at time instant $t = 5 \text{ sec}$. The magnitude of the fault is 0.1 ($F_{mt} = 0.9$). Figure 4.36 shows the results that are obtained by using the approach that is proposed in [2] for comparison.

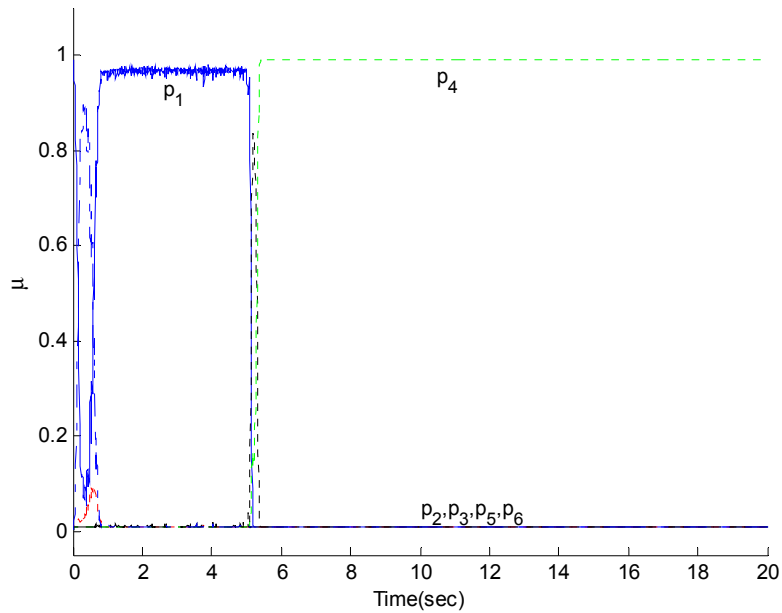


Figure 4.35: The simulation result for the scenario IV by using the proposed method with $W_f = 0.85$. A fault with magnitude 0.1 ($F_{mt} = 0.9$) occurs in the turbine mass flow at $t = 5 \text{ sec}$ (for the mode labels refer to Table 4.5).

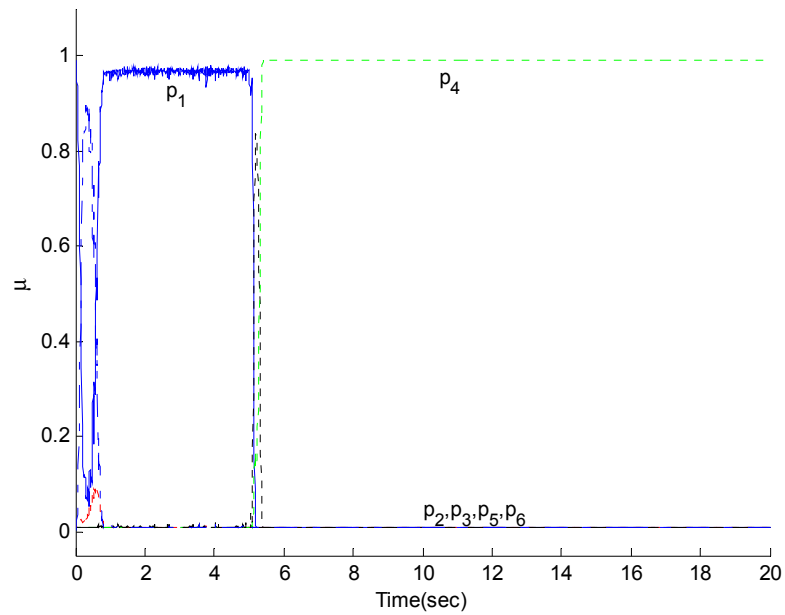


Figure 4.36: The simulation result for the scenario IV by using the approach proposed in [2] with $W_f = 0.85$. A fault with magnitude 0.1 ($F_{mt} = 0.9$) occurs in the turbine mass flow at $t = 5sec$ (for the mode labels refer to Table 4.5).

4.2.4.4. Scenario V

In this scenario a fault occurs in the compressor mass flow at $t = 5sec$. the magnitude of the fault is 0.1 ($F_{mc} = 0.9$). Figure 4.38 shows the results that are obtained by using the approach that is proposed in [2] for comparison.

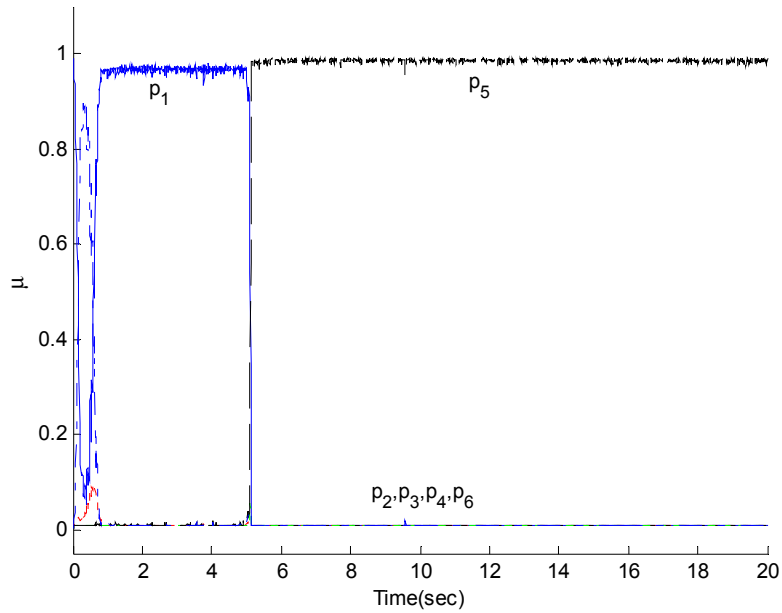


Figure 4.37: The simulation result for the scenario V by using the proposed method with $W_f = 0.85$. A fault with magnitude 0.1 ($F_{mc} = 0.9$) occurs in the compressor mass flow at $t = 5sec$ (for the mode labels refer to Table 4.5).

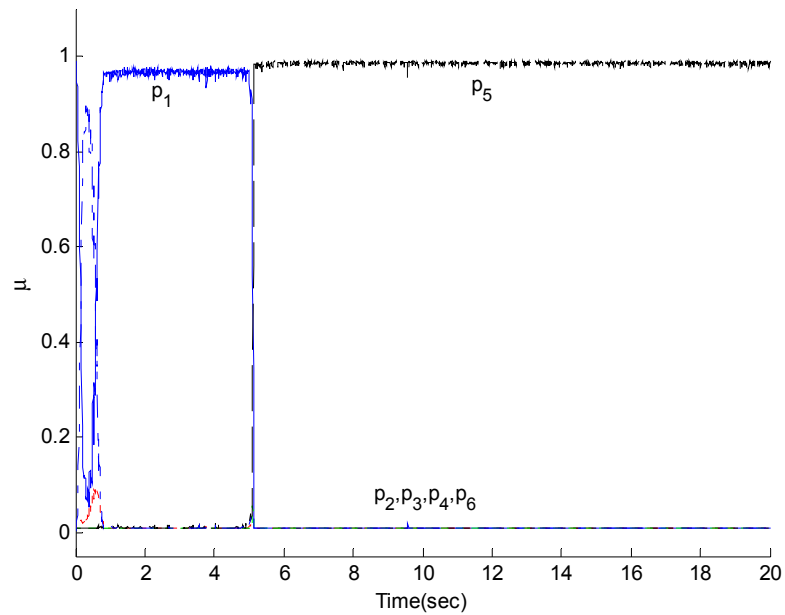


Figure 4.38: The simulation result for the scenario V by using the approach proposed in [2] with $W_f = 0.85$. A fault with magnitude 0.1 ($F_{mc} = 0.9$) occurs in the compressor mass flow at $t = 5sec$ (for the mode labels refer to Table 4.5).

4.2.5. Effectiveness Loss of Fuel Flow

In this scenario, we assume that a loss of effectiveness occurs in the fuel flow actuator at $t = 5 \text{ sec}$. The simulation results for different magnitudes of faults are provided as follows.

4.2.5.1. Fault with Magnitude 5%

Figure 4.39 and Figure 4.40 provide the simulation results for the scenario VI which simulates a single fault in the fuel flow actuator occurring at $t = 5 \text{ sec}$ with a magnitude of 0.05 ($F_{wf} = 0.95$).

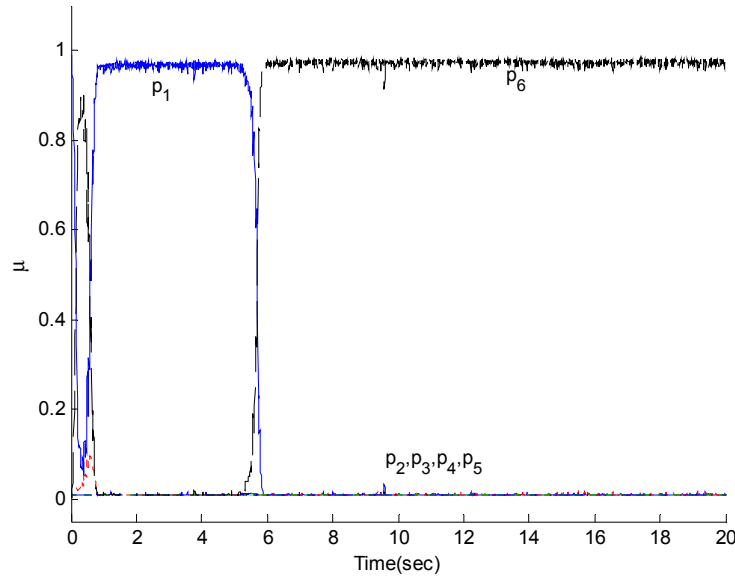


Figure 4.39: The simulation result for the scenario VI by using the proposed method with $W_f = 0.85$. A fault with magnitude 0.05 ($F_{wf} = 0.95$) occurs in effectiveness of fuel flow actuator at $t = 5 \text{ sec}$ (for the mode labels refer to Table 4.2).

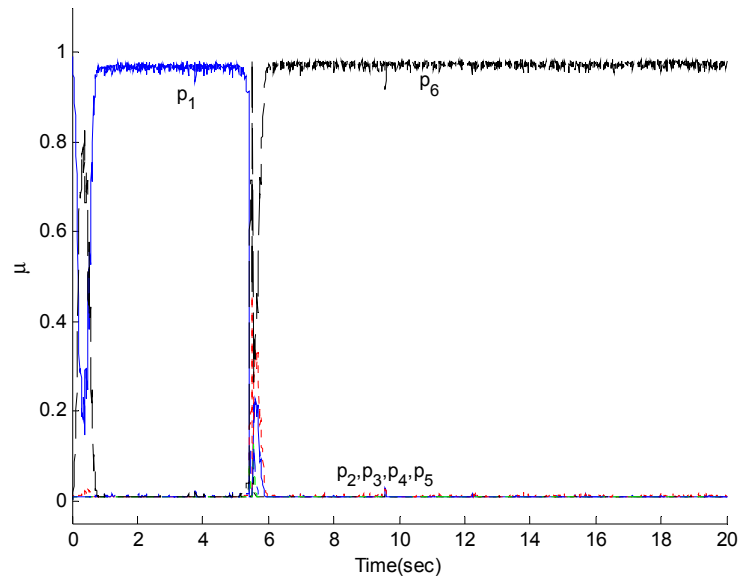


Figure 4.40: The simulation result for the scenario VI by using the approach proposed in [2] with $W_f = 0.85$. A fault with magnitude 0.05 ($F_{wf} = 0.95$) occurs in effectiveness of fuel flow actuator at $t = 5sec$ (for the mode labels refer to Table 4.2).

4.2.5.2. Fault with Magnitude 8%

Figure 4.41 and Figure 4.42 provides the simulation results for the scenario VI which simulates a single fault in the fuel flow actuator occurring at $t = 5sec$ with a magnitude of 0.08 ($F_{wf} = 0.92$).

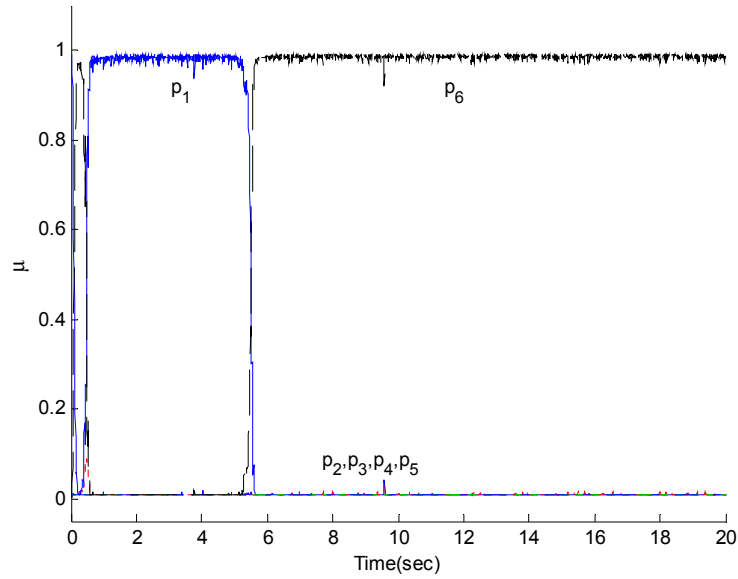


Figure 4.41: The simulation result for the scenario VI by using the proposed method with $W_f = 0.85$. A fault with magnitude 0.08 ($F_{wf} = 0.92$) occurs in effectiveness of fuel flow actuator at $t = 5\text{sec}$ (for the mode labels refer to Table 4.4).

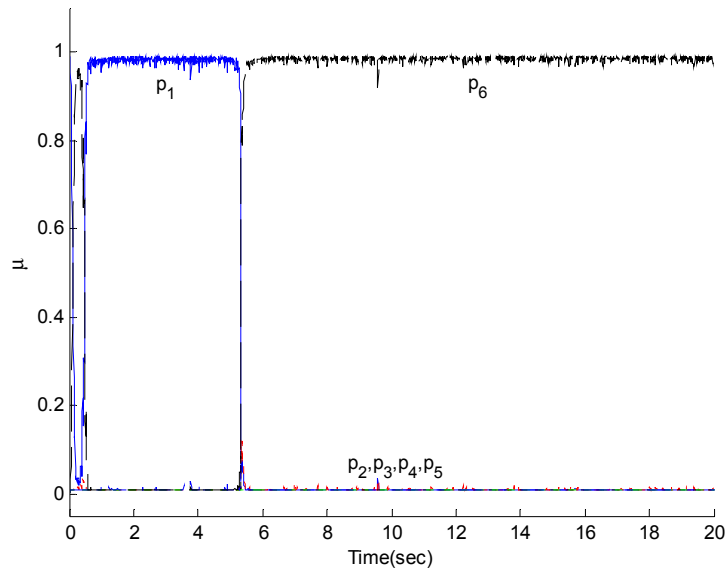


Figure 4.42: The simulation result for the scenario IV by using the approach proposed in [2] with $W_f = 0.85$. A fault with magnitude 0.08 ($F_{wf} = 0.92$) occurs in effectiveness of fuel flow actuator at $t = 5\text{sec}$ (for the mode labels refer to Table 4.4).

4.2.5.3. Fault with Magnitude 10%

Figure 4.43 and Figure 4.44 provides the simulation results for the scenario VI which simulates a single fault in the fuel flow actuator occurring at $t = 5\text{sec}$ with a magnitude of 0.1 ($F_{wf} = 0.9$).

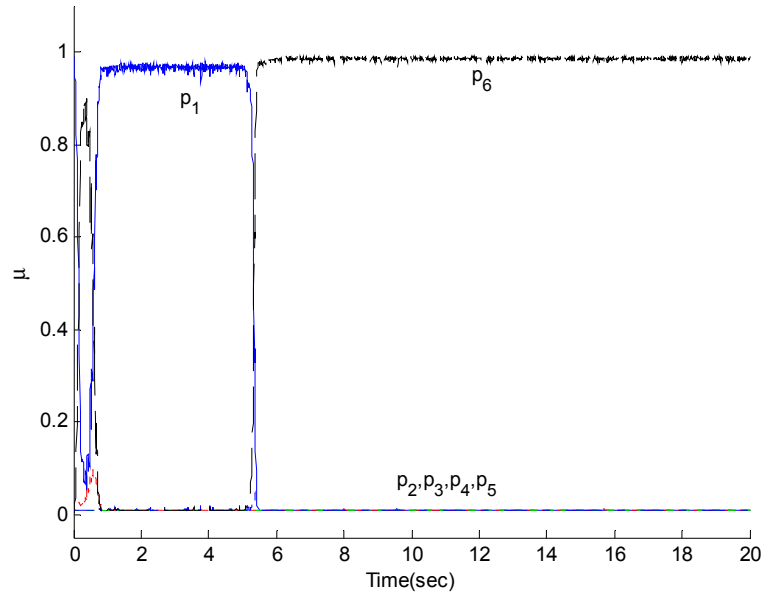


Figure 4.43: The simulation result for the scenario VI with $W_f = 0.85$. A fault with magnitude 0.1 ($F_{wf} = 0.9$) occurs in effectiveness of fuel flow actuator at $t = 5\text{sec}$ (for the mode labels refer to Table 4.5).

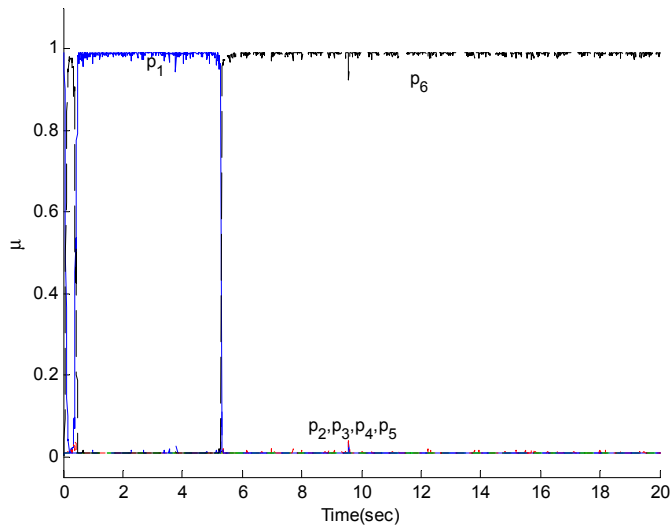


Figure 4.44: The simulation result for the scenario IV by using the approach proposed in [2] with $W_f = 0.85$. A fault with magnitude 0.1 ($F_{wf} = 0.9$) occurs in effectiveness of fuel flow actuator at $t = 5$ sec (for the mode labels refer to Table 4.5).

4.2.6. Summary

In this subsection, we have summarized the simulation results for different values of $W_f = \{0.4, 0.55, 0.7, 0.85\}$. The results are provided in Table 4.6 to Table 4.13.

Table 4.6: The summary of simulation results for different values of w_f by using our proposed approach. t_D and t_I denote the detection and isolation times, respectively. The magnitude of the faults is equal to 2%.

Scenarios	Scenario II		Scenario III		Scenario IV		Scenario V	
	t_D	t_I	t_D	t_I	t_D	t_I	t_D	t_I
$w_f = 0.4$	6.42	7.7	5.66	6.62	5.89	7.18	6.63	13.06
$w_f = 0.55$	5.97	7.27	5.35	6.23	5.61	6.62	5.72	7.83
$w_f = 0.7$	6.31	7.73	5.46	6.13	5.53	6.55	5.38	6.32
$w_f = 0.85$	6.32	7.87	5.36	6.23	5.52	6.4	5.44	6.95

Table 4.7: The summary of simulation results for different values of w_f by using the proposed approach in [2]. t_D and t_I denote the detection and isolation times, respectively. The magnitude of the faults is equal to 2%.

Scenarios Fuel flow	Scenario II		Scenario III		Scenario IV		Scenario V	
	t_D	t_I	t_D	t_I	t_D	t_I	t_D	t_I
$w_f = 0.4$	6.42	7.65	5.71	6.65	5.64	6.62	6.54	12.39
$w_f = 0.55$	6.22	7.49	5.35	5.91	5.6	6.55	5.73	7.83
$w_f = 0.7$	6.32	7.7	5.48	6.98	5.79	6.57	5.58	6.88
$w_f = 0.85$	6.04	6.15	5.36	5.82	5.58	6.02	5.38	7.14

Table 4.8: The summary of simulation results for different values of w_f by using our proposed approach. t_D and t_I denote the detection and isolation times, respectively. The magnitude of the faults is equal to 5%.

Scenarios Fuel flow	Scenario II		Scenario III		Scenario IV		Scenario V	
	t_D	t_I	t_D	t_I	t_D	t_I	t_D	t_I
$w_f = 0.4$	5.59	6.24	5.09	5.43	5.26	5.59	5.36	6.21
$w_f = 0.55$	5.79	6.11	5.1	5.3	5.33	5.62	5.14	5.42
$w_f = 0.7$	5.58	6.1	5.1	5.14	5.33	5.62	5.11	5.34
$w_f = 0.85$	5.58	6.09	5.09	5.22	5.36	5.59	5.1	5.33

Table 4.9: The summary of simulation results for different values of w_f by using the proposed approach in [2]. t_D and t_I denote the detection and isolation times, respectively. The magnitude of the faults is equal to 5%.

Scenarios Fuel flow	Scenario II		Scenario III		Scenario IV		Scenario V	
	t_D	t_I	t_D	t_I	t_D	t_I	t_D	t_I
$w_f = 0.4$	5.94	6.34	5.12	5.29	5.38	5.56	5.38	5.83
$w_f = 0.55$	5.73	6.13	5.11	5.32	5.36	5.57	5.12	5.42
$w_f = 0.7$	5.53	6.1	5.08	5.27	5.52	5.7	5.19	5.42
$w_f = 0.85$	5.58	5.71	5.08	5.2	5.35	5.42	5.14	5.27

Table 4.10 The summary of simulation results for different values of w_f by using our proposed approach. t_D and t_I denote the detection and isolation times, respectively. The magnitude of the faults is equal to 8%.

Scenarios Fuel flow	Scenario II		Scenario III		Scenario IV		Scenario V	
	t_D	t_I	t_D	t_I	t_D	t_I	t_D	t_I
$w_f = 0.4$	5.51	6.06	5.04	5.15	5.14	5.29	5.15	5.58
$w_f = 0.55$	5.51	5.73	5.05	5.09	5.26	5.48	5.09	5.19
$w_f = 0.7$	5.5	5.88	5.04	5.07	5.26	5.34	5.08	5.19
$w_f = 0.85$	5.52	5.8	5.04	5.11	5.25	5.37	5.07	5.19

Table 4.11: The summary of simulation results for different values of w_f by using the proposed approach in [2]. t_D and t_I denote the detection and isolation times, respectively. The magnitude of the faults is equal to 8%.

Scenarios Fuel flow	Scenario II		Scenario III		Scenario IV		Scenario V	
	t_D	t_I	t_D	t_I	t_D	t_I	t_D	t_I
$w_f = 0.4$	5.52	5.91	5.05	5.28	5.25	5.38	5.17	5.36
$w_f = 0.55$	5.66	5.86	5.05	5.08	5.26	5.37	5.08	5.16
$w_f = 0.7$	5.47	5.85	5.04	5.16	5.27	5.39	5.09	5.23
$w_f = 0.85$	5.45	5.72	5.04	5.07	5.25	5.39	5.1	5.17

Table 4.12: The summary of simulation results for different values of w_f by using our proposed approach. t_D and t_I denote the detection and isolation times, respectively. The magnitude of the faults is equal to 10%.

Scenarios Fuel flow	Scenario II		Scenario III		Scenario IV		Scenario V	
	t_D	t_I	t_D	t_I	t_D	t_I	t_D	t_I
$w_f = 0.4$	5.7	5.85	5.04	5.16	5.12	5.37	5.11	5.36
$w_f = 0.55$	5.47	5.61	5.03	5.07	5.24	5.33	5.08	5.15
$w_f = 0.7$	5.46	5.83	5.03	5.05	5.25	5.38	5.08	5.16
$w_f = 0.85$	5.36	5.61	5.03	5.09	5.1	5.37	5.05	5.15

Table 4.13: The summary of simulation results for different values of w_f by using the proposed approach in [2]. t_D and t_I denote the detection and isolation times, respectively. The magnitude of the faults is equal to 10%.

Scenarios Fuel flow	Scenario II		Scenario III		Scenario IV		Scenario V	
	t_D	t_I	t_D	t_I	t_D	t_I	t_D	t_I
$w_f = 0.4$	5.47	5.77	5.06	5.3	5.21	5.35	5.14	5.29
$w_f = 0.55$	5.44	5.77	5.04	5.18	5.25	5.34	5.08	5.22
$w_f = 0.7$	5.44	5.75	5.03	5.09	5.25	5.32	5.08	5.16
$w_f = 0.85$	5.43	5.6	5.03	5.13	5.23	5.32	5.05	5.13

It follows from the results provided in the above tables that

1. By increasing the magnitude of a fault not only the detection time decreases (which is expected because of the difference between the faulty and the healthy systems), but also the isolation time is lower as compared with smaller fault magnitudes.
2. Although our proposed method has lower computational cost (note we symbolically linearized the jet engine only once), the detection and isolation times are almost the same another ones obtained by using the approach introduced in [2].

4.3. NUMBER OF OBSERVERS

In the previous section, the number of modes in the multiple model is equal to 21 (that is one healthy mode and 20 faulty modes (for different values of W_f) as shown in

Tables 4.2 to 4.5). In this section, we investigate the impact of the banks with larger number of modes (observers) in our proposed approach. A bank with larger number of filters enables one to identify the fault magnitudes more accurately (that is higher resolution). However, increasing the number of the filters can decrease the efficiency of the MM method [7]. In this part, we run all the filters (one healthy model and 20 faulty models for the fault 2%, 5%, 8% and 10%) in parallel. However, we investigate the scenarios that the injected fault severities are not equal to these values. In other words, the injected faults have the severities 3%, 6%, 7% and 9% in the scenarios II-V in the previous section.

In this section, the probabilities of different modes are defined in follows: p_1 denotes the probability of the healthy mode. p_2, p_7, p_{11} and p_{15} denote the modes corresponding to $F_{et} = 0.98, F_{et} = 0.95, F_{et} = 0.92$ and $F_{et} = 0.9$, respectively. The probabilities of the modes corresponding to $F_{ec} = 0.98, F_{ec} = 0.95, F_{ec} = 0.92$ and $F_{ec} = 0.9$ are shown by p_3, p_8, p_{12} and p_{16} , respectively. p_4, p_9, p_{13} and p_{17} denote the probabilities of the modes corresponding to $F_{mt} = 0.98, F_{mt} = 0.95, F_{mt} = 0.92$ and $F_{mt} = 0.9$, respectively. The faulty modes $F_{mc} = 0.98, F_{mc} = 0.95, F_{mc} = 0.92$ and $F_{mc} = 0.9$ are denoted by p_5, p_{10}, p_{14} and p_{18} , respectively. Finally, p_6, p_{19}, p_{20} denote the faulty modes corresponding to $F_{wf} = 0.95, F_{wf} = 0.92$ and $F_{wf} = 0.9$.

Figure 4.45 to Figure 4.48 show the results for scenario II with the magnitudes 3%, 6%, 7% and 9%. As can be seen in these figures, the filter which simulates the fault with lower to the injected fault is valid. For example, in Figure 4.46 filter with magnitude 2% is valid for fault 3%.

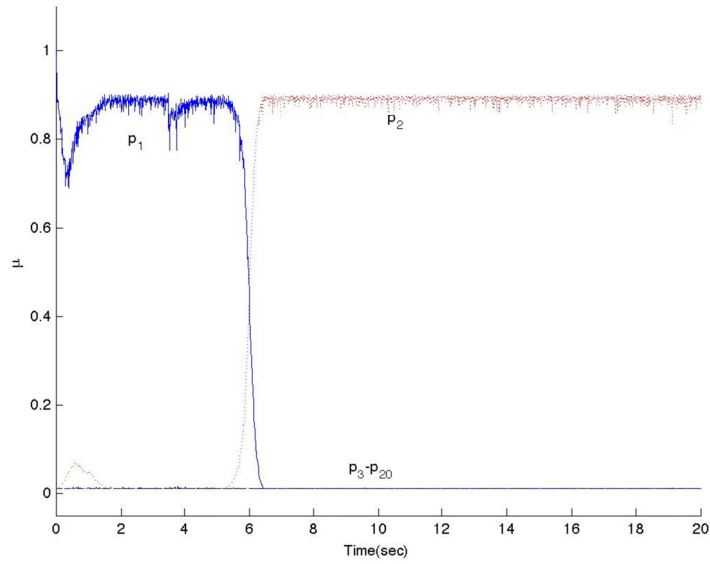


Figure 4.45: The simulation result for the scenario II by using our proposed method. A fault with magnitude 3% ($F_{et} = 0.97$) occurs in the compressor efficiency at $t = 5sec$ (in this simulation we run all filters in parallel).

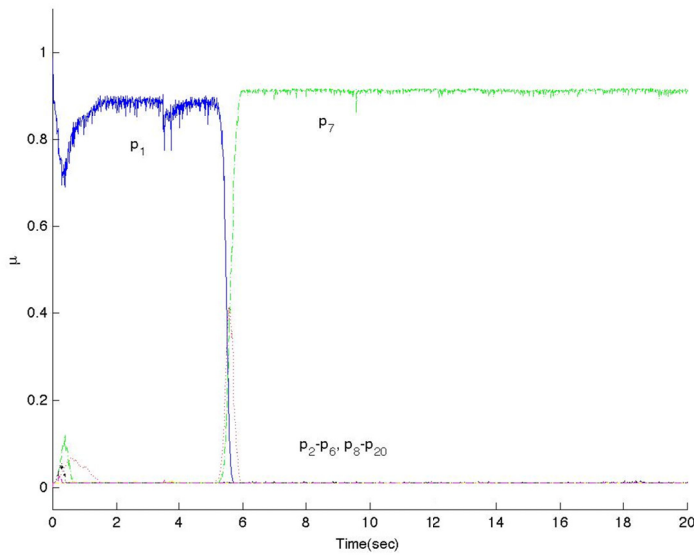


Figure 4.46: The simulation result for the scenario II by using our proposed method. A fault with magnitude 6% ($F_{et} = 0.94$) occurs in the compressor efficiency at $t = 5sec$ (in this simulation we run all filters in parallel).

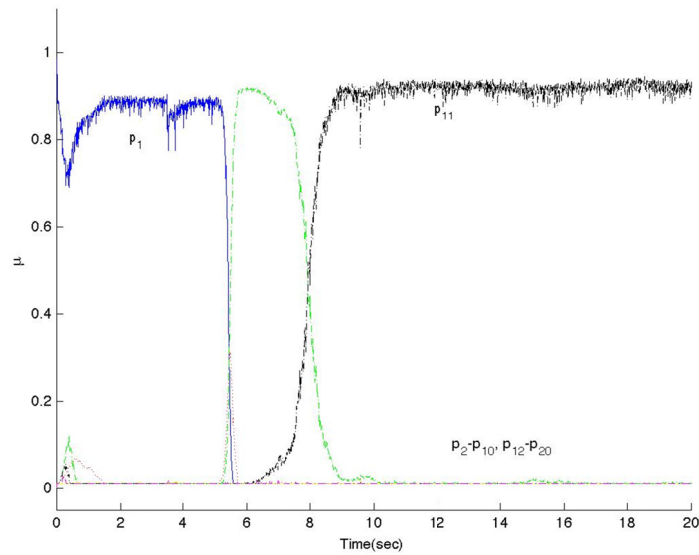


Figure 4.47: The simulation result for the scenario II by using our proposed method. A fault with magnitude 7% ($F_{et} = 0.93$) occurs in the compressor efficiency at $t = 5sec$ (in this simulation we run all filters in parallel).

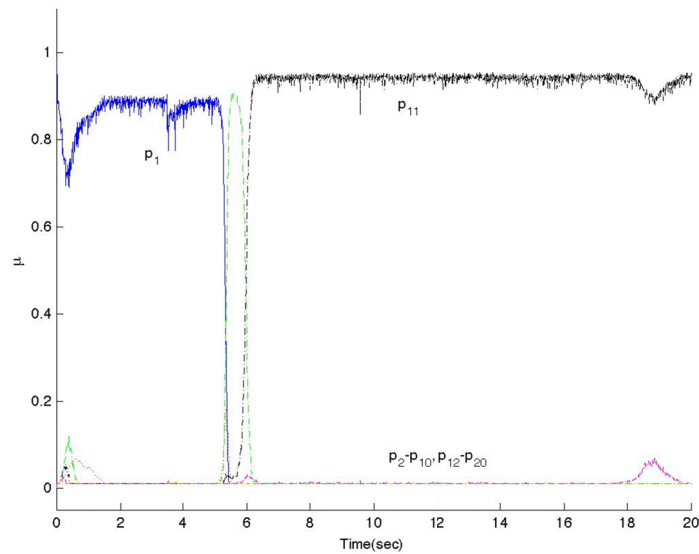


Figure 4.48: The simulation result for the scenario II by using our proposed method. A fault with magnitude 9% ($F_{et} = 0.91$) occurs in the compressor efficiency at $t = 5sec$ (in this simulation we run all filters in parallel).

The results of all scenarios are summarized in Table 4.14. In this table, it is shown

the valid filter is shown by the corresponding fault. For example the valid filter for Scenario II with a magnitude 3% is the filter simulate the faulty model for $F_{et} = 0.98$.

Table 4.14: The summary of simulation results for different severity of faults such that these magnitudes are not match with the filters.

Fault Severity \ Scenario	3%	6%	7%	9%
II	$F_{et} = 0.98$	$F_{et} = 0.95$	$F_{et} = 0.92$	$F_{et} = 0.92$
III	$F_{ec} = 0.98$	$F_{ec} = 0.95$	$F_{ec} = 0.95$	$F_{ec} = 0.92$
IV	$F_{mt} = 0.98$	$F_{mt} = 0.95$	$F_{mt} = 0.95$	<i>Not Isolated</i>
V	$F_{mc} = 0.98$	$F_{mc} = 0.95$	$F_{mc} = 0.95$	$F_{mc} = 0.92$

As can be seen from Table 4.14, except for Scenario IV (fault in m_t) with magnitude 9%, the faults are accurately detected and isolated, although the magnitudes of the fault cannot be determined. The result for this scenario is shown in Figure 4.49.

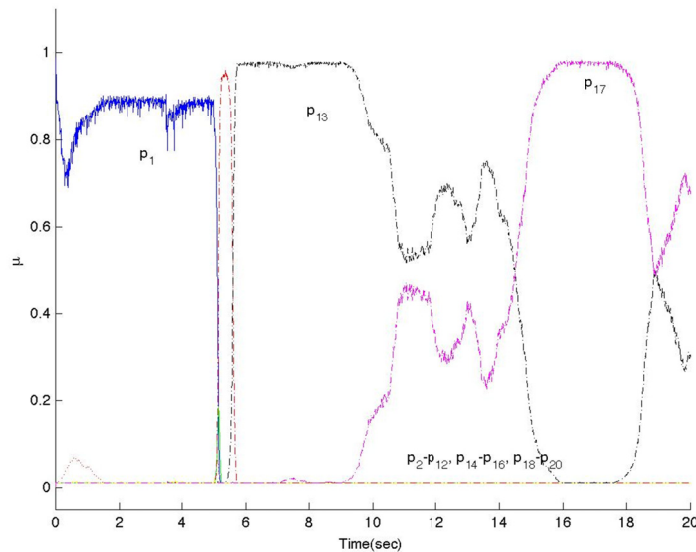


Figure 4.49: The simulation result for the scenario IV by using our proposed method. A fault with magnitude 9% ($F_{mt} = 0.91$) occurs in the compressor efficiency at $t = 5\text{sec}$ (in this simulation we run all filters in parallel).

One reason for this result lies on the fact that the filters corresponding to $F_{mt} = 0.92$ and $F_{mt} = 0.9$ are almost the same after the faults these two filters have the highest

probabilities. Note that in this case, the fault is accurately detected.

4.4. CONCLUSION

In this chapter, the FDI logic that is used in this thesis is presented. In the proposed method a set of observer banks is used for the FDI propose. This method has been applied to the single spool gas turbine. The banks of Kalman filters are constructed based on different operating points that are determined by the value of the fuel flow. It is shown that by considering a predefined threshold for the model probabilities one can decrease the false flags. By using this technique, it is shown that if the operating points that are selected such that $\Delta W_f = 0.2$ the proposed method can detect and isolate all faults that are introduced in Chapter 1.

Chapter 5 MODIFICATIONS TO THE FDI APPROACH

In this chapter, two further issues related to the proposed approach are investigated. We first address the multiple-fault scenarios in which the FDI approach introduced in the previous chapter is not applicable. Then the robustness of the FDI method with respect to total faults in the sensors is investigated. This study not only shows the applicability of the proposed method in the sensor failure cases, but also indicates that one can use a smaller set of measurements for the FDI purpose.

5.1. FDI DIAGNOSIS OF MULTIPLE FAULTS

As explained in the previous chapter, the proposed method can detect and isolate a single fault. However, this approach is not applicable for multiple-fault scenarios. For instance, Figure 5.1 shows the result of the proposed method for a multiple-fault scenario. In this scenario, a decreasing fault (with a magnitude of 2%) in the turbine efficiency occurs at the time instant $t = 8sec$, and a loss in the turbine mass flow (with a magnitude of 5%) occurs at $t = 20sec$. As shown in Figure 5.1, although the proposed method can detect and isolate the first fault, it is not able to isolate the second fault.

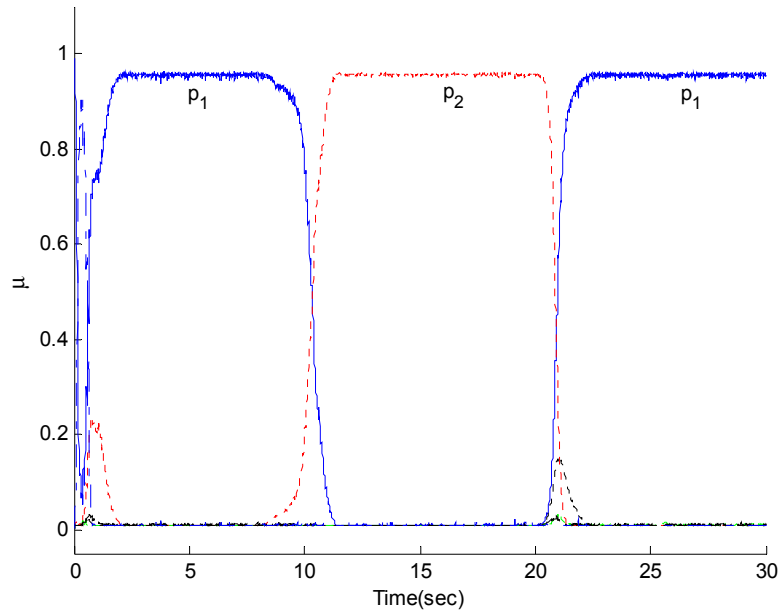


Figure 5.1: The probability of the models for a multiple-fault scenario. The faults with magnitude 2% and 5% occur in the turbine efficiency and mass flow at $t=8\text{sec}$ and $t=20\text{sec}$, respectively. The proposed method in the previous chapter cannot isolate the second fault.

Below a modified approach that is proposed in [3, 59] is utilized to overcome the problem that is shown in Figure 5.1. Note that we apply this method to the linear banks constructed by the method proposed in Chapter 3. As the method provided in the previous chapter, the new approach is based on the multiple model methodology. In this method a bank of observers are run in parallel in order to detect and isolate the first fault. After the isolation of the first fault the bank is updated with the new structure that is called the Level 2 bank such that the second fault can be detected and isolated.

More precisely, this method is a hierarchical approach. Based on the assumption that the engine starts from the healthy condition, first Level 1 banks are active. The Level 1 banks are those that are used in the previous chapters to detect and isolate the first fault. It is worth nothing that the active bank is selected based on the value of W_f and at each time only one bank is active (the details for Level 1 banks have been

provided in Section 4.1). After detection and isolation of the first fault, the corresponding Level 2 bank (based on the isolated fault and W_f) is utilized to detect and isolate the second fault.

Remark: The Level 2 bank used only when the first fault is isolated, and based on the isolated fault only one Level 2 bank will be activated. Also, after the corresponding Level 2 bank activation, the Level 1 bank is deactivated. This technique enables us to decrease the computational cost as compared with the approach in which one runs all models (models for a single fault and models for multiple faults) in parallel. Moreover, in this approach we assume that there is no simultaneous multiple fault occurrence and there is a minimum time interval between the first fault and the second one, and this minimum time interval is greater than the time is needed to isolate the first fault (for instance, see Table 4.6).

For more clarification, assume that at the time instant $t = t_1 \text{ sec}$ the fault $F_{et} = 0.98$ (a fault in the turbine efficiency with a magnitude of 2%) is isolated. The corresponding Level 2 bank for this case is shown in Table 5.1.

Table 5.1: The selected Level 2 bank after isolating the fault $F_{et} = 0.98$. Note that all models include this fault.

Model Modes	#1	#2	#3	#4	#5	#6
Model	$F_{et} = 0.98$	$F_{et} = 0.95$	$F_{et} = 0.98$ $F_{ec} = 0.98$	$F_{et} = 0.98$ $F_{mt} = 0.98$	$F_{et} = 0.98$ $F_{mc} = 0.98$	$F_{et} = 0.98$ $F_{wf} = 0.95$

Note that all models include the isolated fault $F_{et} = 0.98$. The model for $F_{et} = 0.95$ can be viewed as a model with a fault $F_{et} = 0.98 - 0.03$. One can construct the Level 2 bank for the other faults in the same way. Table 5.2 and Table 5.3 summarize the Level 1 and Level 2 banks that are used for the faults with a magnitude of 2% in F_{et} , F_{ec} , F_{mt} ,

and F_{mc} and 5% in F_{wff} .

Table 5.2: The Level 1 bank used for multiple fault diagnosis.

Models Modes	Healthy	$F_{et} = 0.98$	$F_{ec} = 0.98$	$F_{mt} = 0.98$	$F_{mc} = 0.98$	$F_{wff} = 0.95$
-----------------	---------	-----------------	-----------------	-----------------	-----------------	------------------

Table 5.3: The Level 2 banks that are used for multiple fault diagnosis.

Bank Label	First Fault	Corresponding Level 2 Bank					
1	F_{et}	$F_{et} = 0.98$	$F_{et} = 0.95$	$F_{et} = 0.98$ $F_{ec} = 0.98$	$F_{et} = 0.98$ $F_{mt} = 0.98$	$F_{et} = 0.98$ $F_{mc} = 0.98$	$F_{et} = 0.98$ $F_{wff} = 0.95$
2	F_{ec}	$F_{ec} = 0.98$	$F_{ec} = 0.95$	$F_{ec} = 0.98$ $F_{et} = 0.98$	$F_{ec} = 0.98$ $F_{mt} = 0.98$	$F_{ec} = 0.98$ $F_{mc} = 0.98$	$F_{ec} = 0.98$ $F_{wff} = 0.95$
3	F_{mt}	$F_{mt} = 0.98$	$F_{mt} = 0.95$	$F_{mt} = 0.98$ $F_{et} = 0.98$	$F_{mt} = 0.98$ $F_{ec} = 0.98$	$F_{mt} = 0.98$ $F_{mc} = 0.98$	$F_{mt} = 0.98$ $F_{wff} = 0.95$
4	F_{mc}	$F_{mc} = 0.98$	$F_{mc} = 0.95$	$F_{mc} = 0.98$ $F_{et} = 0.98$	$F_{mc} = 0.98$ $F_{ec} = 0.98$	$F_{mc} = 0.98$ $F_{mt} = 0.98$	$F_{mc} = 0.98$ $F_{wff} = 0.95$
5	F_{wff}	$F_{wff} = 0.95$	$F_{wff} = 0.92$	$F_{wff} = 0.95$ $F_{et} = 0.98$	$F_{wff} = 0.95$ $F_{ec} = 0.98$	$F_{wff} = 0.95$ $F_{mt} = 0.98$	$F_{wff} = 0.95$ $F_{mt} = 0.98$

5.1.1. Simulation Results

In this section, we provide the simulation results for the following scenarios. It is worth noting that all the parameters, except the fault magnitude and occurrence time are the same as in Section 4.2.

Scenario I (multiple faults in the turbine efficiency and compressor mass flow):

In this scenario we assume that a fault with a magnitude of 2% (decrease in the turbine efficiency) occurs at the time instant $t=8\text{ sec}$, and then at the time instant $t=20\text{ sec}$ another fault with a magnitude of 2% occurs in the compressor mass flow. The results are shown in Figure 5.2.

Scenario II (multiple faults in the turbine): In this scenario a fault with a magnitude of 2% (decrease in the turbine efficiency) occurs at the time instant $t = 8 \text{ sec}$, and then at the time instant $t = 20 \text{ sec}$ another fault with a magnitude of 2% occurs in the turbine mass flow. The results are shown in Figure 5.3.

Scenario III (multiple faults in the turbine efficiency and fuel flow): This scenario simulates multiple faults (decrease) in the turbine efficiency and fuel flow which occur at the time instant $t = 8 \text{ sec}$ and $t = 20 \text{ sec}$ with magnitudes 2% and 5%, respectively. The results are shown in Figure 5.4.

Scenario IV (multiple faults in the compressor mass flow and fuel flow): In this scenario, multiple faults (decrease) in the compressor mass flow and fuel flow occur at the time instant $t = 8 \text{ sec}$ and $t = 20 \text{ sec}$ with magnitudes 2% and 5%, respectively. The results are shown in Figure 5.5.

Scenario V (multiple faults in the turbine mass flow and compressor efficiency): This scenario simulates multiple faults (decrease) in the turbine efficiency and compressor mass flow and fuel flow which occur at the time instant $t = 8 \text{ sec}$ and $t = 20 \text{ sec}$ with magnitudes 2% and 2%, respectively. The results are shown in Figure 5.6.

Figure 5.2 provides the result of Scenario I by using the proposed Level 2 method. As can be seen, first the turbine efficiency fault is detected and then the bank label 1 in Table 5.3 is activated. Then the second fault which is a fault in the compressor mass flow is detected and isolated.

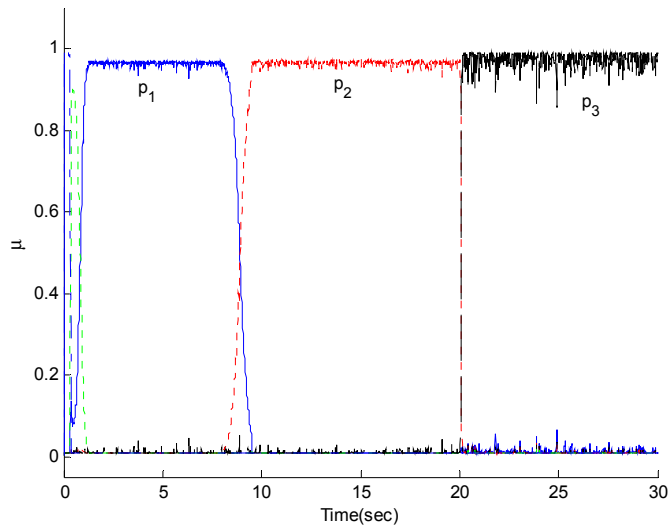


Figure 5.2: Simulation results of Scenario I, multiple faults in the turbine efficiency and compressor mass flow with a magnitude of 2% occurs at $t=8sec$ and $t=20sec$, respectively.

Figure 5.3 shows the result of Scenario II by using the Level 2 method. As Figure 5.3 shows, first a fault in the turbine efficiency is detected and isolated and again the bank label 1 in Table 5.3 is activated. However, in this scenario a fault in the turbine mass flow is detected and isolated as the second fault.

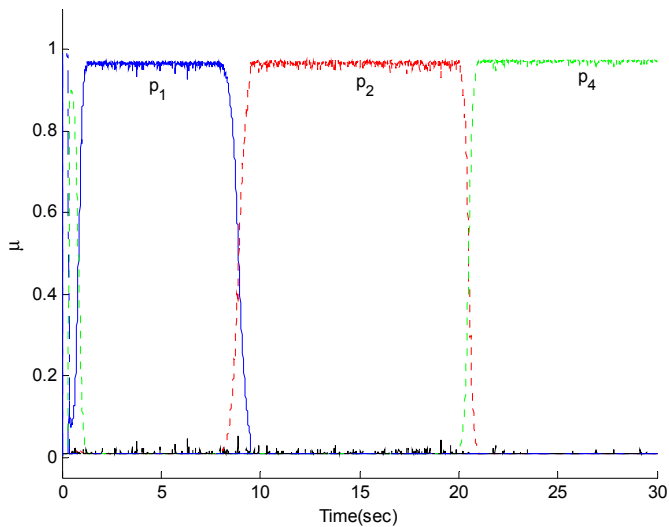


Figure 5.3: Simulation results of Scenario II, multiple faults in the turbine efficiency and mass flow with a magnitude of 2% occurs at $t=8sec$ and $t=20sec$, respectively.

The result of Scenario III by using the Level 2 method is shown in Figure 5.4. Again in this simulation, first a fault in the turbine efficiency is detected and isolated, and then a fault in the fuel flow effectiveness is isolated.

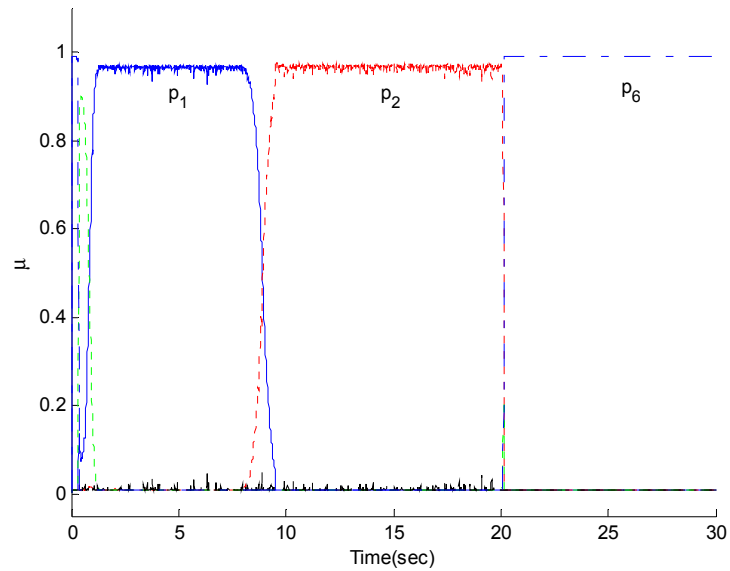


Figure 5.4: Simulation results of Scenario III, multiple faults in the turbine efficiency and fuel flow with a magnitude of 2% and 5% occur at $t=8sec$ and $t=20sec$, respectively.

The result of Scenario IV by using the Level 2 method is shown in Figure 5.5.

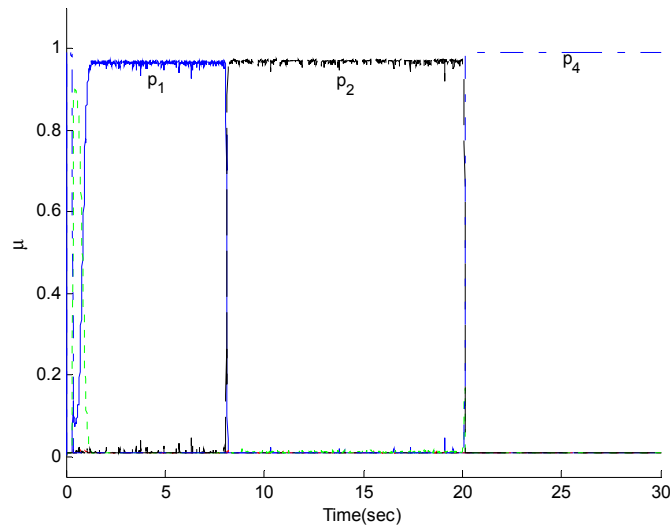


Figure 5.5: Simulation results of Scenario IV, multiple faults in the compressor mass flow and fuel flow with a magnitude 2% and 5% occur at $t=8sec$ and $t=20sec$, respectively.

In Figure 5.5, a fault in the compressor mass flow is detected and isolated as the first fault. Then the bank number 4 in Table 5.3 is activated. The second fault which is a fault in the fuel flow effectiveness is detected and isolated.

Figure 5.6 shows the result of Scenario V by using the Level 2 method. The first fault that is a fault in the turbine mass flow is detected and isolated. Then the Bank label 3 is activated and a fault in the compressor efficiency is detected and isolated as the second fault.

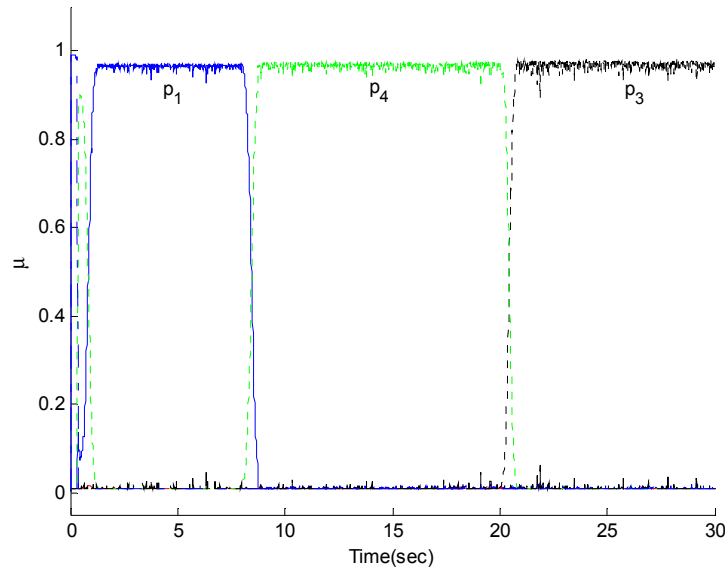


Figure 5.6: Simulation results of Scenario V, multiple faults in the turbine mass flow and compressor efficiency with a magnitude 2% occur at $t=8\text{sec}$ and $t=20\text{sec}$, respectively.

Table 5.4 summarizes the results corresponding to Scenarios I-V

Table 5.4: The detection and isolation time of scenarios I-V. T_D and T_I denote the detection and isolation time, respectively. In all the scenarios, first fault occurs at $t=8\text{sec}$ and second one occurs at $t=20\text{sec}$.

Scenarios	First fault		Second fault	
	T_D	T_I	T_D	T_I
I	8.36	9.48	20.05	20.11
II	8.35	9.48	20.19	20.82
III	8.35	9.48	20.09	20.17
IV	8.06	8.17	20.09	20.19
V	8.16	8.73	20.2	20.69

5.2. OUTPUT SELECTION

As mentioned in Chapter 2, we consider the following outputs for a single spool jet engine, that is

$$y = [N, T_c, T_t, P_c, P_t]^T \quad (5.1)$$

where N, T_c, T_t, P_c, P_t denote the fan speed, the compressor temperature, the turbine temperature, the compressor pressure and the turbine pressure. In this section, we show that with lower number of measurements the FDI can still be accomplished. However, detection and isolation times are increased. The output selection enables us to investigate the robustness of the proposed methodology due to loss of measurements. In this case we analysis two different set of outputs as follow

1. $y = [N, T_c, P_c, P_t]$.
2. $y = [T_c, P_c, P_t]$.

In this section, we first investigate the system observability for different sets of outputs which is then followed by the simulation results.

5.2.1. Investigation of the Observability

Let us consider the nonlinear system (2.14), where one can find the linear model for the different values of W_f (recall that the steady state points are determined with values of W_f). For example, the fault free linear model for $W_f = 0.4$ is given by

$$A = \begin{bmatrix} -10.24 & 1015 & -0.92 & 0 \\ 0.09 & 83 & 3.2 & 13.2 \\ 3.2 & 1548 & -111 & -0.001 \\ 0 & -0.001 & -0.002 & 20.25 \end{bmatrix}$$

$$B = \begin{bmatrix} 2 \times 10^4 \\ 136 \\ 0 \\ 0 \end{bmatrix}, \quad C = \begin{bmatrix} 0 & 1 & 0 & 0 \\ 0 & 24.25 & 0.01 & 0 \\ 0.77 & -46.2 & 0.01 & 141.25 \\ 0 & 0 & 1 & 0 \\ 0 & 0 & 0 & 1 \end{bmatrix} \quad (5.2)$$

in which we consider equation (5.1) as the output function.

By using the matrices A and C one can test the observability of the corresponding linear system. Therefore, we can investigate the observability of the linear systems for different values of W_f and different sets of output equations. Table 5.5 summarizes the results for this investigation. It is worth noting that the symbols \surd and \times denote that the corresponding linear system is observable and unobservable, respectively.

Table 5.5: The Observability test results by using different sets of outputs and different values of W_f . The symbols \surd and \times designate the observability and unobservability, respectively.

W_f	0.4	0.5	0.6	0.7	0.8	0.9
Outputs						
$[N, T_C, P_C, P_t]^T$	\surd	\surd	\surd	\surd	\surd	\surd
$[T_C, P_C, P_t]^T$	\times	\surd	\times	\surd	\surd	\surd
$[P_C, P_t]^T$	\times	\times	\times	\times	\times	\times
P_t	\times	\times	\times	\times	\times	\times
$[N, P_C, P_t]^T$	\surd	\times	\surd	\surd	\times	\surd
$[N, P_t]^T$	\times	\times	\times	\times	\times	\times
$[T_C, P_C]^T$	\times	\surd	\surd	\surd	\surd	\times
$[T_C, P_t]^T$	\times	\times	\times	\times	\times	\times

As can be observed, for the output sets $y = [N, T_C, P_C, P_t]^T$ the linear models for all steady state points are observable.

5.2.2. Simulation Results

In the following simulation results, we consider the following scenarios with $W_f = 0.8$.

Scenario I: A fault in the turbine efficiency occurs at $t=5\text{sec}$ with a magnitude of 2% ($F_{et} = 0.98$).

Scenario II: A fault in the compressor efficiency occurs at $t=5\text{sec}$ with a magnitude of 2% ($F_{ec} = 0.98$).

Scenario III: A fault in the turbine mass flow occurs at $t=5\text{sec}$ with a magnitude of 2% ($F_{mt} = 0.98$).

Scenario IV: A fault in the compressor mass flow occurs at $t=5\text{sec}$ with a magnitude of 2% ($F_{mc} = 0.98$).

Scenario V: A loss of effectiveness of fuel flow occurs at $t=5\text{sec}$ with a magnitude of 5% ($F_{wf} = 0.95$).

5.2.2.1. Simulation Results for $y_1 = [N, T_C, P_C, P_t]$

The simulation results for the Scenarios I to V are shown in Figure 5.7 to Figure 5.11 . In these simulations we consider $y_1 = [N, T_C, P_C, P_t]$ as the available measurement. As can be observed from Figure 5.7 to Figure 5.11, the faults in all scenarios are detected and isolated. Note that the system with $y_1 = [N, T_C, P_C, P_t]$ as measurement is observable

for all value of W_f (Table 5.5).

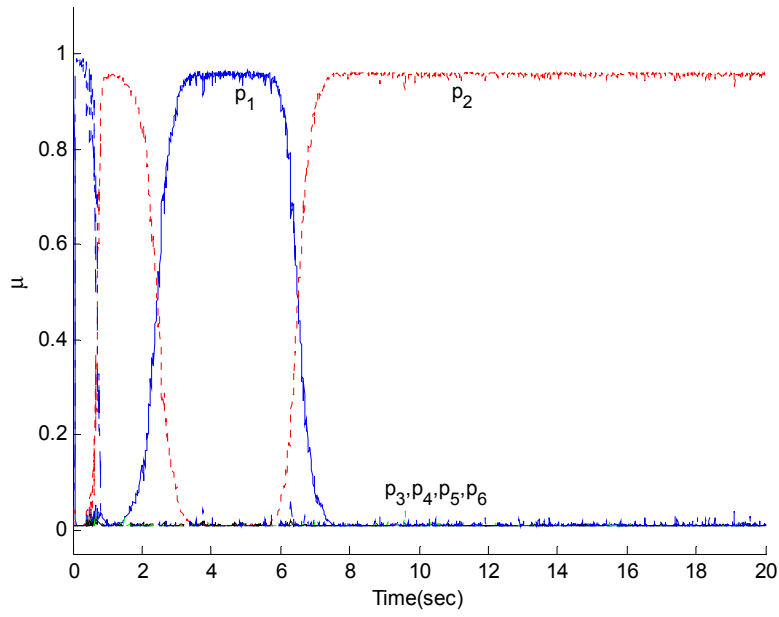


Figure 5.7: The probability of the models for Scenario I with $y = [N, T_C, P_C, P_t]$. A fault with a magnitude of 2% occurs in the turbine efficiency at $t=5sec$.

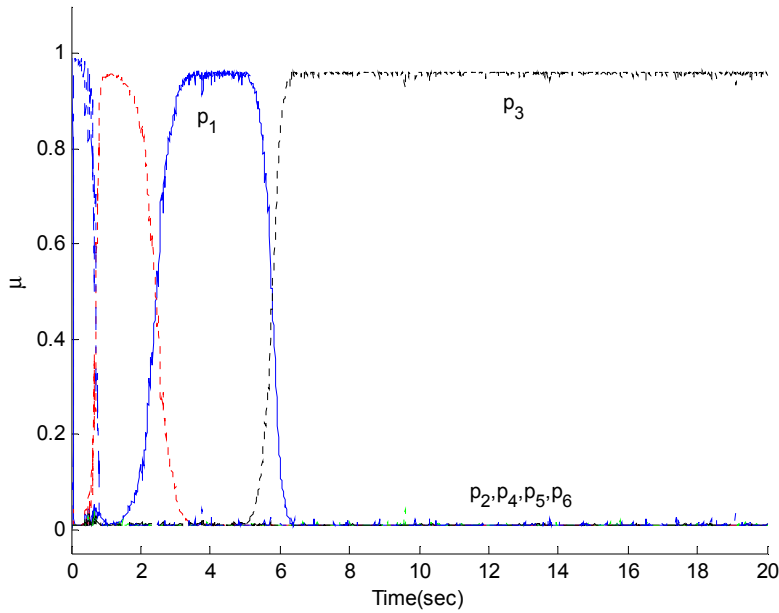


Figure 5.8: The probability of the models for Scenario II with $y = [N, T_C, P_C, P_t]$. A fault with a magnitude of 2% occurs in the compressor efficiency at $t=5\text{sec}$.

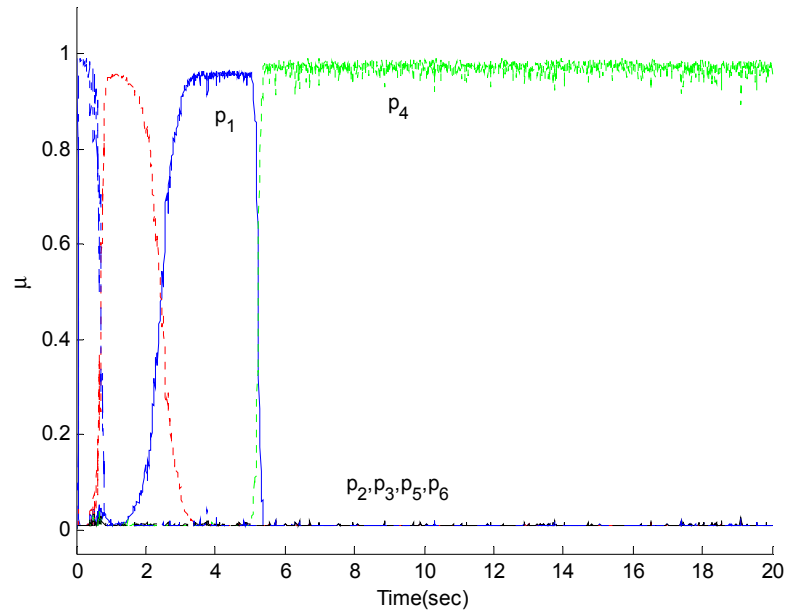


Figure 5.9: The probability of the models for Scenario III with $y = [N, T_C, P_C, P_t]$. A fault with a magnitude of 2% occurs in the turbine mass flow at $t=5\text{sec}$.

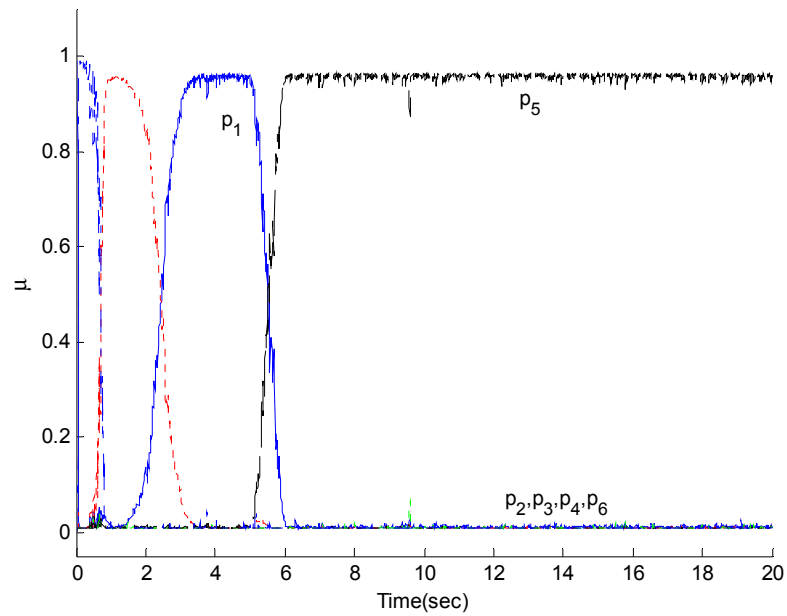


Figure 5.10: The probability of the models for Scenario IV with a $y = [N, T_C, P_C, P_t]$. A fault with a magnitude of 2% occurs in the compressor mass flow at $t=5\text{sec}$.

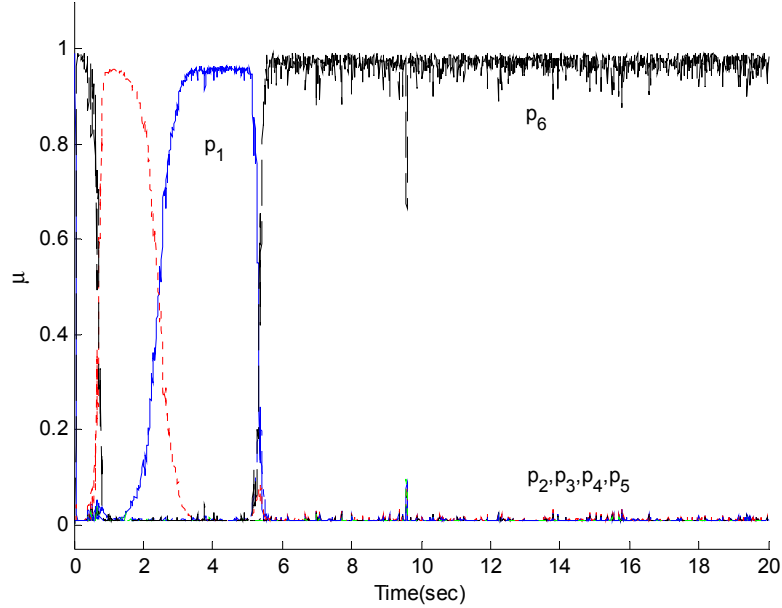


Figure 5.11: The probability of the models for Scenario V with $y = [N, T_C, P_C, P_t]$. A loss of effectiveness of fuel flow with a magnitude of 5% occurs at $t=5\text{sec}$.

5.2.2.2. Simulation Results for $y = [T_C, P_C, P_t]$

The simulation results for the Scenarios I to V are shown in Figure 5.12 to Figure 5.16. In these simulations we consider $y = [T_C, P_C, P_t]$ as the available measurement. By using $y = [T_C, P_C, P_t]$ the system is not observable for all W_f (refer to Table 5.5). However, for $0.7 \leq W_f \leq 0.9$, the system is observable. Therefore, as can be observed from Figure 5.12 to Figure 5.16, the FDI unit can detect and isolate the faults properly.

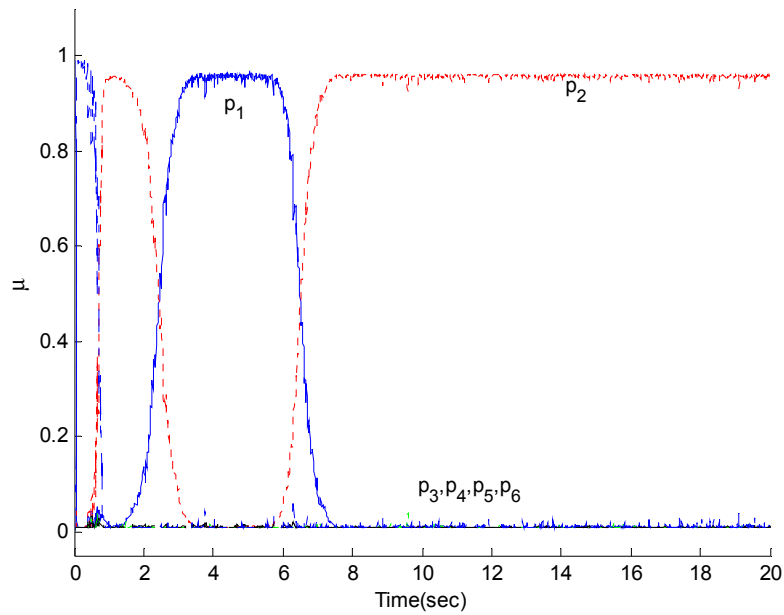


Figure 5.12: The probability of the models for Scenario I with $y = [T_C, P_C, P_t]$. A fault with a magnitude of 2% occurs in the turbine efficiency at $t=5sec$.

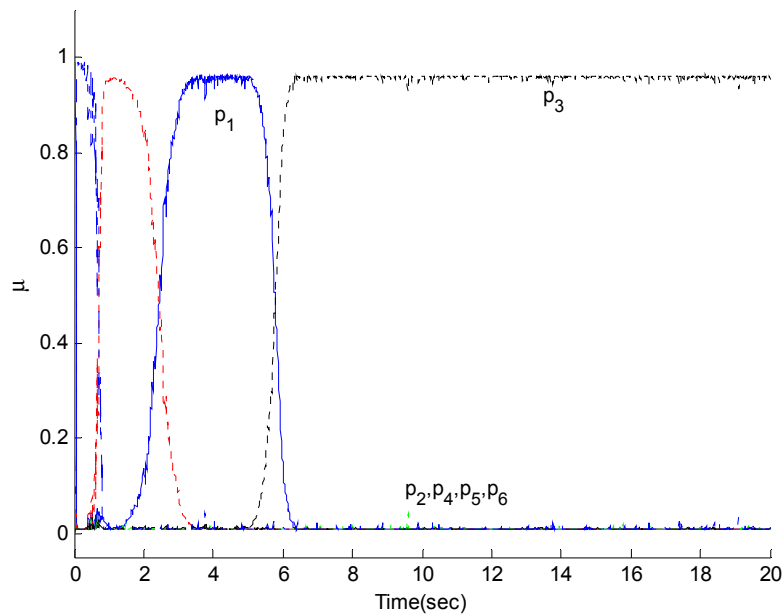


Figure 5.13: The probability of the models for Scenario II with $y = [T_C, P_C, P_t]$. A fault with a magnitude of 2% occurs in the compressor efficiency at $t=5sec$.

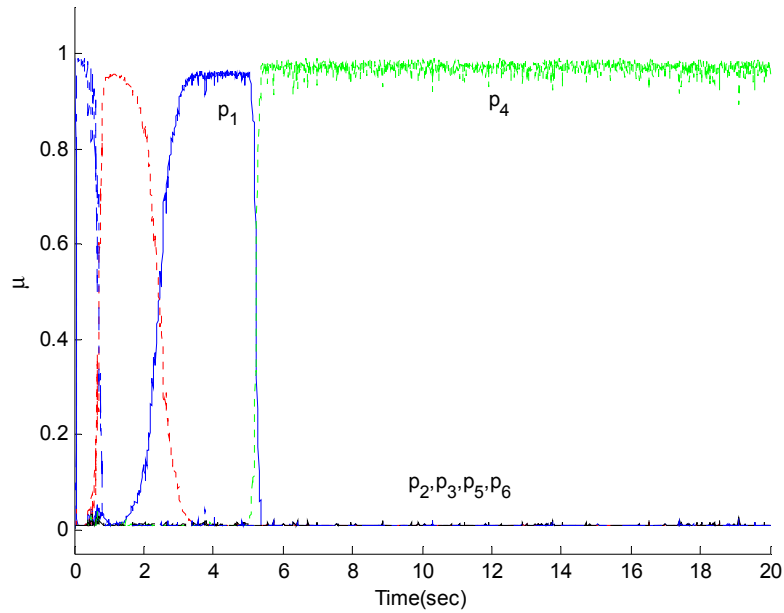


Figure 5.14: The probability of the models for Scenario III with $y = [T_c, P_c, P_t]$. A fault with a magnitude of 2% occurs in the turbine mass flow at $t=5\text{sec}$.

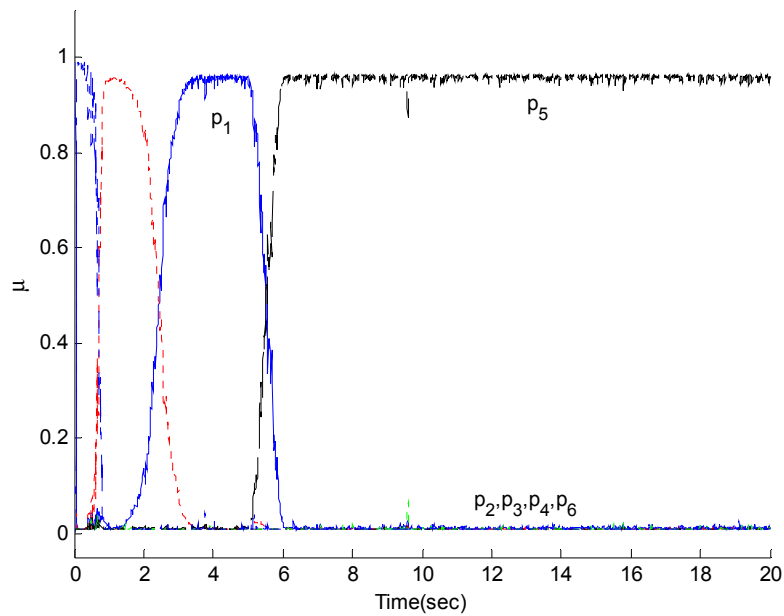


Figure 5.15: The probability of the models for Scenario IV with $y = [T_c, P_c, P_t]$. A fault with a magnitude of 2% occurs in the compressor mass flow at $t=5\text{sec}$.

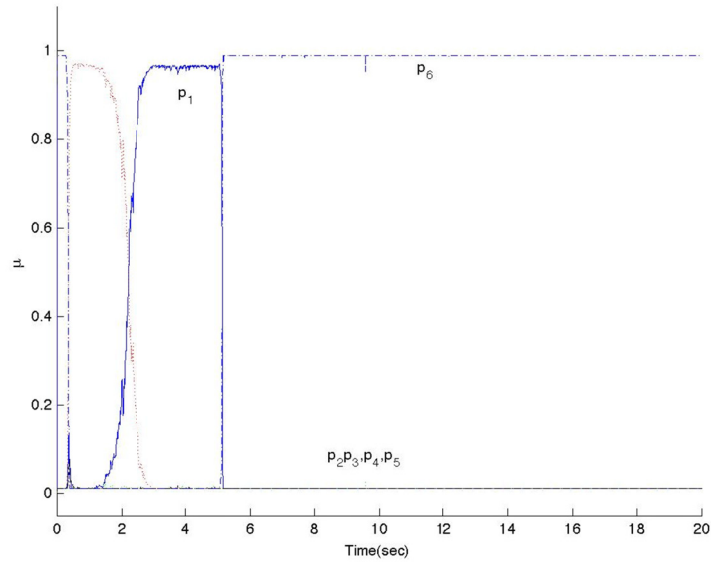


Figure 5.16: The probability of the models for Scenario V with $y = [T_C, P_C, P_I]$. A loss of effectiveness of fuel flow with a magnitude of 5% occurs at $t=5sec$.

5.2.2.3. Summary

As can be observed from the preceding subsections, decreasing the number of measurements affects the accuracy of the FDI results. Table 5.6 summarizes the simulation results. In this table, t_D and t_I denote the detection and isolation times, respectively. It follows that the proposed approach is robust even when there are total failures in some of the sensors.

Table 5.6The summary of simulation results for different set of measurements by using $W_f = 0.8$. t_D and t_I denote the detection and isolation times, respectively.

Scenarios \ Outputs	Scenario I		Scenario II		Scenario III		Scenario IV		Scenario V	
	t_D	t_I	t_D	t_I	t_D	t_I	t_D	t_I	t_D	t_I
$y = [N, T_C, P_C, P_I]$	6	7.02	5.27	6.14	5.1	5.33	5.12	5.9	5.2	5.57
$y = [T_C, P_C, P_I]$	5.99	7.03	5.27	6.15	5.1	5.34	5.13	5.9	5.12	5.7

5.3. CONCLUSION

In this chapter, the proposed FDI approach in chapter 4 has been modified such that the multiple-fault scenarios can be handled. Particularly, a hierarchical structure is utilized in order to detect and to isolate multiple faults. In this structure, after isolating the first fault a new bank is replaced. This bank which is called the Level 2 bank is in charge of detecting and isolating the second fault. Furthermore, the robustness of the proposed approach in the previous chapter is analyzed. We investigated the observability of the linear models for different sets of outputs and steady state points. It has been shown that the linear models with $y = [N, T_C, P_C, P_t]^T$ (without measuring the turbine temperature) are still observable and the FDI mission can be accomplished. Also, the simulation results for different fault scenarios indicate the capability of the proposed FDI method even when one has a lower number of measurements.

Chapter 6 CONCLUSIONS AND SUGGESTIONS

In this thesis, the FDI problem of a special gas turbine (single spool jet engine in cruise mode) has been investigated. Broadly speaking, we first develop a novel symbolic linearization method for a class of nonlinear systems. By using the linearized models for fault-free and faulty systems, we develop an FDI algorithm based on the multiple-model approach. Finally, we applied our proposed method to single spool gas turbine jet engine. Below, we first summarize the thesis by providing the main contributions of the thesis in more precise terms, and then the suggestions for the future work are provided.

6.1. CONTRIBUTIONS OF THE THESIS

6.1.1. Develop a Novel Symbolic Linearization Method

In this approach, we combine the numerical methods with a novel symbolic computation approach to obtain a linear model of a nonlinear system such that the fault variables affect the linear model symbolically. In particular, in order to implement the proposed symbolic linearization method, the original nonlinear model is first decomposed to sub-blocks such that the fault variables are multiplied with the outputs of a certain set of these sub-systems, and then each sub-block is linearized numerically. Finally, these linear sub-blocks (by considering faults as the symbolic variables) are combined to obtain the linear symbolic model.

6.1.2. Develop the Modified Multiple Model FDI

The proposed FDI algorithm is based on the symbolic linear system that is obtained in the previous step. More precisely, by using the symbolic model, the linear models of the system for different operating points are obtained (this set of models contains the linear fault-free and faulty systems). Then a modified linear multiple model FDI algorithm (based on linear models) is performed on the original nonlinear system. This modified approach is equipped with an observer selecting unit such that for each vicinity around a certain operating point the corresponding bank of observer is select. The observer of this bank is constructed based on the linear model of the original nonlinear system at the corresponding operating point. Also, a hierarchical structure is used to improve the FDI unit. By this modification the FDI algorithm can detect and isolate multiple faults.

In summary, the proposed FDI algorithm has two main features namely linearity and hierarchical structure. The linearity enables one to accomplish the FDI mission with lower computational time as compared to the nonlinear model while the hierarchical structure has been developed to handle multiple fault scenarios.

6.1.3. The FDI problem of the Single Spool Gas Turbine

In this part, as the case study, we consider a nonlinear model of a single spool gas turbine engine. Because of the complexity of the model, particularly compressor and turbine map, this system cannot be linearized symbolically by using the existing symbolic computation toolboxes. Therefore, the proposed symbolic linearization method has been applied to this system. Simulation results show that linear model obtained by using the proposed method can capture the behavior of the nonlinear system in a vicinity of the corresponding operating point.

Also, for the FDI purpose the modified multiple model is applied to the investigated system. This approach has two main features namely linearity and hierarchical structure. To decrease the negative effects of the measurement noise, we provide a relatively simple (however efficient) method that can decrease the false alarms significantly. Moreover, to investigate the robustness of the proposed method we performed the approach by using different set of measurements. The observability of linear models has been investigated and it was shown that with a smaller set of measurements, one can still accomplish the FDI mission. The simulation results support the capability of the proposed method.

6.2. SUGGESTIONS

In this section, we provide the suggestions for future work. These suggestions are categorized into two different groups as theoretic and application. In the theoretic part, we focus on the proposed linearization method, while in the application subsection the suggestions for the case study (gas turbines) are provided.

6.2.1. Suggestions on the Theory

In this thesis, we use the multiple model approach to determine the fault severity. This suffers from a drawback of high computational cost when one needs to estimate the fault severity accurately. Based on the fact that the symbolic linear model includes the fault variables as parameter, this symbolic model can also be used for fault severity estimation.

Also, the proposed approach can be extended to modify the nonlinear multiple-model approach such as the extended Kalman filter (EKF). More precisely, in the EKF one needs to numerically linearize the original nonlinear system and for different faulty

systems. Therefore, by using the proposed symbolic linearization methods the system is first linearized and then by substituting different fault severities, one can obtain different faulty models.

Moreover, in this thesis we assume a perfect model for the original system. In presence of modeling error, one has to use the hybrid approaches by using artificial intelligence and model based methods. Generalizing the proposed method for the hybrid systems is another suggestion for future work. In other words, if the neural network that is used to compensate for the modeling error is updated, can one compute the linear model without performing the linearization process completely?

6.2.2. Suggestions on the Application

As mentioned in Chapter 1, the behavior of the power station plant and jet engine (at cruise mode) are almost the same. Therefore, by applying the proposed method on different types of gas turbines can be the first step for future work on the application side.

The dual spool gas turbines have two compressors and turbines namely as high pressure and low pressure. Hence, the nonlinear model of these engines is more complicated as compared with the single spool ones. The proposed symbolic linearization methodology can be investigated as well for dual spool gas turbines.

BIBLIOGRAPHY

- [1] J. Gertler, "Survey of model-based failure detection and isolation in complex plants," *Control System Magazine*, vol. 8, no. 6, pp. 3-11, 1998.
- [2] N. Meskin, E. Naderi and K. Khorasani, "Fault diagnosis of jet engines by using a multiple model-based approach," in *ASME Conference*, Glasgow, 2010.
- [3] N. Meskin, E. Naderi and K. Khorasani, "A multiple model-based approach for fault diagnosis of jet engines," *IEEE Tran. Control System Technology*, vol. 21, no. 1, pp. 254-262, 2013.
- [4] R. Patton, L. Toribio and S. Simani, "Robust fault diagnosis in a chemical process using multiple-model approach," *Proceedings of the 40th IEEE Conference on Decision and Control*, pp. 149-154, 2001.
- [5] P. Frank, "Fault diagnosis in dynamical systems using analytical and knowledge-based redundancy: A survey and some new results," *Automatica*, vol. 26, no. 3, pp. 459-474, 1990.
- [6] R. Isermann, *Fault-diagnosis systems: an introduction from fault detection to fault tolerance*, Berlin: Springer, 2005.
- [7] Y. Zhang and J. Jiang, "Bibliographical review on reconfigurable fault-tolerant control systems," vol. 32, no. 2, pp. 229-252, 2008.
- [8] R. Patton, P. Frank and R. Clark, *Issues of fault diagnosis for dynamic systems*, Berlin: Springer, 2000.
- [9] Z. Sadough, "Fault detection and isolation in gas turbine engines," Master of Applied Science thesis, Concordia University, 2012.
- [10] V. Venkatasubramanian, R. Rengaswamy, K. Yin and S. Kavuri, "A review of process fault detection and diagnosis- part I: Quantitative model-based methods," *Computer and Chemical Engineering*, vol. 27, no. 3, pp. 293-311, 2003.
- [11] V. Venkatasubramanian, R. Rengaswamy, K. Yin and S. Kavuri, "A review of process fault detection and diagnosis- part II: Qualitative models and research strategies," *Computer and Chemical Engineering*, vol. 27, no. 3, pp. 313-326, 2003.
- [12] V. Venkatasubramanian, R. Rengaswamy, K. Yin and S. Kavuri, "A review of process fault detection and diagnosis-part III: History based methods," *Computer and Chemical Engineering*, vol. 27, no. 3, pp. 327-346, 2003.

- [13] S. Sarkar, X. Jin and A. Ray, "Data-driven fault detection in aircraft engines with noisy sensor measurements," *Transactions of the ASME*, vol. 133, no. 8, pp. 1-10, 2011.
- [14] P. M. Frank, "A fuzzy FDI decision-making system for the support of the human operator," in *Proceedings of the IFAC Symposium SAFEPROCESS'97, (Hull, UK)*, pp. 721-726, 1998.
- [15] H. Lee, D. Park, B. Ahn, Y. Park, J. Park and S. Venkata, "A fuzzy expert system for the integrated fault diagnosis," *IEEE Transactions on Power Delivery*, vol. 15, no. 2, pp. 833--838, 2000.
- [16] H. Saravanamuttoo, G. Rogers and H. Cohen, *Gas turbine theory*, Person Education, 2001.
- [17] Y. Lee, D. Mavris, V. Volovoi, M. Yuan and T. Fisher, "A fault diagnosis method for industrial gas turbines using Bayesian data analysis," *Journal of Engineering for Gas Turbines and Power*, vol. 132, pp. 041602(1-6), 2010.
- [18] T. Giampaolo, *The gas turbine handbook: Principle and Practice*, New York: Fairmont Press, 2003.
- [19] E. Naderi, N. Meskin and K. Khorasani, "Nonlinear fault diagnosis of jet engines by using a multiple model-based approach," *Journal of Engineering for Gas Turbines and Power*, vol. 134, no. 1, pp. 1-10, 2011.
- [20] "Documentation Center," Mathworks-MATLAB, 2011. [Online]. Available: www.mathworks.com.
- [21] J. Marzat, H. Piet-Lahanier, F. Damongeot and E. Walter, "Model-based fault diagnosis for aerospace systems: a survey," *Journal of Aerospace Engineering*, vol. 226, pp. 1329-1360, 2012.
- [22] V. Panov, "GasTurboLib: simulink library for gas turbine engine modelling," in *ASME, Orlando*, 2009.
- [23] M. Roemer, G. Kacprzyński, M. Schoeller, R. Howe and R. Friend, "Advanced test cell diagnostics for gas turbine engines," in *IEEE, Aerospace Conference*, Montana, 2001.
- [24] W. Yan, "Application of random forest to aircraft engine fault diagnosis," in *IMACS Multiconference on Computational Engineering in Systems Applications*, 2006.
- [25] L. Changzheng and L. Yong, "Fault diagnosis for an aircraft engine based on information fusion," in *IEEE International Conference on Mechatronics*, 2006.
- [26] T. Kobayashi and D. Simon, "Application of a bank of Kalman filters for aircraft engine fault diagnostics," NASA, 2003.
- [27] M. Salman and B. Chang, "Analysis of aircraft dynamics near the flight envelope boundary," in *8th Asian Control Conference (ASCC)*, Kaohsiung, Taiwan, 2011.

- [28] G. Yen and L. Ho, "Online multiple-model-based fault diagnosis and accommodation," *IEEE Transactions on Industrial Electronics*, vol. 50, no. 2, pp. 296-312, 2003.
- [29] T. Lefebvre, H. Bruyninckx and J. De Schutter, "Kalman filters for non-linear systems: a comparison of performance," *International journal of Control*, vol. 77, no. 7, pp. 639-653, 2004.
- [30] R. J. Patton, C. Lopez-Toribio and F. Uppal, "Artificial intelligence approaches to fault diagnosis," in *Condition Monitoring: Machinery, External Structures and Health*, Birmingham, UK, 1999.
- [31] M. Ramesh and A. J. Laxmi, "Fault identification in HVDC using artificial intelligence—Recent trends and perspective," in *IEEE International Conference on Power, Signals, Controls and Computation (EPSCICON)*, Thrissur, 2012.
- [32] Y. Duan and H. Toliyat, "A review of condition monitoring and fault diagnosis for permanent magnet machines," in *IEEE Power and Energy Society General Meeting*, San Diego, 2012.
- [33] B. Mahdi Ebrahimi and J. Faiz, "Feature extraction for short-circuit fault detection in permanent-magnet synchronous motors using stator-current monitoring," *IEEE Transactions on Power Electronics*, vol. 25, no. 10, pp. 2673-2682, 2010.
- [34] M. Rosu, V. Nahkuri, A. Arkkio, T. Jokinen, J. Mantere and J. Westerlund, "Permanent magnet synchronous motor for ship propulsion drive," Istanbul, Turkey, 1998.
- [35] R. Jiang and J. Xie, "Gas turbine gas path fault diagnosis technology based on the fuzzy Petri net," in *IEEE International Conference on Transportation, Mechanical, and Electrical Engineering (TMEE)*, ChangChun, 2011.
- [36] R. Mohammadi, "Fault diagnosis of hybrid systems with applications to gas turbine engines," PhD Thesis, Concordia University, 2009.
- [37] W. Yang, K. Y. Lee, S. Junker and H. Ghezal-Ayagh, "Fuzzy fault diagnosis and accommodation system for hybrid fuel-cell/gas-turbine power plant," *Energy Conversion, IEEE Transactions on*, vol. 25, no. 4, pp. 1187--1194, 2010.
- [38] S. Tayarani-Bathaie, Z. Sadough Vanini and K. Khorasani, "Fault detection of gas turbine engines using dynamic neural networks," in *25th IEEE Canadian Conference on Electrical & Computer Engineering (CCECE)*, Montreal, 2012.
- [39] F. Xia, H. Zhang, D. Peng, H. Li and Y. Su, "Turbine fault diagnosis based on fuzzy theory and SVM," *Artificial Intelligence and Computational Intelligence*, pp. 668-676, 2009.
- [40] K. Satyanarayana, M. Sarcar and S. Purushothaman, "Condition monitoring of a turbine using echo state neural network," *European Journal of Scientific Research*, vol. 85, no. 4, pp. 591-599, 2012.
- [41] Y. Qi-Ping, L. Meng-Qun, M. Xue-Yun and W. Jun, "Application of artificial intelligence

- (AI) in power transformer fault diagnosis," in *IEEE International Conference on Artificial Intelligence and Computational Intelligence AICI'09.*, 2009.
- [42] L. Yuan, Y. He, J. Huang and Y. Sun, "A new neural-network-based fault diagnosis approach for analog circuits by using kurtosis and entropy as a preprocessor," *Instrumentation and Measurement, IEEE Transactions on*, vol. 59, pp. 586-595, 2010.
- [43] Z. Liu, J. Chen and C. Song, "A new RBF neural network with GA-based fuzzy C-means clustering algorithm for sins fault diagnosis," in *Control and Decision Conference. CCDC'09. Chinese*, Guilin, 2009.
- [44] S. Huang and K. K. Tan, "Fault detection and diagnosis based on modeling and estimation methods," *Neural Networks, IEEE Transactions on*, vol. 20, pp. 872-881, 2009.
- [45] C. C. Wang, Y. Kang, P. C. Shen, Y. P. Chang and Y. L. Chung, "Applications of fault diagnosis in rotating machinery by using time series analysis with neural network," *Expert Systems with Applications*, vol. 37, no. 2, pp. 1696-1702, 2010.
- [46] T. A. Lemma and F. M. Hashim, "Wavelet analysis and auto-associative neural network based fault detection and diagnosis in an industrial gas turbine," in *Business Engineering and Industrial Applications Colloquium (BEIAC)*, Kuala Lumpur, 2012.
- [47] P. P. Lin, D. Ye, Z. Gao and Q. Zheng, "Intelligent process fault diagnosis for nonlinear systems with uncertain plant model via extended state observer and soft computing," *Intelligent Control and Automation*, vol. 3, no. 4, pp. 346-355, 2012.
- [48] Z. Yang, Y. Wang and J. Lv, "Survey of modern fault diagnosis methods in networks," in *IEEE International Conference on Systems and Informatics (ICSAI)*, Yantai, 2012.
- [49] M. I. Steinder and S. Sethi, "A survey of fault localization techniques in computer networks," *Science of Computer Programming*, vol. 53, no. 2, pp. 165-194, 2004.
- [50] J. KOSZLAGA, "Application of artificial intelligence methods for fault detection in analogue electronic circuits," *Zeszyty Naukowe. Elektryka*, vol. 1, no. 109, pp. 41-50, 2006.
- [51] S. Lin and Z. Ying, "Fault diagnosis of navigation satellite attitude control system based on data-driven combined with artificial intelligence," in *Springer Proceedings China Satellite Navigation Conference (CSNC)*, China, 2012.
- [52] H. Cohen, G. Rodgers and H. Saravanamuttoo, *Gas turbine theory*, John Wiley and Sons Inc., New York, NY, 1987.
- [53] A. N. Tudosie, "Fuel injection controller with barometric and air flow rate correctors," in *International Conference on System Science and Simulation in Engineering*, Genova, Italy, 2009.
- [54] R. D. Flack, *Fundamentals of jet propulsion with applications*, New York: Cambridge University Press, 2005.
- [55] [Online]. Available: <http://images.yourdictionary.com/gas-turbine>.

- [56] K. Mathioudakis, C. Romessis and A. Stamatis, "Probabilistic methods for gas turbine fault diagnostics," *Gas Turbine Condition Monitoring and Fault Diagnosis*, CH Sieverding and K. Mathioudakis, eds., von Karman Institute, Belgium, pp. 1-28, 2003.
- [57] R. Hallouzi, "Multiplemodel based diagnosis for adaptive fault tolerant control," Ph.D. Thesis, Delft Center for Systems and Control, 2008.
- [58] Y. Zhan and J. Jiang, "An interacting multiple-model based fault detection, diagnosis and fault-tolerant control approach," in *38th IEEE Conference on Decision and Control*, Phoenix, 1999.
- [59] P. Maybeck, "Multiple model adaptive algorithms for detecting and compensating sensor and actuator/surface failures in aircraft flight control systems," *International Journal of Robust and Nonlinear Control*, vol. 9, pp. 1051-1070, 1999.
- [60] T. Menke and P. Maybeck, "Sensor/actuator failure detection in the vista F-16 by multiple model adaptive estimation," *IEEE Transaction on Aerospace and Electronic Systems*, vol. 31, no. 4, pp. 1218-1229, 1995.
- [61] P. Maybeck, *Stochastic models, estimation and control*, vol. 1, New York: Academic Press, 1979.
- [62] A. Gelb, *Applied optimal estimation*, Cambridge: MIT press, 1974.
- [63] R. Brown, P. Hwang and others, *Introduction to random signals and applied Kalman filtering*, John Wiley and Sons Inc., New York, NY, 1992.
- [64] F. Lewis and F. Lewis, *Optimal estimation: with an introduction to stochastic control theory*, Wiley New York et al., 1986.
- [65] O. Jacobs, *Introduction to control theory*, vol. 2, Oxford University Press Oxford, UK, 1993.
- [66] P. Eide and P. Maybeck, "An MMAE failure detection system for the F-16," *IEEE Transactions on Aerospace and Electronic Systems*, vol. 32, no. 3, pp. 1125-1136, 1996.
- [67] S. Haykin and others, *Kalman filtering and neural networks*, Wiley Online Library, 2001.